

**Ecole Doctorale 139**

**Connaissances, Langages, Modélisation**

# THÈSE

Présentée

en vue de l'obtention du

**grade de Docteur**

de

**l'Université Paris Ouest Nanterre La Défense**

*en Sciences pour l'Ingénieur*

**José Luis RAMIREZ ARIAS**

## **Development of an artificial muscle for a soft robotic hand prosthesis**

**Développement d'un muscle artificiel pour une prothèse de  
main robotique souple**

soutenue le 09 décembre 2016 devant le jury composé de :

T. WALLMERSPERGER	Prof., Dr.-Ing, Technische Universität Dresden	Rapporteur
P. WENGER	Prof., Ecole Centrale de Nantes	Rapporteur
C. LASCHI	Prof., Scuola Superiore Sant'Anna, Pisa	Examinatrice
Y. AOUSTIN	Prof., Ecole Centrale de Nantes	Examineur
N. JOUANDEAU	Asst. Prof. HDR, Université Paris 8	Examineur
M. D'OTTAVIO	Asst. Prof., Université Paris Ouest Nanterre La Défense	Examineur
O. POLIT	Prof., Université Paris Ouest Nanterre La Défense	Directeur
L. GALLIMARD	Prof., Université Paris Ouest Nanterre La Défense	Directeur

Laboratoire Énergétique Mécanique Électromagnétisme

LEME - EA 4416

50 rue de Sèvres - 92410 Ville d'Avray



# Acknowledgments

First and foremost I am extremely grateful to my supervisors Prof. Laurent Gallimard (head of the theoretical and numeric modeling of structures and systems team) and Prof. Olivier Polit (head of the LEME laboratory) who have supported me throughout this three years and made possible this amazing path. Likewise, I acknowledge M. Michele D'Ottavio and M. Nicolas Jouandeau who share with me their knowledge and expertise during all the useful discussions and brainstorming sessions.

I would also like to take this opportunity to thank my thesis examiners, Prof. Dr.-Ing. Thomas Wallmersperger (Chair of Mechanics of Multifunctional Structures at the Institute of Solid Mechanics of the Technische Universität Dresden in Germany) and Prof. Philippe Wenger (Director of Research at CNRS IRCCyN Ecole Centrale de Nantes in France), for their very helpful comments and suggestions.

I acknowledge Prof. Cecilia Laschi (Full Professor of Biorobotics and Rector's delegate to Research at the BioRobotics Institute of the Scuola Superiore Sant'Anna in Italy) for agreeing to take part in the jury of my thesis and for her valuable comments; and Prof. Yannick Aoustin (full professor at Ecole Centrale de Nantes in France) who accept to be the president of my jury and offered me very interesting ideas.

My sincere gratitude is reserved for M. Pol Le Borgne (Managing Director at Cogitobio in France), who was always enthusiast regarding my project and helped me with profound insights at various stages of my research. Very special thanks to Mme. Sophie Longuet (research coordinator at école supérieure de biomécanique appliquée à l'ostéopathie - OSTEOBIO in France) for her invaluable insights and suggestions.

I wish to express my gratitude to all colleagues and friends, Alexander Nikitin, Jonas Maruani, Zhaoyi Jiang, Thi Huyen Cham Le, Mohand Ouarabi, Patrick Ribeiro, Romain Pawelko and El Hadji Boubacar Seck, who have contributed to this thesis and supported me in one way or the other during this wonderful journey. Very special thanks to the team of master students that worked together with me, especially Aurélien Scola, Adrian Lyonnet and Quentin Bomberault.

Very special thanks to the Colciencias Colombia for giving me the opportunity to carry out my doctoral research and for their financial support. Likewise, I acknowledge Université Paris lumières for the founding through the ProMain Project. Furthermore, I acknowledge the Université franco-allemande Deutsch-Französische Hochschule for the support during my thesis.

---

Last but not the least, I would like to thank my family, my wife, my mother and my grandfather for supporting me spiritually throughout writing this thesis and my life in general, you are my source of inspiration.

# Summary

Up to now, several efforts have been carried out aiming to improve flexibility, usability, and adaptability of robotic hands. Despite these efforts, the problem of robot's dexterous grasping is not completely solved, and actual robots are not able to mimic human grasping movements. The principal research activities concerning the improvement of robotic hands have been focused mainly on prehension analysis, automatic control, and mechanisms. Recently, the utilization of smart and soft materials has led to the development of new adaptive devices known as soft robots, which are useful for physical rehabilitation and improvement of human skills.

In the field of robotic hand prosthesis, the use of smart and soft materials is helpful in improving flexibility, usability, and adaptability of the robots, which simplify daily living activities of prosthesis users. However, regarding the smart materials for artificial muscles, technologies are considered to be far from implementation in anthropomorphic robotic hands.

Therefore, the target of this research work seeks to reduce the gap between smart material technologies and robotic hand prosthesis. Five central axes address the problem: i) identification of useful grasping gestures and reformulation of the robotic hand mechanism [1], ii) analysis of human muscle behavior to mimic human grasping capabilities [2], iii) modeling robot using the hybrid model DHKK-SRQ [3] for the kinematics and the virtual works principle for dynamics. iv) definition of actuation requirements considering the synergy between prehension conditions and robot mechanism [2], and v) development of a smart material based actuation system [4].

Bearing in mind that most of the daily living activities are related to accurate manipulation of objects, the design approach was focused on precision grasping gestures, which requires three fingers. Thus, the first prototype of the robotic hand prosthesis, so-called ProMain-I [4], is equipped with three fingers, placed in the palm of the hand in such a way that they collaborate to facilitate the grasping of several kinds of objects.

Furthermore, the ProMain-I is underactuated and equipped with a drive mechanism based on tendons, which mimic the human musculoskeletal system. The tendon system is fabricated using an elastic material. Thus, it furnishes a flexible or soft behavior to the fingers joints. Due to the flexibility of the driving mechanism, a modeling methodology is introduced to describe the finger behavior accurately.

Taking into account the necessity of representing the different hand poses that arise when soft robotics chains are used, a hybrid model, called DHKK-SQR, was proposed. The model

---

uses the positions of finger's links and joints computed with the Denavit-Hartenberg (DH) parameters associated with the quaternions representation to avoid singularities and to reduce the number of DH parameters.

The proposed kinematic and dynamic models were combined with experimental data to identify the actuation requirements of the robotic hand prosthesis. These specifications were used in a review of smart materials, which allows the identification of two potential candidates to design a smart material based actuator, i) the ionic polymer metal composites (IPMCs) and ii) the shape memory alloys (SMAs). The IPMCs has a huge potential due to their kinematic behavior, and the SMAs has a large actuation force.

Therefore, a new actuation system was proposed based on the theoretical and experimental evaluation of the robotic finger and its mechanism, and the smart material review. This actuation system comprises a servomotor and an active tendon driving system, which is composed of SMA wires in parallel with the elastic tendon.

The active tendon driving system allows controlling joint stiffness, so it is possible to adapt the behavior of the hand based on the grasping requirements and thus, address a solution to some of the main challenges in the domain of robotic hands flexibility and adaptability. The SMA based actuation system is issued of the proposed smart actuation design methodology; a model for SMA wires is introduced and identified experimentally. Moreover, the actuation system was tested and a second prototype of the Robotic hand ProMain-II is introduced.

# Contents

<b>Acknowledgments</b>	<b>i</b>
<b>Summary</b>	<b>iii</b>
<b>Introduction</b>	<b>1</b>
<b>1 Human hand movement analysis toward the hand prosthesis requirements</b>	<b>7</b>
1.1 Equivalent biomechanical model of human hand . . . . .	10
1.2 Human grasping . . . . .	14
1.3 Human force analysis . . . . .	16
1.3.1 Hand and forearm muscles . . . . .	16
1.3.2 Hill's Model of human muscle . . . . .	18
1.3.3 Characteristics issued from experimental analysis of the human hand . . . . .	22
1.4 Discussion . . . . .	25
<b>2 Design and modeling of the soft robotic hand ProMain-I</b>	<b>27</b>
2.1 Review of robotic hands . . . . .	27
2.2 Precision grasping hand set up . . . . .	32
2.3 Design of the soft robotic finger . . . . .	33
2.4 Robotic hand ProMain-I . . . . .	38
2.5 Kinematic model . . . . .	39
2.5.1 DHKK parameterization merged With Quaternions Formulation . . . . .	40
2.5.1.1 DHKK parameterization . . . . .	40
2.5.1.2 Formulation of Rotations Using Quaternions . . . . .	41
2.5.1.3 Hybrid Model DHKK-SRQ . . . . .	43
2.5.2 Modeling of the Robotic Hand Prosthesis Promain-I . . . . .	46
2.6 Dynamic model . . . . .	48
2.7 Discussion . . . . .	50
<b>3 Mechatronic assessment of the prosthetic hand</b>	<b>53</b>
3.1 General experimental set-up . . . . .	54
3.2 Validation of kinematic model DHKK-SRQ . . . . .	57

3.3	Robotic finger pinch force . . . . .	60
3.4	Kinematic and force of the ProMain-I finger . . . . .	61
3.5	Artificial muscle design methodology . . . . .	65
3.5.1	Particularized methodology for robotic fingers . . . . .	66
3.5.2	Characteristics issued from the human hand . . . . .	67
3.5.3	Characteristics issued from ProMain-I hand . . . . .	68
3.5.3.1	Required active strain . . . . .	68
3.5.3.2	Required actuator force . . . . .	69
3.6	Smart actuator characteristics . . . . .	70
3.7	Discussion . . . . .	72
<b>4</b>	<b>Development of an artificial muscle based on smart materials</b>	<b>73</b>
4.1	Smart materials review and comparison . . . . .	74
4.2	Modeling of a SMA–based actuator . . . . .	77
4.2.1	SMA–based actuator . . . . .	77
4.2.2	SMA constitutive model . . . . .	79
4.2.2.1	1D constitutive model of SMA . . . . .	84
4.2.3	Parametric identification of SMA based actuator . . . . .	86
4.3	Smart material based mechanism of Promain-II Hand . . . . .	93
4.4	Discussion . . . . .	97
<b>5</b>	<b>Conclusions</b>	<b>99</b>
<b>6</b>	<b>Perspectives</b>	<b>103</b>
	<b>Bibliography</b>	<b>122</b>

# List of Tables

1.1	Proposed categories used to cluster research studies . . . . .	8
1.2	Carpal bones acronyms . . . . .	11
1.3	Joint rotational limits of the hand articulations[48] . . . . .	13
1.4	Muscles involved in the flexion movement of finger’s articular joints . . . . .	17
1.5	Mean value of the human pinch force. . . . .	24
2.1	Physics characteristics: over-actuated hands . . . . .	29
2.2	Actuation characteristics: over-actuated hands . . . . .	29
2.3	Physics characteristics: fully-actuated hand . . . . .	30
2.4	Actuation characteristics: fully-actuated hand . . . . .	30
2.5	Physics characteristics: under-actuated hand . . . . .	31
2.6	Actuation characteristics: under-actuated hand . . . . .	32
2.7	Adopted notation for ProMain-I hand. . . . .	46
2.8	DHKK parameters for the ProMain-I Hand . . . . .	47
3.1	Mean absolute position error and fingertip force. . . . .	60
3.2	Mean pinch force (two-finger platform). . . . .	61
3.3	Comparison of ProMain-I hand requirements and actuator characteristics. . . . .	72
4.1	summary of requirements of artificial muscles for robotic hands. . . . .	74
4.2	Main characteristics of smart materials (B: Bending, E: Extension). . . . .	75
4.3	Stiffness and voltage excitation of smart materials. . . . .	76
4.4	ProMain-I hand actuation requirements . . . . .	77
4.5	Physical parameters description of Helmholtz $\Psi$ and Gibbs $G$ specific free energies . . . . .	80
4.6	General constitutive model equations and parameters . . . . .	84
4.7	1–D Constitutive model equations and parameters . . . . .	86
4.8	Sources and methods used to identify material parameters . . . . .	86
4.9	Measured Young’s modulus in martensite and austenite phases . . . . .	88
4.10	Initial parameter values for 1–D model simulation. . . . .	89
4.11	Optimized parameter values for 1–D model simulation. . . . .	90

4.12 Sources and methods used to identify parameters for governing equations (4.4) and (4.7). . . . .	91
4.13 Actuator parameters obtained using Matlab Ident toolbox. . . . .	92

# List of Figures

1.1	Time line of research around human grasping. . . . .	7
1.2	co-occurrence density view of the main research topics on grasping. . . . .	9
1.3	Human hand requirements identification work flow . . . . .	10
1.4	Human hand (a) Bones (b) Joints. . . . .	11
1.5	Equivalent mechanical joints. . . . .	12
1.6	Equivalent proposed biomechanical model. . . . .	13
1.7	Least used grasping gestures. . . . .	15
1.8	Most used grasping gestures. . . . .	15
1.9	Work flow proposed to identify hand requirements regarding force. . . . .	16
1.10	Intrinsic muscles involved in finger flexion-extension movements. . . . .	17
1.11	Extrinsic muscles involved in finger flexion-extension movements.. . . .	18
1.13	Model proposed by <b>Hatze</b> , image adapted from [86] . . . . .	19
1.14	Model proposed by <b>Winters</b> , image adapted from [87] . . . . .	19
1.15	Model proposed by <b>Tondu and Zagal</b> , image adapted from [88] . . . . .	19
1.16	Model proposed by <b>Winters</b> , image adapted from [87] . . . . .	19
1.17	Model proposed by <b>Zajac</b> , image adapted from [90] . . . . .	20
1.18	Model proposed by <b>Delp</b> , image adapted from [91] . . . . .	20
1.19	Model proposed by <b>Hayashibe et al.</b> , image adapted from [92] . . . . .	20
1.20	Model proposed by <b>Pang et al.</b> , image adapted from [93] . . . . .	20
1.21	Model proposed by <b>Millard et al.</b> , image adapted from [94] . . . . .	20
1.22	Retained Hill based model. . . . .	21
1.23	Damped example of movement simulation. . . . .	21
1.24	Non-damped example of movement simulation. . . . .	21
1.25	Experimental set-up to measure the human pinch force. . . . .	22
1.26	Steady state of the pinch force performed by the subject 2 during trial 3. . . . .	23
1.27	Absolute frequency of the pinch force performed by the subjects. . . . .	23
1.28	Measure of the settling time Pinch force versus time $t$ . . . . .	24
2.1	Review robotic hands . . . . .	28
2.2	Support chassis of the ProMain-I. . . . .	33
2.3	Early “alpha” prototype of the robotic finger. . . . .	34

2.4	Epicyclic mechanism. . . . .	35
2.5	Soft epicyclic mechanism. . . . .	35
2.6	Promain-I hand phalange description . . . . .	36
2.7	Promain Hand-I main components . . . . .	36
2.8	Parallel between soft epicyclic mechanism and the Hills-based muscle model. . . . .	38
2.9	ProMain-I Hand. . . . .	38
2.10	Graphical representation of DHKK parameters . . . . .	41
2.11	Rotation $\gamma$ applied $\vec{r}$ to around . . . . .	42
2.12	Rotation around the axes $x_i$ , $y_i$ , and $z_i$ . . . . .	43
2.13	Model of hybrid joint using DHKK and SRQ. . . . .	44
2.14	Grasp Conditions. . . . .	45
2.15	ProMain-I Hand with angles $\theta_{ji}$ and lengths $l_{ji}$ . . . . .	47
2.16	Kinematic model of the robotic finger with $S_{ji}, x_{ji}, y_{ji}, z_{ji}, \alpha_{ji}, \beta_{ji}, \theta_{ji}$ . . . . .	48
2.17	Dynamic model of the robotic finger. . . . .	49
3.1	Relationship between the experiments . . . . .	54
3.2	Automatic detection of finger joints an fingertip position . . . . .	55
3.3	Positions of the robotic finger articulations during flexion . . . . .	56
3.4	Angles and final position measure . . . . .	56
3.5	Interpretation of measured kinematic data. . . . .	56
3.6	Experiment Set-up . . . . .	57
3.7	CAD Model of the test platform . . . . .	58
3.8	Work flow of the kinematic method error estimation. . . . .	58
3.9	Results of the position tracking using the HS-422 servo motor. . . . .	59
3.10	CAD Model of the pinch force test platform. . . . .	60
3.11	ProMain-I finger test platform. . . . .	61
3.12	Results of the position tracking of ProMain-I finger. . . . .	62
3.13	Results of the position tracking of ProMain-I finger. . . . .	63
3.14	Probability density function of $\theta_{j2}$ absolute error. . . . .	63
3.15	Probability density function of $\theta_{j3}$ absolute error. . . . .	63
3.16	Calculated position of center masses $R_{ji} = (x'_{ji}, y'_{ji})$ . . . . .	64
3.17	Position of $R_{j2}$ with respect to the framework $(x_{j2}, y_{j2}, z_{j2})$ . . . . .	65
3.18	Measured fingertip force $F_j$ during contact. . . . .	65
3.19	Actuator displacements: (a) Extension-based (b) Bending-based. . . . .	68
3.20	Parameter quantification workflow. . . . .	69
3.21	Temperature vs strain for NiTi SMAs. . . . .	70
3.22	Schema of the SMA-based actuator. . . . .	71
3.23	Identified transfer function of the normalized strain (based on the strain of NiTi SMA wire in response to a current step input). . . . .	72

## LIST OF FIGURES

---

4.1	Schematic representation of the SMA-based actuator. . . . .	78
4.2	Schematic representation of the SMA-based actuator. . . . .	79
4.3	Experimental set-up to measure Young's Modulus . . . . .	87
4.4	Placement of SMA wire specimen . . . . .	87
4.5	Temperature vs strain for NiTi SMAs at constant stress $\sigma_{11} = 172\text{Mpa}$ . . . . .	88
4.6	Optimization results. . . . .	90
4.7	Experiment to identify and test the SMA-based actuator. . . . .	91
4.8	Angular position tracking of the actuator. . . . .	91
4.9	Simulink simulation of the complete proposed model. . . . .	92
4.10	Simulation an experimental result of the SMA actuator. . . . .	93
4.11	Promain Hand-II . . . . .	94
4.12	Schematic representation of the ProMain Hand-II's soft epicyclic tendon-driven actuation system based on SMA . . . . .	94
4.13	Promain Hand-II . . . . .	95
4.14	Promain Hand-II . . . . .	95
4.15	Parallel disposition of the flexible tendon and the SMA wire in the MCP joint . . . . .	96
4.16	ProMain-II finger prototype . . . . .	96
4.17	ProMain-II finger flexion cycle . . . . .	97



# Introduction

The human dexterous manipulation has long been a question of keen interest in a wide range of fields e.g. medicine, biomechanics, and robotics. In the area of robotics, the study of dexterous manipulators has led to the development of devices aiming at the automation of industrial processes. Principally, robotic manipulator and grippers have been introduced in the last two decades seeking to: i) replace human intervention in dangerous environments or ii) speed up and improve accuracy in productive processes. However, recent progress in the field of dexterous robotic manipulation has led to a renewed interest in the development of robotic devices for rehabilitation or improvement of human skills.

Studies over the past two decades have provided valuable information on the considerations for robotic hands development. Two main research axes can be clearly defined around the development of robotic hands: i) the control and operation ii) the mechanic and actuation. The first axis concerns the development of control and automation strategies to improve robots' performance, and the design of facilities to operate robotic devices. The second axis concerns the analysis, improvement, and design of mechanisms and actuation technologies, and the study of materials. In all cases, the target is the enhancement of dexterous manipulation skills of robotic hands.

The utilization of smart and soft materials has led to the development of new adaptive devices known as soft robots [5], which due to their adaptability and compliance are useful for physical rehabilitation and improvement of human skills. The main idea of soft robotics is to equip robots with new bio-inspired capabilities, allowing adaptive and flexible interactions with unknown or incomplete information about the operation environments. The dexterous manipulation in robotic hand prostheses can be considered as a problem with incomplete information because the task (grasping of objects) is clearly defined, but the operation conditions (object's shape, size, and weight) are unknown.

The current commercial robotic hand prostheses [6–9] are rigid and not compliant, and follow an approach that attempts to completely mimic the human hand, neglecting its functionality which is the primary target in the rehabilitation of amputated patients. Consequently, the development of new adaptable devices using a bio-inspired approach, taking into account not only the mechanics of the hand but also the functionality, is crucial for the progress of robotic hand prostheses. Thus, the soft robotic constitute a fascinating approach for developing robotic hand prostheses.

---

The main advantage offered by soft robotic in the dexterous manipulation is the adaptation capacity, which allows the robotic hand to be used in several uncertain grasping situations. However, it implies to address several challenges. The first challenge concerns the design of a robotic mechanism, which is sufficiently flexible to grasp objects with different shapes and sizes, and is rigid enough to perform prehension task in a steady way. The second challenge concerns the development of soft muscle-like actuation technologies, which are still one of the major challenges in the creation of soft-bodied robots that can move, deform their body, and modulate body stiffness[10].

The central topic of this thesis dissertation is the development of a soft actuation strategy using smart materials for a soft robotic hand prosthesis. Our approach takes into account the different matters of interest that can influence the development of an actuation strategy or an artificial muscle. Thus, we focus our study in: i) The mechanics and functionality of the human hand to identify human prehension requirements. ii) The analysis and improvement of the robotic hand mechanism to endow the prosthesis with a soft behavior iii) The experimental assessment of the robotic hand prostheses to identify actuation requirements regarding the kinematic and dynamics of the robot. iv) The development and modeling of an actuation strategy using smart materials. These topics are addressed in four chapters as follows:

1. Human hand movement analysis toward the hand prosthesis requirements.
2. Design and modeling of the soft robotic hand ProMain-I.
3. Mechatronic assessment of the prosthetic hand.
4. Development of an artificial muscle based on smart materials.

Chapter one begins by laying out the theoretical dimensions of the research regarding the prehension of humans, and looks at how it influences the development of different research areas as medicine, biomechanics, and robotics among others. An evolution and a state of art about human grasping are introduced, the investigation outlines the connection between the research subjects to identify their impact on the development of robotic hand prosthesis. As a result, we address our approach to assessing the human hand and its functionality toward the identification of grasping requirements.

Subsequently, we carry out an analysis of the human hand, identifying the most critical elements and functionalities from a biomechanical point of view. The proposed biomechanical model takes into account the equivalent mechanical model of the human hand joints and bones. Furthermore, we introduce the kinematic operational limits of the hand joints. This model is the basis for the further design of the soft robotic hand prosthesis ProMain-I.

Afterward, we analyze the information reported in state of the art regarding the daily living and working necessities concerning grasping. This analysis allows us to select the seven most used prehension gestures. This group of movements is used to bound the motion requirements of our robotic prosthesis. Moreover, we perform a study of the human muscles and an experimental

---

evaluation of the human pinch force. The human muscle is analyzed using: i) a modified Hill-based model that allows the description of muscle behavior, and ii) an experimental evaluation allows us to identify requirements of pinch force and time response that must be taken into account for the design of the robotic hand prosthesis.

The second chapter is concerned with the design of the soft robotic hand prosthesis ProMain-I. First, we introduce a review of the current hand prosthesis in the literature, analyzing mechanical and functional features as the grasping force capacity, the working space, the degrees of freedom, the weight, the size, the number of fingers, the actuators, and the driving mechanisms. The hands are categorized into under-actuated, fully-actuated or hyper-actuated, according to the degrees of freedom and the number of actuators.

Then, we introduce the design process of the soft robotic hand. The bio-inspired soft robotic hand prosthesis ProMain-I<sup>1</sup>, has been developed, tested and manufactured entirely in the LEME laboratory. It has three fingers disposed to perform precision grasping. Each finger has three joints: Metacarpophalangeal (MCP), Proximal interphalangeal (PIP) and distal interphalangeal (DIP). The design process is addressed in three parts:

1. The Precision grasping hand set-up: In this part, we introduce a support chassis that host the fingers in such a way that they are correctly placed for grasping, guaranteeing that the thumb is abducted facing index and middle fingers; and the index and middle fingers have the right abduction angle to perform precision grasping.
2. The design of the soft robotic finger and the soft epicyclic mechanism: the finger is under-actuated, so that the rotation angle of the PIP and DIP joints are linked with the rotation angle of the MCP joint. The driving mechanism is inspired by the epicyclic gear train but instead of gears we introduce a tendon based mechanical transmission that incorporates a flexible behavior to finger joints.
3. The complete assembly of the soft robotic hand prosthesis ProMain-I: Here the complete prototype of the soft robotic hand is introduced and the mechanical angular relations of the soft epicyclic driving mechanism are presented.

Due to the tendons introduced in the soft epicyclic mechanism, the designed robotic hand ProMain-I has a flexible behavior in the joints. These soft responses boost new movements that cannot be predicted by classical robotic models. The modeling of those unpredicted motions requires new considerations regarding kinematic modeling. Consequently, we introduce a new hybrid model that improves the representation of rotations that arise from soft robotics prosthesis movements. Our model merges the parameterization of Denavit-Hartenberg (DH) method with quaternions to formulate soft rotations. This new method allows to: improve the computation of rotations in the neighborhood of rotational singularities, reduce the number of rotation parameters, and unify the formulation to describe the kinematic of a soft robot. Likewise, a dynamic model based on the principle of virtual displacements and virtual work [1] is

---

<sup>1</sup>Patent Number: FR1656914[4]

---

introduced. Both dynamic and kinematic models are applied to the soft robotic hand prosthesis ProMain-I.

The third chapter is concerned with the methodology used to design artificial muscles using smart materials. The method takes into account the human hand capabilities to establish the range and operation limits of the actuator considering the influence of mechanical and functional characteristics of the robotic hand. The method is applied to our robotic hand but can be readily extrapolated to any robotic hand. The experimental data is analyzed using the proposed kinematic and dynamic models, and we present several experiments aiming to: i) validate the DHKK-SRQ model, ii) evaluate mechanical features of the robot, and iii) extract actuation requirements.

The experiment carried out with the ProMain finger aims to measure kinematic and force. The information obtained experimentally is used to feed the kinematic and the dynamic models to define actuation requirements. Furthermore, we compare the expected rotation relations fixed in the soft epicyclic mechanism and the measured ones to verify the behavior of the finger. In the last part of the chapter, we propose a general methodology which aims at designing smart material based actuators for grasping application defining the main features of an smart material based actuator (force  $f_a$ , active strain  $\varepsilon$  and frequency  $\omega_n$ ). This methodology is based on the following four stages:

1. Application requirements modeling: in this phase the main parameters and their relationships are modeled, allowing to establish the operating conditions of the actuators.
2. Experimental parameters identification: once the key parameters and their relationships have been modeled, it is necessary to carry out an experiment. The experimental protocol is designed in agreement with proposed models, to measure the required parameters.
3. Parameters quantification: Experimental data is analyzed using the defined models to characterize the artificial muscle and quantify operational limits of the actuator.
4. Material selection: the retrieved information is used to approximate the actuator dynamic behavior, allowing the selection of a smart material that fits the application requirements.

The fourth and last chapter presents the final development of the smart material based artificial muscle. First, we perform a review of state of art to examine and compare the smart materials following key actuation features that are formulated regarding actuation requirements. The study is centered on the smart materials that, due to their characteristics, are suitable for grasping applications.

Moreover, a general constitutive model that uses thermo-mechanical formulation to describe SMAs behavior is presented. The constitutive model of the SMAs is identified and validated through an experimental approach as follows:

1. Identify the Young's modulus of SMA in martensite and austenite phases: this identification is performed using a test machine in which Seven specimens of an SMA wires are

tested under uniaxial tension. first the wires are tested with thermal stimulus to measure the Young's modulus in full austenite phase and then the thermal stimulus is removed to measure the Young's modulus in full martensite phase.

2. Identify thermal SMA characteristics: the transformation temperatures  $M_s$ ,  $M_f$ ,  $A_s$ ,  $A_f$  and the reference entropy difference  $\Delta s_0$  are identified by an optimization algorithm in which we seek to fit our model result with the temperature vs strain response of the SMA wire.
3. Kinematic evaluation of an SMA rotary actuator: a experiment to identify the parameters of the complete model of the actuator is proposed.

Finally, we introduce the simulation, and the experimental evaluation of a rotary SMA based actuator, which is suitable to fulfill human grasping requirements. Based on this analysis the shape memory alloys (SMA) are chosen to improve the ProMain-I hand mechanism adding the possibility of control the stiffness of the soft epicyclic mechanism.



# Chapter 1

## Human hand movement analysis toward the hand prosthesis requirements

The human hand is one of the most adaptable and complex mechanisms and has a significant role in the way individuals interact with their environment. Notably, the hand is the default tool in daily living activities, allowing persons to feel and handle objects. Several fields of knowledge (as medicine, anatomy, biomechanics and robotics among many others) are deeply concerned by the understanding of anatomy, mechanics, and functionality of the human hand. Studies over the past years have provided valuable information on different approaches to model, understand, and mimic the human hand [11–17].

These studies, carried out by researchers of different fields, have as common subject the grasping, which is the final goal of the human hand. Figure 1.1 summarizes the evolution of the research around grasping in the last century in the different science fields and also the most relevant studies in a time line.

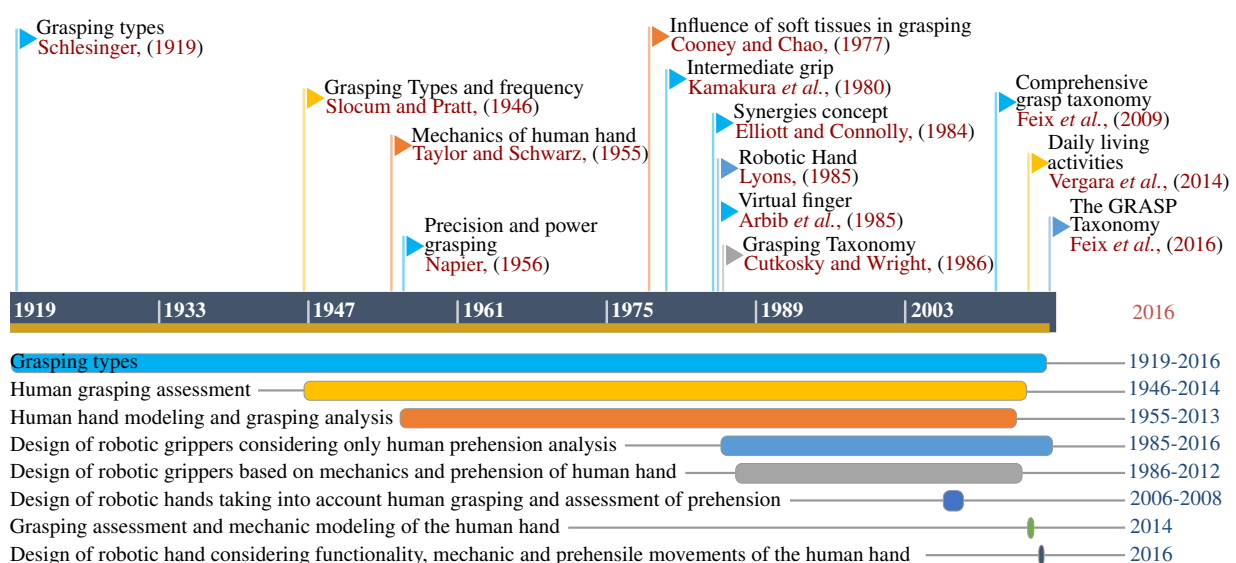


Figure 1.1: Time line of research around human grasping.

## 1. Human hand movement analysis toward the hand prosthesis requirements

The research about grasping has addressed mainly two problems: the analysis of the human hand for medical and rehabilitation purposes and the development of devices or robots able to mimic human hand capabilities. Regarding the research about medical and rehabilitation purposes, the main research lines are: i) Human grasping assessment, ii) Human hand modeling and grasping analysis, and iii) Grasping evaluation and mechanic modeling of the human hand.

On the other hand, the primary research milestones, on engineering science and robots, are: i) Design of robotic grasping systems based on human prehension analysis and considering mechanics of human hand, ii) Design of robotic hands taking into account human grasping and assessment of prehension movements, and iii) Design of robotic hands considering functionality, mechanics and prehensile movements of the human hand.

There is a growing body of recent literature which recognizes that people only employ a limited quantity of hand gestures in daily living activities, adapting hand movements to perform several tasks. Therefore, the analysis of requirements for the development of prosthesis must be enhanced to consider the functionality of the human hand. Consequently, the new central challenge, facing the development of artificial hands to be used as a prosthesis, is synergistically merging anatomy mechanics and functionality considerations in the design process.

Concerning the combination of mechanics and functionality considerations in the robotic hand design process, we carried out a study of state of the art, in which the links of grasping research topics reported in scientific papers [11–78] are analyzed and clustered into four categories as follows: i) study of human prehension, ii) biomechanics, iii) human hand assessment, and iv) development of robotic devices. Each category is composed by several topics that are summarized in Table 1.1. The analysis attempts to identify the connection between the topics of the four categories to determine how the research about the human hand have influenced the development of robotic grasping devices and more specifically the robotic hand prosthesis.

<b>Study of human prehension</b>	<b>Biomechanics</b>	<b>human hand assessment</b>	<b>Development of robotic devices</b>
Synergies	Hand Anatomy	Daily living activities	Prosthetic devices
Taxonomy	Mechanic analysis	Dexterity	Design considerations
Grasp Types	Force analysis	Disability evaluation	Robotic hands
Grasping assessment	Soft tissues	External influences	Control and sensors
Objects' influence		Frequency of grasping	

Table 1.1: Proposed categories used to cluster research studies

The results of the analysis are summarized in figure 1.2, in which the co-occurrence, the total strength of all links, and the number of carried out studies are reported following the bibliographic mapping method proposed by Van Eck and Waltman, [79]. The distance between

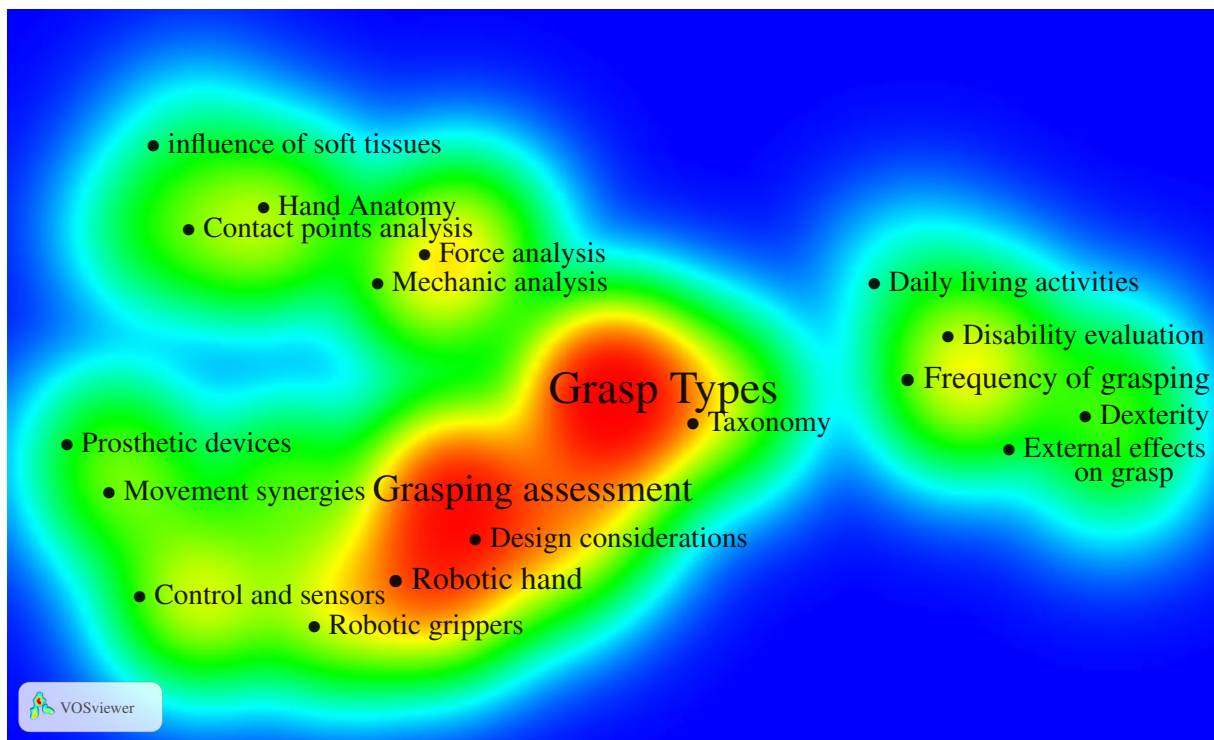


Figure 1.2: co-occurrence density view of the main research topics on grasping.

items illustrates co-occurrence, smaller the distance, larger the number of co-occurrences. The font size depends on the total strength of all links between the item and the other topics. The gradient of color between red and blue indicates the number of items in the neighborhood of a point, red for high densities and blue for small concentrations.

Undoubtedly, the research about robotic hands and grippers (red and yellow zones in the lower part of figure 1.2) has been significantly influenced by the study of human grasping (red zones in center of figure 1.2). This connection is reasonable considering the advantages of the human hand. Consequently, the combination of knowledge around grasping has led to the development of: i) Robots for manipulation of objects, say robotic hands and grippers, considering the human prehension assessment, and the classification of the human movements and ii) Prosthetic devices designed to take into account the human grasping gestures, and more recently movement and postural synergies, which expresses the coordinated action of the perception and the motor systems with the environment that enable a functional grasping.

On the other hand, recently studies have focused their interest in the evaluation of daily living activities and their influence of grasping, as is shown in the right-hand side of figure 1.2. However, a necessary connection between grasping, hand functionality and mechanics has not been thoroughly established. This link would be valuable in the development of new mechanism and actuators for prosthetic devices, which up to now are rigid and not compliant [6–9]. Nevertheless, it implies to undertake two main challenges: 1. the first concerns design a robot mechanism sufficiently flexible to grasp objects with different shapes and sizes, and rigid enough to perform prehension task in a steady way, and 2. the second, which is still one of

## 1. Human hand movement analysis toward the hand prosthesis requirements

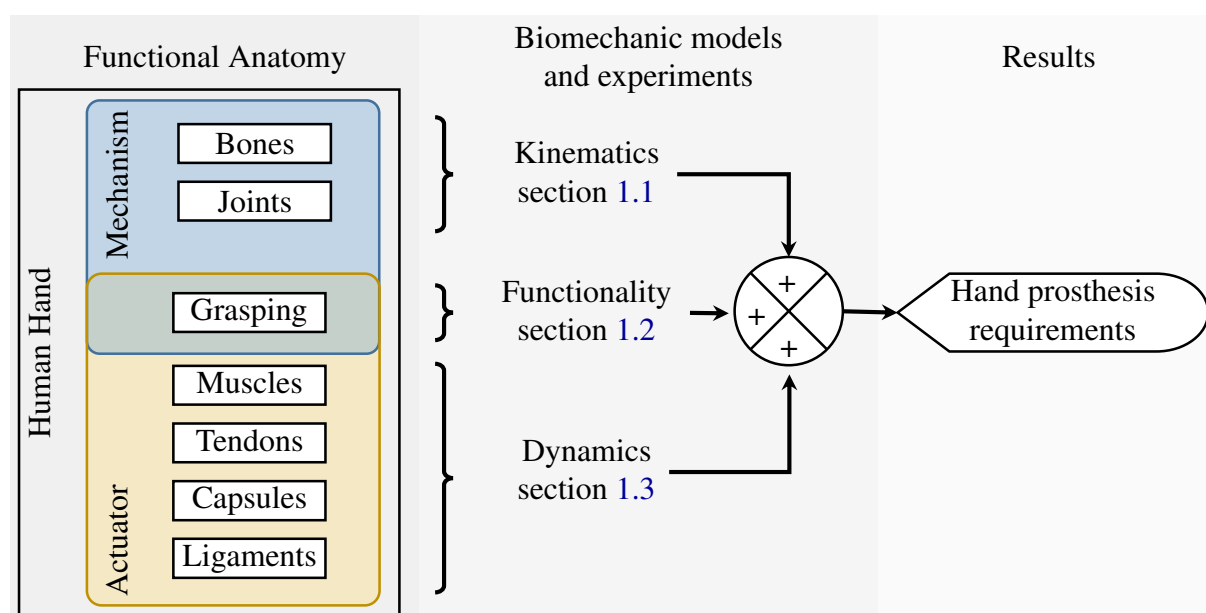


Figure 1.3: Human hand requirements identification work flow

the major challenges, concerns the development of soft muscle-like actuation technologies[10]. Consequently, our targets are set to develop new mechanism and actuators for prosthetic devices, and are addressed in a first stage through the study of the hand anatomy and functionality considering three main elements: i) the equivalent biomechanical model of the human hand, ii) the grasping, and iii) the actuation model.

These three aspects grant a better understanding and identification of the real artificial muscle requirements for prosthetic hands, and are introduced in the following sections as follows: i) section 1.1 Equivalent biomechanical model of human hand: introduces a biomechanical model of the human hand that is used to identify kinematic requirements ii) section 1.2 Human grasping: presents an analysis of grasping to evaluate the functional requirements in terms of prehension movements iii) section 1.3 Human force analysis: addresses the a Hill-based muscle model used to define human muscle behavior and an experiment to identify human pinch force requirements. Figure 1.3 shows the requirements identification work flow that is followed in this chapter.

### 1.1 Equivalent biomechanical model of human hand

From a functional point of view, the hand is composed of muscles, tendons, and bones; and is divided into three main parts, wrist, palm, and fingers. The muscles can be assimilated to actuators, the bones are the mechanical structure understood as rigid mechanism linked by soft or flexible rotational joints, and the tendons are the driving mechanism linking bones with muscles.

Regarding the structural part of the hand, the wrist is composed of the carpal bones, divided

Region	Group	Bone	Acronym				
Wrist	Distal Carpals	Trapezium	TZ				
		Trapezoid	TD				
		Capitate	C				
		Hamate	H				
	Proximal Carpals	Pisiform	P				
		Triangular	T				
		Lunate	L				
		Schaphoid	S				
Palm	Metacarpus	Metacarpal series	M-I	M-II	M-III	M-IV	M-V
Finger	Phalanges	Proximal series	PP-I	PP-II	PP-III	PP-IV	PP-V
		Middle series	-	MP-II	MP-III	MP-IV	MP-V
		Distal series	DP-I	DP-II	DP-III	DP-IV	DP-V
	Number	-	I	II	III	IV	V
	Name	-	Thumb	Index	Middle	Ring	Pinky

Table 1.2: Carpal bones acronyms

into proximal and distal carpal bones [13, 44, 48]. The palm is constituted of metacarpal bones, and the fingers consist of proximal, middle and distal series of phalanges. The only finger that does not have middle phalanx is the thumb finger. Table 1.2 summarizes the bones and its acronyms used henceforth. Furthermore, figure 1.4a shows the hand bones.

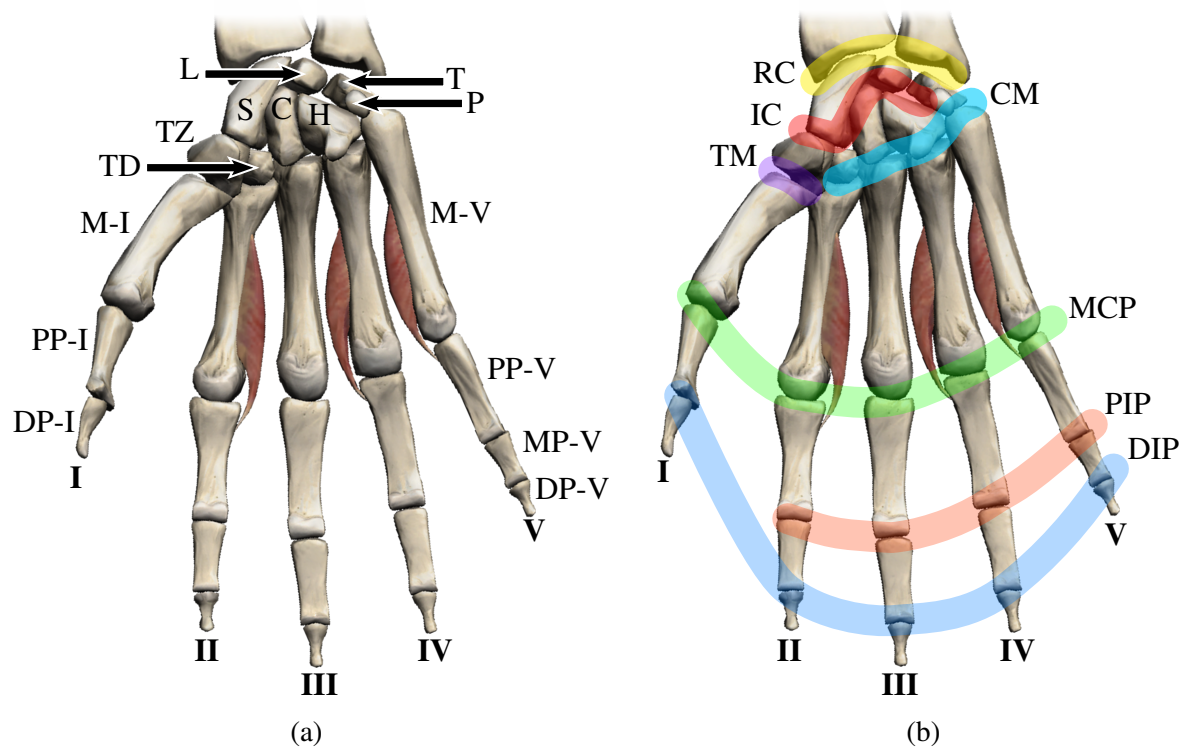


Figure 1.4: Human hand (a) Bones (b) Joints.

## 1. Human hand movement analysis toward the hand prosthesis requirements

Moreover, the hand articulated joints are: 1. radiocarpal (RC) between radius-humerus and proximal carpal bones, 2. intercarpal (IC) between proximal and distal carpal bones, 3. Carpometacarpal (CM) between distal carpals and metacarpal bones, 4. Trapezometacarpal (TM) between trapezoid and thumb's metacarpal, 5. Metacarpophalangeal (MCP) between distal carpals and metacarpal series of fingers II to V, 6. Proximal interphalangeal (PIP) between proximal and medial series of phalanges of digits II to V, and 7. Distal interphalangeal (DIP) between the middle and distal set of phalanges of digits II to V, and between proximal and distal phalanges of thumbs. Figure 1.4b shows each group of articulations.

The wrist is a complex articulation composed of two kinds of joints (radiocarpal and intercarpal) that allow the hand, considered as a final effector, to reach an optimal prehension gesture. This articulation is modeled as a kinematic joint with two degrees of freedom (DoF) allowing the hand to perform flexion-extension and abduction-adduction movements [48]. Frequently, the wrist is considered to have a third DoF corresponding to prono-supination, this DoF is not taken into account for the present analysis because it is part of the elbow joint.

Carpometacarpal (CM) joints have a significant role enhancing the workspace of the fingers [80]. Nevertheless, the (CM) joints are more meaningful, from a functional perspective, to allow effective finger motion. Thus, the effect of the CM joints is embedded in the fingers capacity of motion. Concerning Trapezometacarpal (TM) articulation, it plays a meaningful role in the thumbs opposition. The joint has two DoF coupled with a rotation of the thumb's metacarpal bone. As a consequence, it can be modeled as a 2-DoF kinematic joint with a dependent rotation. Metacarpophalangeal (MCP) joints have two DoF allowing the flexion-extension and abduction-adduction finger movements. Likewise, the proximal and distal interphalangeal joints have one DoF, providing flexion-extension movements. Figure 1.5 shows the equivalent mechanical joints for the hand.

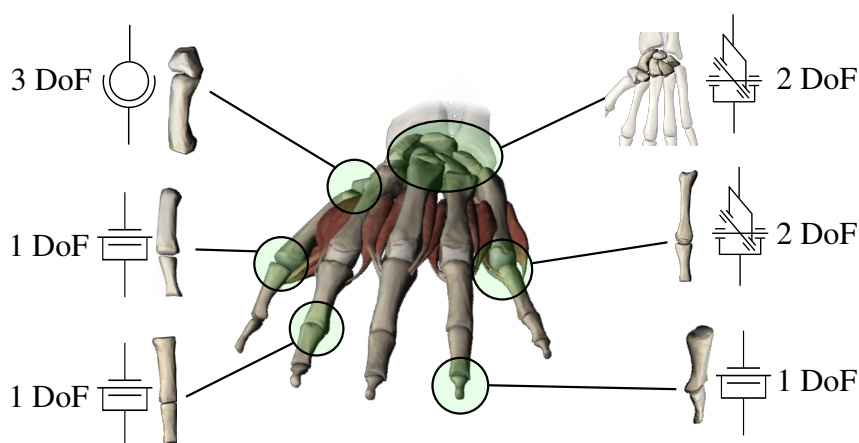


Figure 1.5: Equivalent mechanical joints.

Besides, it is necessary to define the joint ranges or movement amplitude. These values, are determined with respect to a reference position, which in the case of the wrist is the axis formed by the third metacarpal aligned with the forearm. Likewise, the reference position

Joint	Finger	1st DoF		2nd DoF		3rd DoF
		flexion [°]	extension [°]	abduction [°]	adduction [°]	Rotation [°]
Wrist	-	85	85	15	45	-
MCP	I	60-90	0	-	-	-
	II	100	30	30	30	-
	III	90	30	30	30	-
	IV	80	30	30	30	-
	V	70	30	30	30	-
PIP	I	80	10	-	-	-
	II-V	90	0	-	-	-
DIP	II-V	90	5	-	-	-
TM	I	60	0	0	60	120

Table 1.3: Joint rotational limits of the hand articulations[48]

to measure the metacarpophalangeal and interphalangeal motion amplitude is the axis formed when the finger is brought into line with metacarpal bone. Furthermore, the thumb opposition is measured around an axis parallel to the wrist reference axis and laying the trapezometacarpal joint. Table 1.3 summarizes the joint rotational limits of the hand articulations.

As a result, a biomechanic model of the human hand is proposed. The model takes into account the wrist and the finger joints bounded by the angular limits established in table 1.3. Moreover, the model uses three kinds of simplified angular joints, hinge saddle, and spherical. Figure 1.6 shows the equivalent proposed biomechanical model.

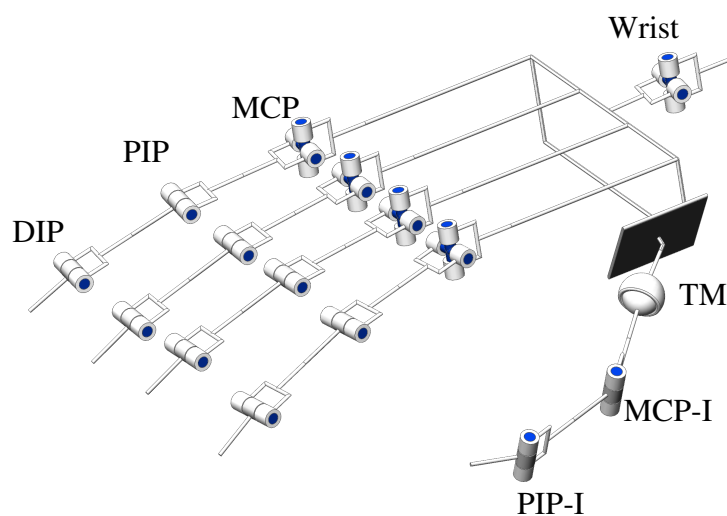


Figure 1.6: Equivalent proposed biomechanical model.

## **1.2 Human grasping**

The prehension or grasping is the capacity to grip an object with precision in a steady way. One of the first definitions [12], states that the grasping is the combined action of the fingers against the opposed thumb and the palm of the hand. From then on, several concepts have been added, for example, the prehensile functions of precision and power grasping [14], or the idea of handling instead of grasping objects [44].

Moreover, the advent of robots introduces a new challenge concerning the analysis of grasping. As a result, concepts as intermediate grasping are introduced [19]. From that, several approaches have been tested and grasping taxonomies are added, *e.g.* the classification of grasping based on security and dexterity of prehension [21, 64]. The newest taxonomy [17], developed taking into account the most relevant researches in the field of grasping, include 33 grasping gestures and suggest a grasping taxonomy divided into three categories: precision, force, and intermediate grasping.

The different grasping taxonomies, introduced up to now [11, 14, 15, 17, 19, 42, 48, 64], are based on the analysis of people movements during the prehension of objects. Admittedly, all prehension gestures have been classified into two broad categories: power and precision grasping. During power grasping, the object may be held in a clamp formed by the partly flexed fingers and the palm, counter pressure being applied by the thumb lying more or less in the plane of the palm. During precision grasping, the object may be pinched between the flexor aspects of the fingers and the opposing thumb. The hand gestures that do not match the power or precision categories are classified in a middle category so-called intermediate grasping.

On the other hand, There is a growing body of literature that recognizes the adaptability of the human hand as a key point in the analysis of grasping. The concept of adaptability implies that people do not use all the possible movements during grasping or handling of objects, instead, they adopt a simple gesture to perform several tasks. Following the approach of hand motion adaptability, two notions are introduced, the analysis of employment frequency of grasping gestures and the movement synergies, which expresses the coordinated action of the perception and the motor systems with the environment that enable a functional grasping. The purpose of movement synergies [20], is the analysis of finger coordination during motion attempting to identify common movement patterns. This concept of synergies has evolved [31] introducing the postural synergies to illustrate the hand action.

Correspondingly, the analysis of employment frequency of grasping gestures has been recently proposed by [17, 60, 61, 69–73, 81] and attempts to identify the most used hand gestures in daily work activities of people who have different professions. These research works have shown that in the literature several efforts have been carried out to study grasping movements that are rarely used by human and consequently are not needed in prosthetic devices, figure 1.7 shows the less used prehension gestures. Even more significantly, Feix *et al.*, [17] have shown the most used grasping gestures, which consequently must be acknowledged in the design of a hand prosthesis, figure 1.8 shows the most used prehension gestures.

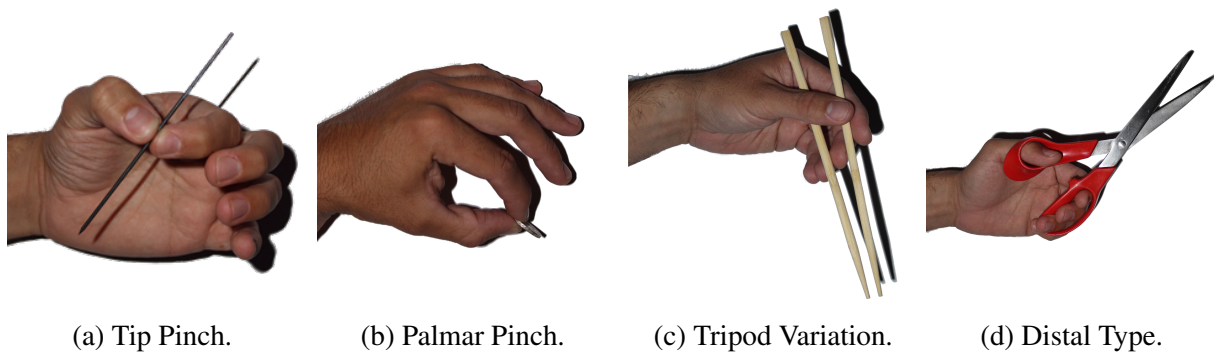


Figure 1.7: Least used grasping gestures.

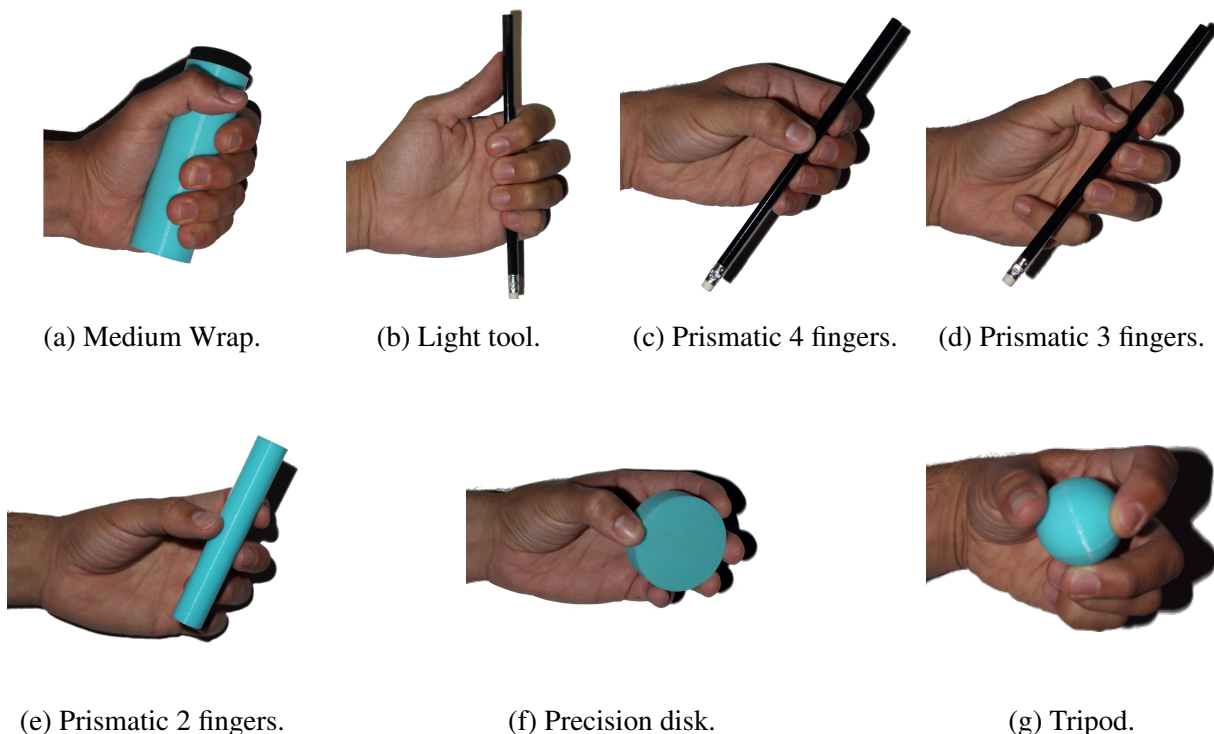


Figure 1.8: Most used grasping gestures.

The following statements can be identified based on analysis of the utilization frequency of objects: i) the most current object shapes are cylinders, discs, and spheres, ii) regarding hand movements, the thumb is abducted in six of the seven movements, and Furthermore, the performed movements illustrated in figures 1.8a and 1.8c to 1.8g are performed using from two to four fingers opposed to the thumb. However, all of them are feasible using two fingers opposed to the thumb. All things considered, our robotic hand prosthesis is designed to perform precision grasping taking into account the following characteristics proposed considering the most used prehension gestures: i) hand opening of 10cm during grasping and ii) index and middle fingers must have a minimum abduction angle set to  $15^\circ$  [48]. The force considerations are introduced in the following chapter.

### 1.3 Human force analysis

The joint capsules, ligaments, tendons, and muscles are crucial for the function of the human hand. However, these structures are extremely complex and vary between individuals[80]. As far as we know, it does not exist any standard method allowing to measure tendon and muscle forces in real time [82]. Consequently, our approach to extract hand requirements regarding force consists of two main phases: i) introduce a model based on equivalent biomechanic elements, to qualify the dynamic behavior of muscles and tendons during prehension movements and ii) outline the principal muscles involved in the precision grasping, to establish the applied force while the most used prehension gestures are performed. Figure 1.9 sketch the work flow proposed to identify hand requirements regarding force.

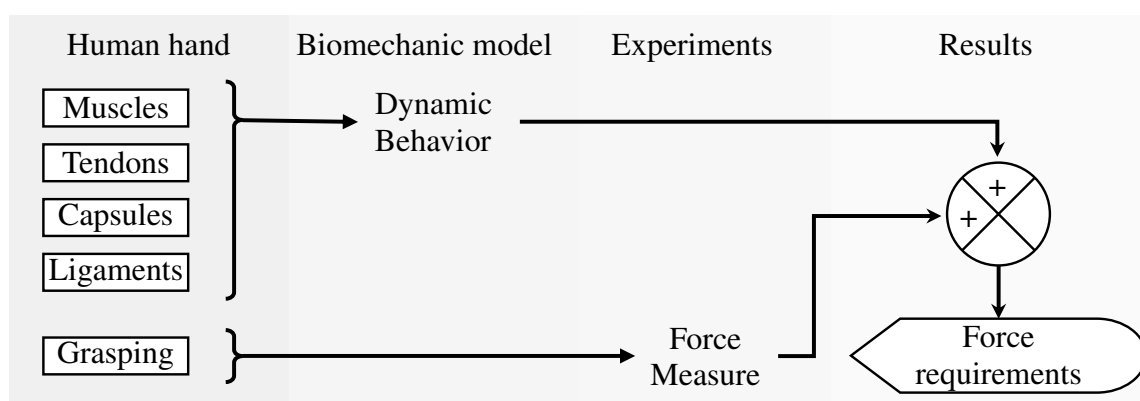


Figure 1.9: Work flow proposed to identify hand requirements regarding force.

#### 1.3.1 Hand and forearm muscles

The muscles involved in the hand movement are divided into extrinsic and intrinsic [48]. The extrinsic muscles arise outside of the hand, in the forearm, but act on the considered hand structure through the tendons that link the muscles with the fingers or the actuated bone. The intrinsic muscles are fully contained in the hand structure. Furthermore, the muscles can perform three types of actions: flexion-extension, adduction-abduction, and supination-pronation.

As presented before in section 1.2, most of the daily working activities are performed using precision grasping gestures with three fingers (thumb, index, and middle). During precision grasping, fingers are bent from a fixed starting position until contact with objects to grasp. Once the fingers get in touch with an object, the sensory system provides necessary information to the subject to apply the required force to hold the object in a steady way.

The muscles involved in adduction-abduction and supination-pronation play an important role preparing the hand for grasping. However, the act of grasping is done mainly flexing the finger to reach the object. Thus, we focus our study on muscles involved in finger flexion-extension movements, which are the most active during the last phase of grasping. The hand and the wrist articulations are actuated by a total of 31 muscles, 10 of them involved in fingers

Placement	Finger	Muscle	Acronym	Flexion of:		
				MCP	PIP	DIP
Intrinsic	I	Flexor Pollicis Brevis	FPB	x		
	II	First Dorsal Interosseous	FDI	x		
		First Palmar Interosseous	FPI	x		
		Index lumbrical	IL	x		
	III	Second Dorsal Interosseous	SDI	x		
		Third Dorsal Interosseous	TDI	x		
		Middle lumbrical	ML	x		
Extrinsic	I	Flexor Pollicis Longus	FPL	x	x	
	II-III	Flexor Digitorum Profundus	FDP	x	x	x
	II-III	Flexor Digitorum Superficialis	FDS	x	x	

Table 1.4: Muscles involved in the flexion movement of finger's articular joints

flexion movement, seven are intrinsic (see figure 1.10), and three are extrinsic (see figure 1.11). The list of muscles involved in the flexion movement of finger's articular joints is presented in table 1.4.

Furthermore, the maximal force produced by a muscle can be defined as the product between the maximal muscular stress constants  $\sigma_{max}$  and the physiological cross-sectional area  $A_{PCSA}$ , which is the area of the cross section of a muscle perpendicular to its fibers, generally at its largest point [83]. Consequently, in our study, we only consider the extrinsic muscles involved in flexion, which produce higher forces.

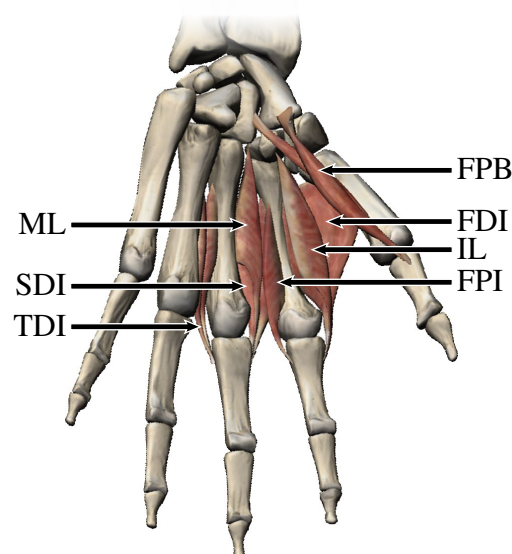


Figure 1.10: Intrinsic muscles involved in finger flexion-extension movements.

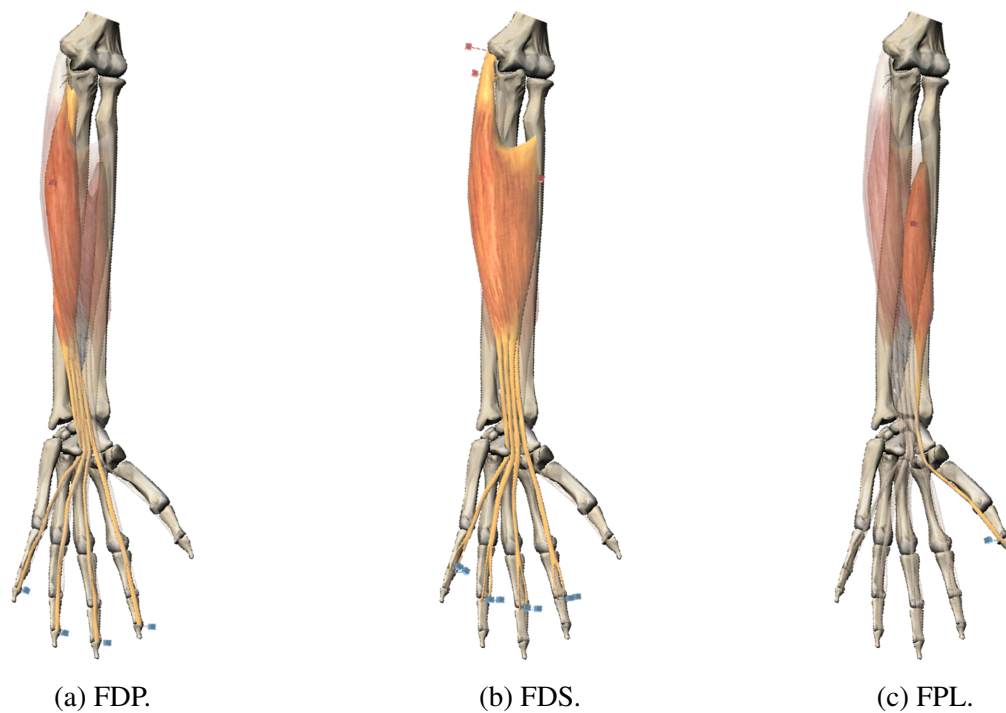


Figure 1.11: Extrinsic muscles involved in finger flexion-extension movements..

### 1.3.2 Hill's Model of human muscle

The modeling approach has been mainly addressed using two methods, the Hill's equivalent model [84], and the finite element analysis [85]. The FEM method has shown to be a performant tool to accurately describe muscles actions, however, the Hill's equivalent models are more suitable to qualify the muscle's behavior through the comparison with mechanical elements. Classical Hill's model was established by Hill, [84], see figure 1.12, it consists of an arrangement of elastic elements that are used as descriptors of the muscle's elastic behavior. Based on Hill's model several authors have appended modifications, *e.g.* Hatze, [86] and Winters, [87] introduced passive damped elements, see figures 1.13 and 1.14. More recently, Tondu and Zagal, [88] suggested an internal non-linear viscous force component, and Perumal *et al.*, [89], not only considered damping, but also a serial motor, see figure 1.16.

The Hill's based models are primarily composed of a representation of the muscle in series with a representation of the tendon. The muscle is depicted as a contractile element in parallel with an elastic element. The tendon is considered as visco-elastic elements; as a result, the tendon is modeled as a damper in parallel to a spring. Furthermore, an important consideration was proposed by Zajac, [90] who determined that the force applied by the muscle is influenced by an angle  $\alpha$ , see figure 1.17. The Zajac's model was complemented by several authors such as Delp, [91], Hayashibe *et al.*, [92], Pang *et al.*, [93], and Millard *et al.*, [94] (see figures 1.18 to 1.21). Muscle-tendon model evolution is listed in the following, sort by the nature of scientific approach, presenting briefly the elements considered and their schematic representation.

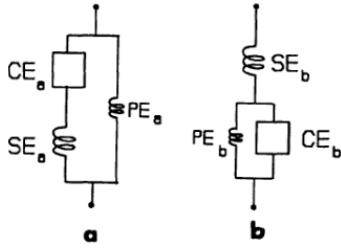
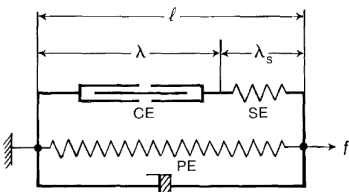
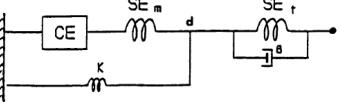
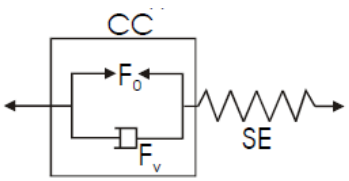
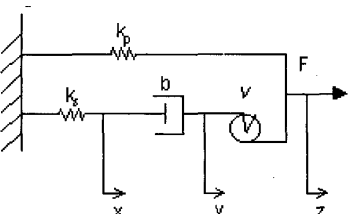
Author (Year)	Elements	Muscle-tendon actuator models
Hill, (1950)	Contractile element (CE), series element (SE), parallel element (PE)	
Hatze, (1977)	Combined muscle-tendon models with active and controllable contractile element (CE), the passive damped series elastic element (SE), the passive, damped parallel elastic element (PE)	
Winters, (1990)	Simple model structure with a "lumped" (SE) viscoelastic element, contractile element (CE) and a passive spring (k).	
Tondu and Zagal, (2006)	Series of elastic element (SE) and a contractile element (CC), which is composed of an internal contractile force $F_0$ and an internal non-linear viscous component $F_V$ .	
Perumal <i>et al.</i> , (2002)	The force generation is modeled by a linear spring ( $K_p$ and $K_s$ ), a damper (b), and a motor in series (V).	

Figure 1.12: Classical Hill's Model [87]

Figure 1.13: Model proposed by Hatze, image adapted from [86]

Figure 1.14: Model proposed by Winters, image adapted from [87]

Figure 1.15: Model proposed by Tondu and Zagal, image adapted from [88]

Figure 1.16: Model proposed by Winters, image adapted from [87]

# 1. Human hand movement analysis toward the hand prosthesis requirements

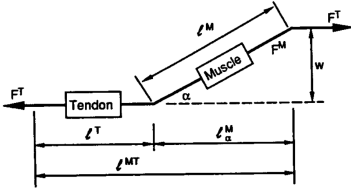
Author (Year)	Elements	Muscle-tendon actuator models
Zajac, (1989)	Relation among muscle fiber length $l^M$ and force $F^M$ tendon length $L_T$ and force $F^T$ , and musculotendon length $L^{MT}$	

Figure 1.17: Model proposed by Zajac, image adapted from [90]

Delp, (1990)	Active contractile element (CE) in parallel with a passive elastic element. The forces in muscle are represented by $F^M$ and tendon $F^T$
--------------	--

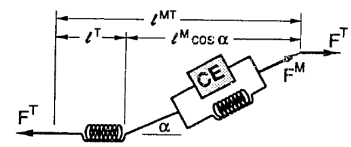


Figure 1.18: Model proposed by Delp, image adapted from [91]

Hayashibe <i>et al.</i> , (2009)	A series of elastic elements (SE) and a contractile element (CC)
----------------------------------	--

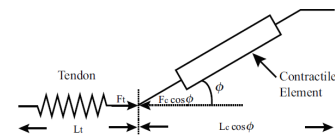


Figure 1.19: Model proposed by Hayashibe *et al.*, image adapted from [92]

Pang <i>et al.</i> , (2013)	A pair of elements arranged in series: the passive serial element (SE) and the active contractile element (CE); and a passive element (PE) arranged in parallel to the previous two.
-----------------------------	--

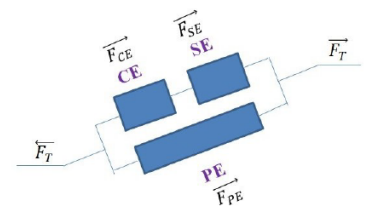


Figure 1.20: Model proposed by Pang *et al.*, image adapted from [93]

Millard <i>et al.</i> , (2013)	Muscle-tendon actuators consist of an active contractile element, a passive elastic element, and an elastic tendon. An active-force-length $f^L$ , force velocity curve $f^V$ , passive force length $f^{PE}$ , and tendon-force-length $f^T$ . The model is also considered by [95, 96]
--------------------------------	--

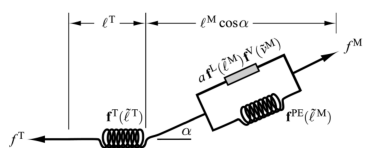


Figure 1.21: Model proposed by Millard *et al.*, image adapted from [94]

In this thesis the chosen model for the muscle is based on the one proposed by Zajac, [90], which considers the pennation angle  $\alpha_m$  that influences the kinematic and the force during movements, but instead of using an elastic element to describe tendons we use a parallel damper-spring to describe more accurately the muscle behavior (as echoed in the following paragraph). Figure 1.22 presents the retained Hill based model where: i)  $CE$  represents the contractile element, ii)  $k_{pee}$  is the parallel elastic element of the muscle, iii)  $k_{see}$  is the muscle's serial elastic element, iv)  $k_{Tee}$  is the tendon's elastic element, v)  $b_{Tde}$  is the tendon's damping element, and vi)  $\alpha_m$  is the angle proposed by Millard *et al.*, (2013).

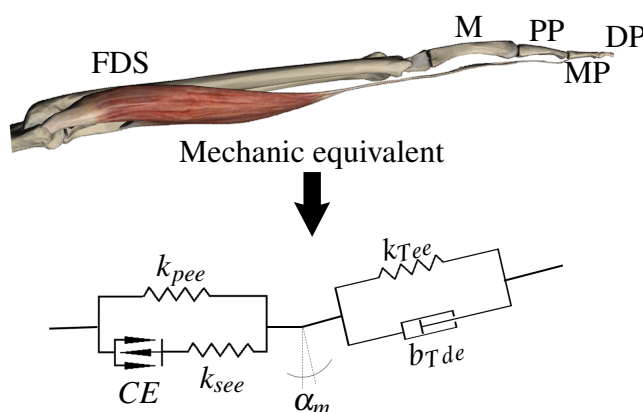


Figure 1.22: Retained Hill based model.

The contractile element  $CE$  is defined by the force–length and force–velocity dependencies. The serial  $k_{see}$  and the parallel  $k_{pee}$  elastic elements are used to account physiologically noticeable effects, such as contraction history effects. The damper  $b_{Tde}$ , included in the tendon part of the model, controls oscillations that may occur when simulating contractions against a mass, predicting muscle forces more realistically [97]. figures 1.23 and 1.24 exemplary show the effect of the damping element in tendons during a flexion of a finger.

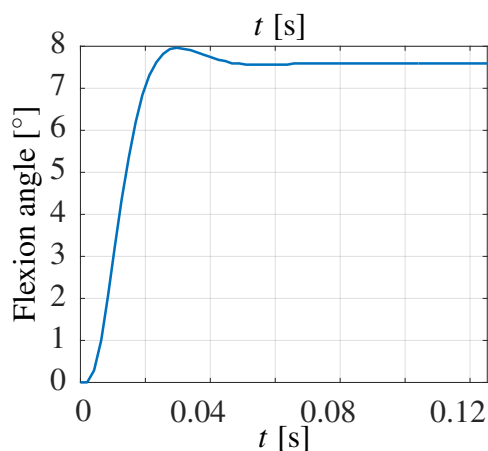


Figure 1.23: Damped example of movement simulation.

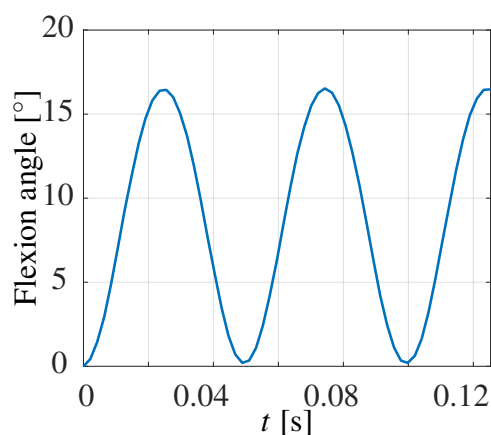


Figure 1.24: Non-damped example of movement simulation.

## 1. Human hand movement analysis toward the hand prosthesis requirements

### 1.3.3 Characteristics issued from experimental analysis of the human hand

The complex organization (anatomic and functional) of the hand contributes to the prehension movements, which are classified into three classes [48] depending on the way in which the force is applied: i) digital, ii) palmar and iii) centered prehension. The digital prehension matches the characteristics of the precision grasping, described section 1.2, because objects are reached using fingertips. Consequently, in this stage of the human force analysis, we seek to study the pinch grasping to bound the necessary force. The target is to identify steady and transient states of the human precision grasping to deduce the pinch force requirements.

The applied force must be adapted to the object's weight, acceleration, surface texture, contour and structure [98]. Consequently, the measure of the pinch force has to be tailored to each particular problem [99], and that is why in this study we carried out an experiment aiming to measure the pinch force applied by two fingers of the hand, the index and the thumb.

#### Experimental set-up

In order to define a reference value of the human pinch force, experimental data are collected within a group of five healthy males (subjects) between 24 and 32 years old. The subjects are asked to apply their maximal pinch force (using thumb and index fingers) over a hand dynamometer Vernier™ D-BTA whose characteristics are:

1. two surfaces of measure (for pinch and grasp)
2. accuracy of  $\pm 0.6\text{N}$
3. resolution of  $0.2141\text{N}$
4. operational range from  $0\text{N}$  to  $600\text{N}$

During the experiment the subjects are sitting and the dynamometer is placed in such a way that the angle between arm and forearm is  $90^\circ$ , reducing the influence of the upper limb muscles in the applied fingertip force. Each subject performs the experiment five times, between trials subjects wait five minutes to avoid muscular fatigue. The data is collected using a digital oscilloscope connected to a computer. Figure 1.25 shows the scheme of the experiment.

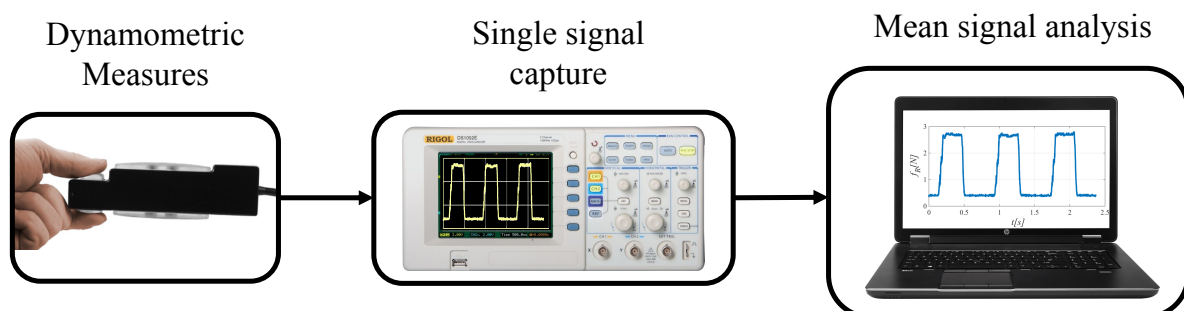


Figure 1.25: Experimental set-up to measure the human pinch force.

### Steady state analysis of the human pinch force

As a result of the experiment, we got a set of signals corresponding to the force performed by each subject with respect to the time. Subsequently, the pinch force steady state values (see figure 1.26) are extracted from the signals. The steady state values are merged for each group in a set of samples representing all trials of the subject. Then the mean values and standard deviations are computed for each subject.

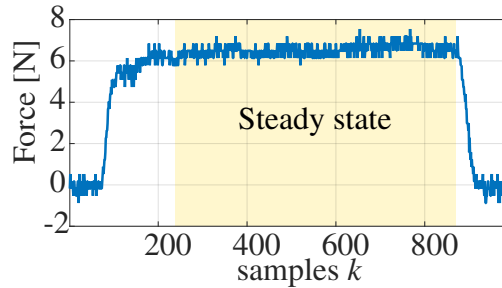


Figure 1.26: Steady state of the pinch force performed by the subject 2 during trial 3.

Figure 1.27 shows the absolute frequencies of the pinch force samples, which correspond to the total number of observations within a given interval of force expressed as probability density function. Furthermore, the plots show a red line for median, a cross for the mean, a blue box around the 25% and 75% quartiles and whiskers bounding 9% and 91%.

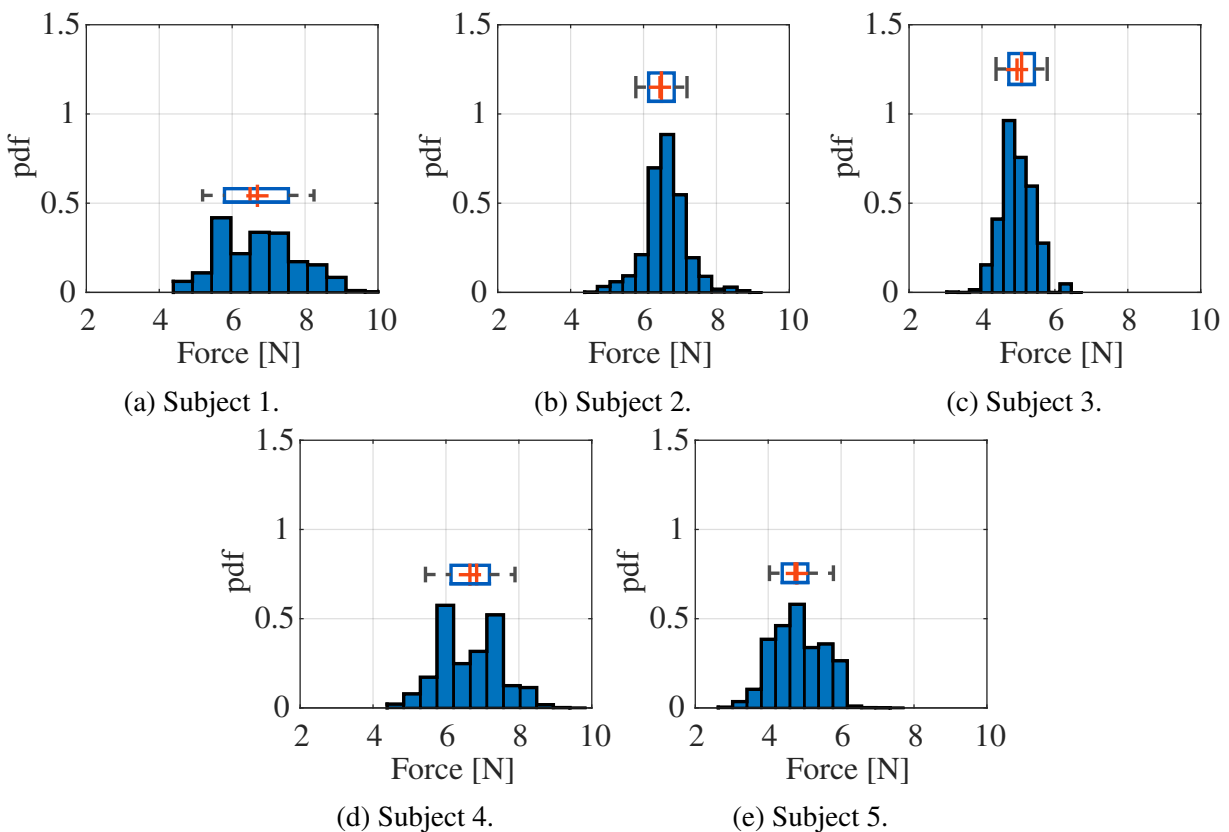


Figure 1.27: Absolute frequency of the pinch force performed by the subjects.

## 1. Human hand movement analysis toward the hand prosthesis requirements

In summary, we have computed mean force and standard deviation for each subject, these experimental results are presented in table 1.5. The measured mean pinch force is in the interval [4.78N, 6.70N].

Subject	Mean pinch force [N]	Standard deviation [N]
1	6.70	1.12
2	6.45	0.58
3	4.97	0.48
4	6.66	0.86
5	4.78	0.65

Table 1.5: Mean value of the human pinch force.

### Transient state analysis to determinate settling time

During the transient state, the measured human pinch force has an exponential behavior (described as  $A(1 - e^{-t/\tau})$  where  $A$  is the amplitude of the signal,  $t$  is the time, and  $\tau$  is the time constant), as is shown in Figure 1.28 for trial 1 of subject 2. These transient phenomena can be approximated by a first order transfer function, whose output (pinch force) is the result of a step input (muscular activation). Thus, the settling time  $t_s$  is defined as the required time to settle the output to the steady state amplitude, within a 2% margin. Considering all subjects and trials, the value of the settling time is in the range  $0.18s < t_s < 0.45s$  with a standard deviation of 0.10s. Moreover, for a first order behavior, the frequency is calculated as  $\omega = 4/t_s$ , see Lu *et al.*, [100]. As a result,  $\omega$  is in the interval [8.89Hz, 22.2Hz].

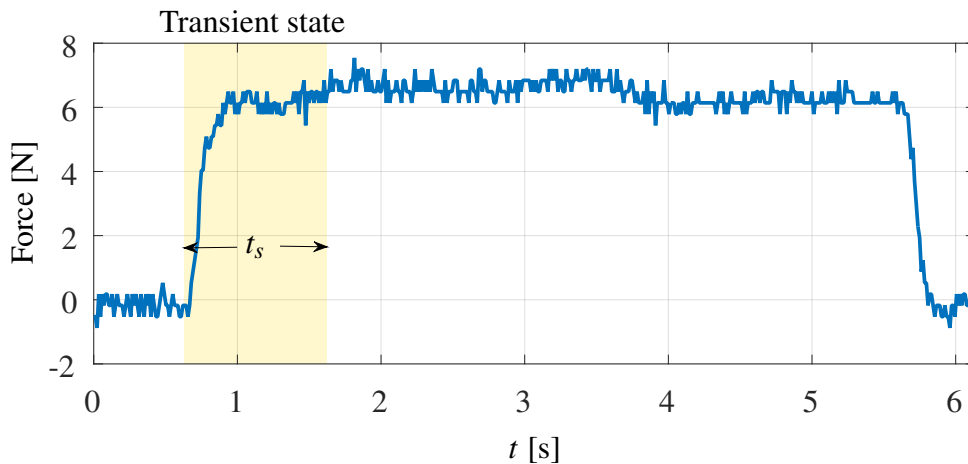


Figure 1.28: Measure of the settling time Pinch force versus time  $t$ .

## 1.4 Discussion

A combination of quantitative and qualitative approaches was used in the data analysis introduced in this chapter. Human hand anatomy was studied from three important aspects: The kinematics, the functionality, and the dynamics. From a kinematic point of view, an equivalent biomechanical model using mechanical equivalents of joints was proposed. Furthermore, a critical study of state of the art, regarding grasping was carried out. This study allows identifying the hand gestures most used in daily living activities. Moreover, an approximation of the dynamic behavior of muscles was introduced through the equivalent Hill-based muscle model. Furthermore, the human force was evaluated experimentally, and the range of pinch force was identified.

The study of the state of the art of human grasping, shows us that most of the movements studied in the literature are not useful in daily life. Instead, a group of seven relevant movements was identified, according to the grasp taxonomy, the hand gestures are: i) medium Wrap, ii) light tool, iii) prismatic 4 fingers, iv) prismatic 3 fingers, v) prismatic two fingers, and vi) precision disk, vii) tripod. The medium wrap and the last five movements are performed using from two to four fingers opposed to the thumb. However, all of them are feasible using two fingers opposed to the thumb. Thus, a robotic prosthetic hand fitted with three fingers can fulfill six of the seven most used hand gestures, restoring 85.7% of the daily working necessities regarding hand usage of an amputated person.

With respect to the experimental result and the biomechanic analysis of hand joints and muscle, we found that for the development of a prosthetic hand, it is necessary to take into account the following consideration:

1. Have an active flexion in the range of [60, 90] degrees in the MCP, PIP, and DIP joints.
2. The adduction and abduction movements are very important to prepare the hand for grasping, even that, if they are fixed in the correct position for the seven identified grasping gestures they can be omitted.
3. According to the study performed in section 1.2, six of the seven grasping movements can be merged in single hand gestures using three fingers, if the prosthetic hand have enough compliance to be adapted to different objects.
4. The behavior of the actuators must follow a viscoelastic scheme as proposed in the Hill-based model.
5. The necessary force range is in the interval [4.78N, 6.70N].
6. The operating frequency must be in the interval [8.89Hz, 22.2Hz].

The collected information is the basis for the development of the hand prosthesis and the actuator based on smart material, which are introduced in the following chapters.



# Chapter 2

## Design and modeling of the soft robotic hand ProMain-I

The task of designing or improving a robotic hand (to replicate the grasping capabilities and the kinematic function of the human hand) involves the consideration of a high complexity sensory and motor functions. The literature (*e.g.* [101]) shows that some robotic hands designed for research have provided solutions for the domain of prosthesis. However, the actual state of the art shows that the requirements of dexterous manipulation, regarding mechanisms, actuation, and kinematic properties, have not been fulfilled [102]. Thus, in this chapter we introduce a contribution regarding the development of a robotic hand prosthesis, designed to take into account the state of the art of robotic hands and requirements of the human hand.

An essential aspect of the development of robotic hands is the actuation system and the drive mechanism. The hands present in state of the art could be classified mainly into three categories: under-actuated, fully actuated, and over-actuated. This classification is based on the number of actuators used to drive a joint. For instance, a robot having three rotational joints, each one provided with one degree of freedom, could be driven by three actuators (one per joint), in that case, the robot is fully-actuated. When the number of actuators is bigger than the number of joints, the robot is over-actuated. Finally, when the number of actuators is lower than the number of joints, two or more joints must be driven by only one actuator, that case is the underactuated scenario.

### 2.1 Review of robotic hands

The last three decades have seen a growing trend towards the development of robotic hand. Thus, it is mandatory to verify the technological progress regarding mechanism, performance, and functionality of robotic hands. With the aim of identifying the actual evolution of robotic hands, we carry out a detailed study of twenty-two robotic hands, which are summarized in figure 2.1.

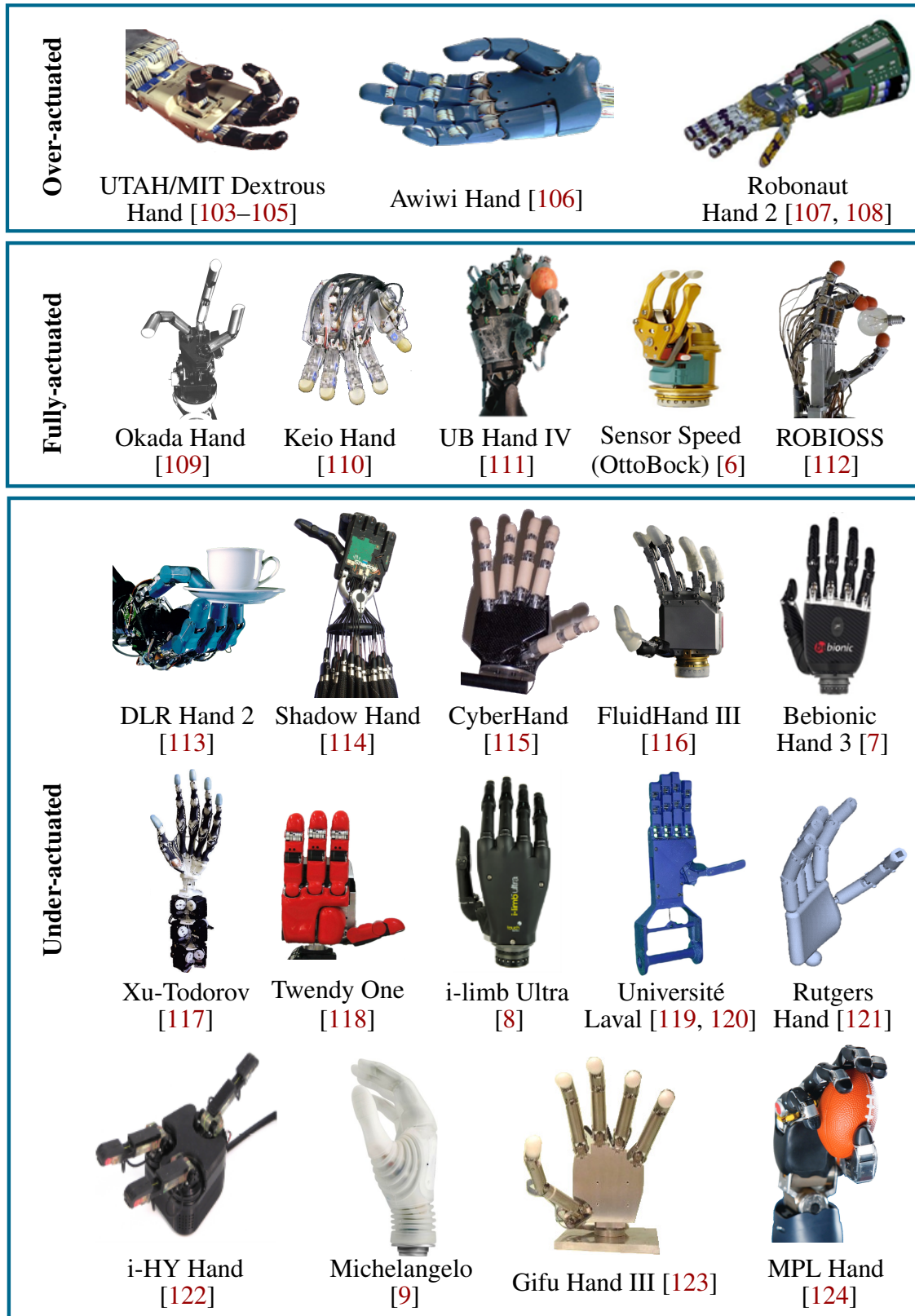


Figure 2.1: Review robotic hands

In our study, we take into account physical characteristics as weight, shape, speed and force. Furthermore, we attempt to identify the used mechanism and the actuators technologies. This information is required to define a framework in which the contribution to robotic hand prosthesis development can be precisely determined and also to define a reference point to start-up the development of a new prosthetic hand.

Physical features of over-actuated hands found in the literature are summarized in table 2.1. Two of the three hands have five fingers, one of them has four. The size is given as a scale factor about the human hand. The grip force is the strength that can be applied by the hand over an object. These robots are designed to be applied as dexterous grippers, and the specifications are quite different from those of robotic prosthetic devices.

Name	Year	Size	Weight	Finger Number	Speed	Force	Ref
UTAH\MIT Dextrous Hand	1986	$\gg 1$	-	4	172°/s	32N	[103–105] [125]
Awiwi Robot Hand	2012	1	-	5	DIP: [1330,1500]°/s PIP: [780,1170]°/s MC: [640,850]°/s	30N	[106]
The Robonaut Hand 2	2011	1	9 kg	5	200 mm/sec	20N	[107, 108]

The speed of the Robonaut Hand 2 is given for the fingertip.

Table 2.1: Physics characteristics: over-actuated hands

The actuation and driving mechanisms are summarized in table 2.2. The hands are driven in all cases by tendons merged with pulleys or with rigid bar mechanisms. Furthermore, the number of actuators is high, which is logical considering the over-actuation concept and the number of degrees of freedom that in all cases is greater than fourteen. Consequently, this kind of actuation concept is not possible for prosthetic devices using traditional actuation technologies, *i.e.*, based on energy sources like electric, pneumatic or hydraulic.

Name	DoF Number	Joints	Type Actuator	Actuator Number	Mechanism	Ref.
UTAH\MIT Dextrous Hand	16	16	electric pneumatic	32	tendon and pulley	[103] [125]
Awiwi Robot Hand	19	15	electric	38	tendon	[106]
The Robonaut Hand 2	14 (12 hand + 2 wrist)	16	electric	16	tendon and 4 bar mechanism	[107, 108]

Table 2.2: Actuation characteristics: over-actuated hands

The fully actuated hands are lighter than the over-actuated ones, which can be explained by the lower number of actuators. In this category, we find the “Sensor Speed” hand which is a hand prosthesis produced by OttoBock. The “Sensor Speed” hand has a size factor of one, i.e., the hand is anthropometric. Furthermore, the hand is configured to perform grasping with three fingers and can apply a force of 100N. The main drawback of this prosthesis is the fact that the position of the fingers and the reduced degrees of freedom limits the usability of the hand. Table 2.3 summarizes the physics characteristics of the considered fully actuated hands.

Name	Year	Size	Weight [Kg]	Finger Number	Speed	Force	Ref
Okada Hand	1979	-	0.240 per finger	3	[500,600] <sup>o</sup> /sec	Grasp Object of 500g	[109]
Keio Hand	2005	1	0.853	5	-	10N	[110]
UB Hand IV	2013	-	-	5	-	-	[111]
Sensor Speed (OttoBock)	2011	1	0.46	3	300mm/sec	100N	[6]
ROBIOSS	2013	1.1	0.113 per finger	4	70 <sup>o</sup> /sec	-	[112]

Table 2.3: Physics characteristics: fully-actuated hand

With respect to the actuators, all hands use electric actuators and excepting the sensor speed hand, which uses rigid drive mechanism, all hands transmit power through cables. In the case of the “Keio” and “UB IV” hands, the number of degrees of freedom is set to 20 allowing each finger to perform flexion-extension and adduction-abduction. The “Okada” hand has eleven joints, eleven DOF and consequently eleven actuators. The utilization of this actuation methodology in robotic hand prosthesis is potentially possible. However, the usage of several joints to perform required grasping tasks lead to the use of a relatively high number of actuators, which results in a high energy consumption and impacts the energetic autonomy of the hand. Table 2.4 summarizes the actuation features of the considered fully actuated hands.

Name	DoF Number	Joints	Type Actuator	Actuator Number	Mechanism	Ref.
Okada Hand	11	11	electric	11	cable	[109]
Keio Hand	20	20	electric	20	tendon and pulley	[110]
UB Hand IV	20	20	electric	24	tendon	[111]
Sensor Speed (OttoBock)	1	2	electric	1	rigid	[6]
ROBIOSS	16	16	electric	16	tendon and pulley	[112]

Table 2.4: Actuation characteristics: fully-actuated hand

The last category corresponds to the under-actuated robotic hand. Here we find three commercial prosthetic hands: i-Limb, BeBionics, and Michelangelo. All of them have a scale factor of one regarding the human hand forces in the range [70,140] N. Their weight is between 420g for the Michaelangelo hand and 557g for the “Bebionic”, in all cases, the weight is under the average human value of 600g.

One important aspect of these prostheses is that they report the speed regarding closing time, which correspond to the time used for the hand to completely close the fingers. Likewise, the speed of the “Shadow” Hand is reported as the operating frequency of full-range joint movement in free space. Furthermore, for the research purposes hands, the heaviest is the shadow hand with 4200g. Table 2.5 summarizes the physics characteristics of the considered under-actuated hands.

Name	Year	Size	Weight	Finger Number	Speed	Force	Ref
DLR Hand 2	2001	-	1.8	4	360°/s	30N	[113]
The Shadow Hand	2003	1	4.2	5	0.2Hz	-	[114]
CyberHand	2006	1	1.8	5	45°/s	70N	[115]
FluidHand III	2009	-	0.4	5	closing time: 1s	65N	[116]
Bebionic Hand 3	2012	1	557	5	closing time: 0.5s	140N	[7]
Xu-Todorov	2016	1	0.942	5	-	-	[117]
Twendy One	2009	1.2	-	4	-	-	[118]
i-limb Ultra	2011	1	0.480	5	closing time: 1.2s	100N	[8]
Université Laval	2008	1	0.4	5	-	50N	[119]
Rutgers Hand	2002	1	1.36	5	-	6.67N	[121]
i-HY Hand	2013	-	1.35	3	-	-	[122]
Michelangelo	2012	1	0.42	5	325mm\sec	70N	[9]
Gifu Hand III	2002	1.3	1.4	5	-	2.8N	[123]
MPL Hand	2010	1	-	5	-	-	[124]

Table 2.5: Physics characteristics: under-actuated hand

Table 2.6 summarizes the actuation features of the considered under-actuated hands. It is interesting to note that the commercial prosthetic hands have four or five DoF and are driven by five electric actuators. Likewise, the hand developed by the Université Laval has 15 DoFs in total, of which one is actuated. Regarding the mechanism, it is not frequently reported due to the complexity of under-actuation, but for the reported cases it is a rigid bars system in two cases and tendons for two others.

Furthermore, only one hand employs a smart material (shape memory alloy) as the actuator. Moreover, regarding actuators of the studied hands, 10 are electric, one is pneumatic, one is hydraulic, one is based on smart materials, and one is activated manually.

Name	DoF Number	Joints	Type Actuator	Actuator Number	Mechanism	Ref.
DLR Hand 2	13	17	electric	12	-	[113]
The Shadow Hand	20	24	pneumatic	20	-	[114]
CyberHand	16	-	electric	6	rigid	[115]
FluidHand III	8	8	hydraulic	8	-	[116]
Bebionic Hand 3	5	-	electric	5	4-bar mechanism	[7]
Xu-Todorov	-	-	electric	10	-	[117]
Twendy One	13	16	electric	13	-	[118]
i-limb Ultra	5	11	electric	5	-	[8]
Université Laval	1	15	manual	1	-	[119]
Rutgers Hand	15	20	SMA	-	tendons	[121]
i-HY Hand	5	9	electric	5	-	[122]
Michelangelo	4	6	electric	-	-	[9]
Gifu Hand III	16	20	electric	16	rigid	[123]
MPL Hand	22	26	electric	15	-	[124]

Table 2.6: Actuation characteristics: under-actuated hand

Summarizing, state of the art allows us to identify that: i) the most used drive mechanism is based on tendons, ii) the mass of a prosthetic hand must be under 600g, iii) the number of actuators must be reduced, but the number of DoF must be as high as necessary to perform the prehension movements identified in chapter 1, and iv) an electric actuator is a right approach for a first test prototype that is going to be used to extract requirements specification to develop an actuation system using smart materials. In the following, we introduce the first prototype of the so-called robotic prosthesis ProMain-I, which uses a new tendon-drive mechanism, and takes into account human hand requirements and state of the art introduced here.

## 2.2 Precision grasping hand set up

As introduced in chapter 1, the adduction-abduction of metacarpophalangeal (MCP) joints play an important role preparing the hand for grasping. Even that, finger's flexion-extension movements are significant to perform the hand grasping gesture. Consequently, if the fingers are correctly placed for grasping, those articulations are not required, and the prosthesis can be simplified without impacting prehension ability. Thus, we introduce a support chassis that host the fingers in such a way that they are correctly placed to perform grasping gestures described in section 1.2.

The support chassis must guaranty that: i) the thumb is abducted facing index and middle fingers and ii) the index and middle fingers must have a minimum abduction angle correspond-

ing to hand opening. This angle is set to  $15^\circ$  allowing a hand opening of 10cm during grasping as introduced in section 1.2. It is to note that to perform the chosen grasping gestures the hand needs to be opened an amount of 5cm.

Fingers' frameworks (2c) are integrated to support chassis (60) as presented in figure 2.2. The rotation axes of the MP joints of the thumb, index, and middle fingers (noted  $z_{11}$ ,  $z_{21}$ , and  $z_{31}$  respectively) are coplanar and create two angles  $\gamma_1$  and  $\gamma_2$ . In order to guarantee the required thumb opposition and the index-middle abduction, we set the following angular values: i) angle  $\gamma_1$  formed between  $z_{11}$  and  $z_{21}$  is set to  $15^\circ$  and ii) angle  $\gamma_2$  formed between  $z_{11}$  and  $z_{31}$  is set to  $15^\circ$ .

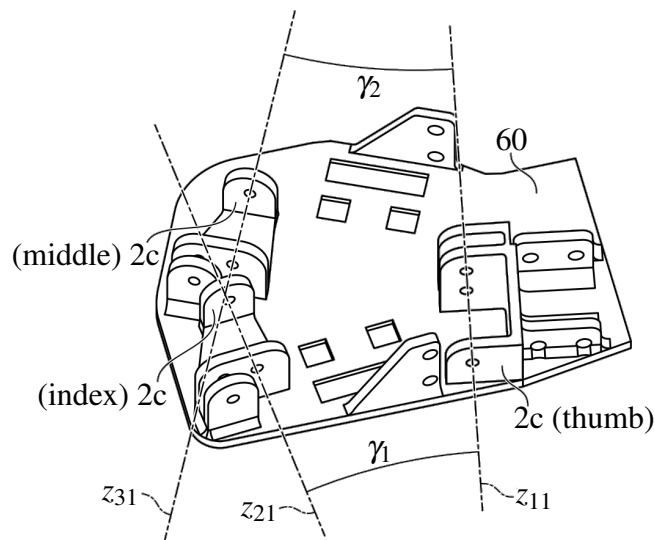


Figure 2.2: Support chassis of the ProMain-I.

Taking into account that angles  $\gamma_1$  and  $\gamma_2$  are measured with respect to the axis  $z_{11}$  of the thumb finger, the abduction angle between the index and the middle fingers is also  $15^\circ$ . As a result, this support chassis offers the ideal configuration<sup>1</sup> to perform the selected prehension patterns. In the following sections, we introduce the prosthetic finger, which is the main component of the hand.

## 2.3 Design of the soft robotic finger

Based on the state of the art of the human (presented in chapter 1) and robotic hands (presented in section 2.1), we chose a tendon-based approach for the finger's driving mechanism to provide flexibility in the articular joints. In order to develop the tendon-based ProMain-I finger, an early "alpha" prototype of the robotic finger is introduced. The "alpha" finger prototype is a bio-inspired tendon-driven finger [1–3] composed of three joints: the metacarpophalangeal (MCP), the proximal interphalangeal (PIP) and the distal interphalangeal (DIP). All the joints have one

<sup>1</sup>The configuration takes into account the grasping conditions reported as part of the grasping taxonomy of Feix *et al.*, [17]

DoF to perform flexion and extension. The finger is controlled by only one actuator, and the drive mechanism uses two tendons for transmitting motion, one for the flexion and one for the extension, as shown in Figure 2.3. Considering that the tendons are fastened to the motor pulley and the fingertip, the clockwise rotation of the actuator produces the flexion, and the counterclockwise rotation provides the extension.

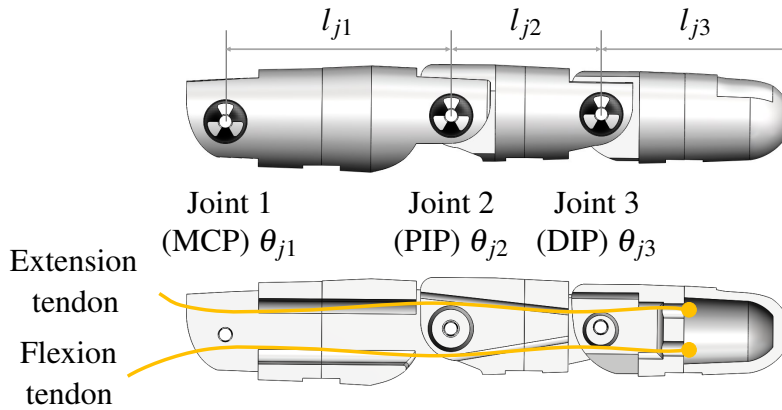


Figure 2.3: Early “alpha” prototype of the robotic finger.

Due to the under-actuation, the rotation angle of the PIP and DIP joints are linked with the rotation angle of the MCP joint. The relations between the angles are calculated using experimental measures presented in section 3.2. As a result, the obtained relations between angles are  $\theta_{j2} = 0.23\theta_{j1}$  and  $\theta_{j3} = 0.72\theta_{j1}$ , where  $\theta_{j1}$  is the MCP joint angle,  $\theta_{j2}$  is the PIP joint angle and  $\theta_{j3}$  is the DIP joint angle. The subindex  $j$  is used to identify the fingers so that  $j = 1$  made reference to thumb,  $j = 2$  the index, and  $j = 3$  the middle. Furthermore, the parameters  $l_{j1}$ ,  $l_{j2}$  and  $l_{j3}$  are the lengths of the proximal, medial and distal phalanges, as shown in Figure 2.3.

The analysis carried out using experimental data, issued from the “alpha” prototype of the robotic finger, gives us valuable and relevant information for the improvement of the finger’s mechanism and actuation systems, and lets us define the following functional requirements: i) higher stiffness into the MCP joints and ii) a fixed mechanical relation between the proximal and metacarpal joints, and between the distal and metacarpal joints. Those improvements are introduced in the ProMain-I finger prototype.

The new driving mechanism is inspired by the epicyclic gear train, which is typically composed of two gears (one fixed and one mobile) whose centers are attached through a rigid link so-called carrier. So that, the rotation of the carrier creates a revolve of the mobile gear center around the fixed gear. As a result, due to the mechanical link between gears, a rotation is provided on the mobile gear. Furthermore, the rotation amount of the carrier can be different from the rotations of the mobile gear, which is controlled by the gears relation. Figure 2.4 exemplary shows an epicyclic gear train (whose gears are labeled with white circles to follow relative rotations) in which the carrier has rotate  $90^\circ$  and the mobile gear  $150^\circ$ .

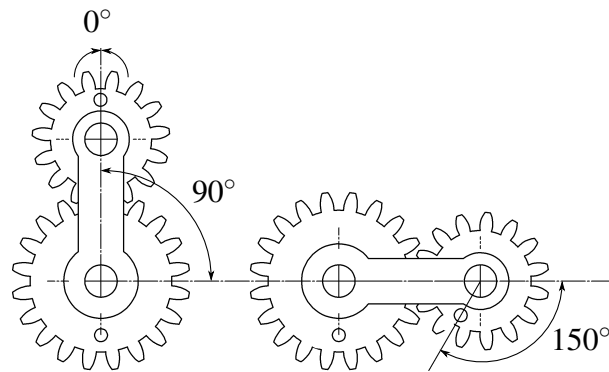


Figure 2.4: Epicyclic mechanism.

Consequently, for our driving mechanism, we proposed a soft epicyclic mechanism in which: i) the finger's phalanges replace the carrier, ii) the gears are replaced by two slotted pulleys, and iii) the mechanical link is guaranteed by two crossed flexible wires, henceforth tendons.

Figure 2.5 shows the scheme of the driven mechanism, in which blue line represents the tendon that drives clockwise rotation, and the yellow one depicts tendon used to produce counterclockwise rotation; clockwise and counterclockwise rotations are assumed regarding the figure orientation. The  $i$ th phalange of the finger  $j$  begins in a vertical position, then after a rotation, it reaches a horizontal position. The center of the mobile pulley orbits around the fixed pulley, and due to the effect of the tendons, the mobile pulley rotates. As a result, a rotation is produced in the  $i + 1$ th phalange, which is fixed to the mobile pulley. If the mobile pulley gets blocked during rotation, the driving tendon is constrained in tension, so that, the elasticity of the tendon's material depicts the stiffness of the joint.

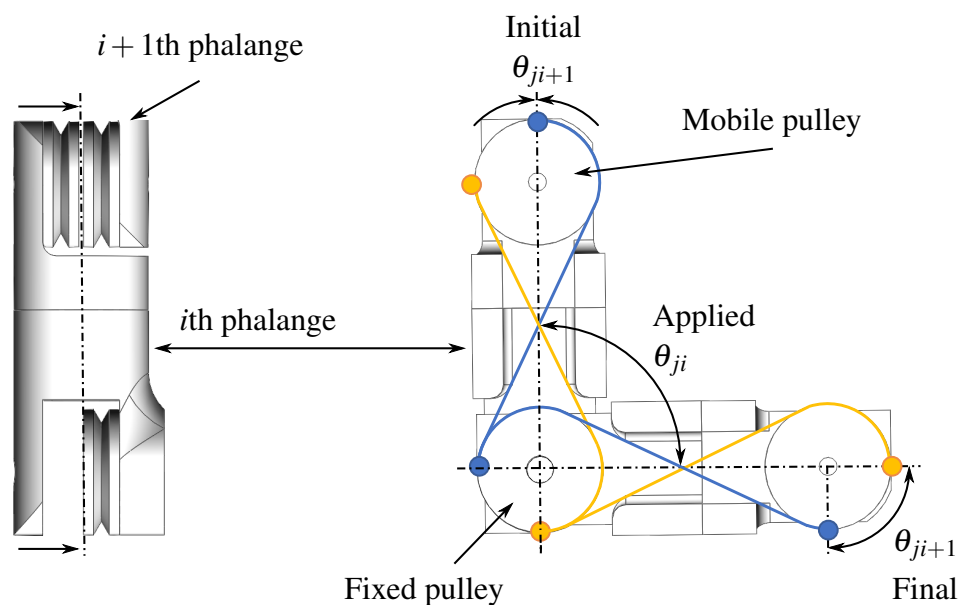


Figure 2.5: Soft epicyclic mechanism.

The proposed soft epicyclic mechanism is used to transmit motion between the MP joint and the DIP joint, and between the DIP joint and the PIP joint. As a result, two groups of tendons are used; each group is composed of one flexion tendon and one extension tendon. Thus Promain-I hand motion consists in the flexion and extension of the robotic fingers which are placed in the support chassis (60) described above. In the following, we introduce the main components of the ProMain-I hand, see figures 2.6 and 2.7. The phalanges are the following: (i.) proximal (10), which is highlighted in blue color in Figure 2.6, (ii.) medial (20), which is highlighted in yellow color, (iii.) distal (40), which is highlighted in gray color.

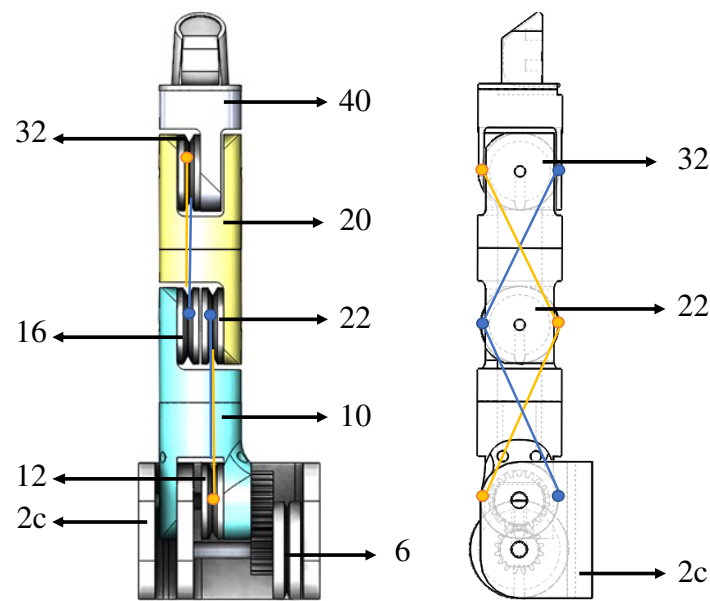


Figure 2.6: Promain-I hand phalange description

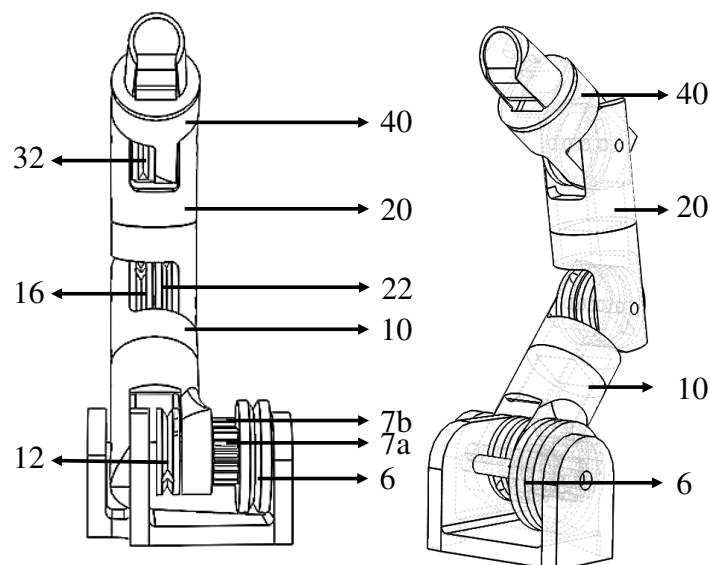


Figure 2.7: Promain Hand-I main components

Robotic finger is under-actuated, hence, the movement is transmitted using only one servomotor, which is the active element, it is linked to the MP joint, through the pulley (6) and the gears (7a and 7b), the gears are used to ensure the rigidity of the proximal phalanx.

Two tendons are crossly placed from pulleys (12) to (22), see figure 2.6, yellow line represents a tendon that executes the flexion of the medial (20) phalange; and blue line illustrates a tendon that executes the extension of medial (20) phalange.

Similarly, pulleys (16) to (32) are linked through two tendons that are crossly attached. Yellow line represents a tendon that executes the flexion of the medial (16) phalanx; and blue line illustrates a tendon that executes the extension of medial (32) phalanx. The motion is executed, following the next steps and conditions:

1. Servomotor is linked to the pulley (6), which transfers the motion to the gear (7a) and (7b).
2. Gear (7b) is attached to the proximal (10) phalanx, therefore the rotation in first phalanx is produced.
3. Pulley (12) is linked with the framework (2c), with this in mind, when the element (10) turns, it causes the rotation of the pulley (22).
4. Pulley (22) is linked to the medial (20) phalanx, thus when the pulley (22) turns, it moves the medial (20) phalanx.
5. Pulley (16) is attached to the phalanx (10), thus, due to the soft epicyclic mechanism, when the pulley (22) turns, it causes a rotation in pulley (32).
6. The pulley (32) is attached to the medial (10) phalanx, so, the rotation of the pulley (32) produces the rotation of the distal phalanx (40).

Two wires or tendons are used to transmit movement from the servomotor to the proximal phalanx. From a qualitative point of view, the elastic behavior of those elements allows us to mimic the human muscle behavior. Furthermore, the same effect is used to reproduce the elastic behavior of human tendons presented in section 1.3.2.

The damping element  $b_{Tde}$  introduced in section 1.3.2 is used to describe more accurately the muscle behavior avoiding undesired oscillations. In this case, considering that no oscillation is present we consider that the element is embedded in the global behavior of the soft epicyclic mechanism. The following figure 2.8 shows the equivalence between the proposed mechanism and the Hills-based muscle model.

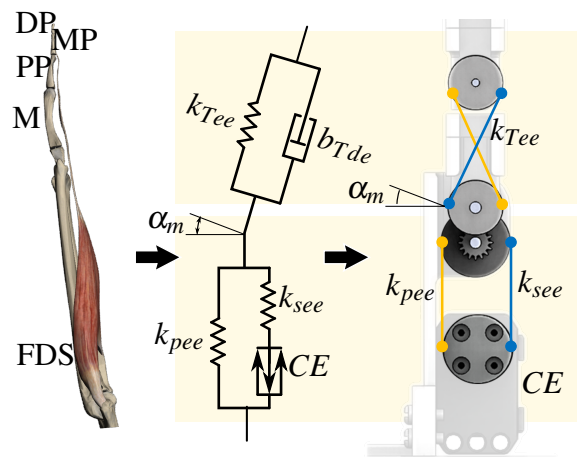
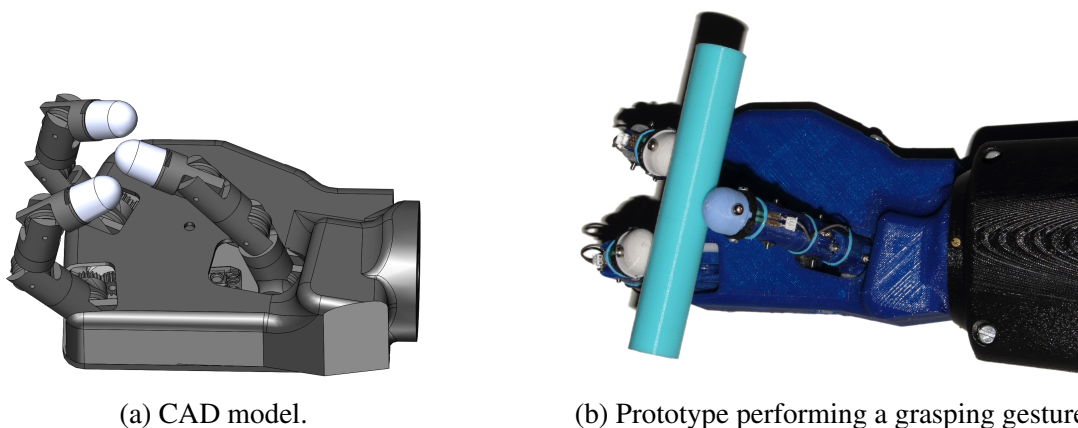


Figure 2.8: Parallel between soft epicyclic mechanism and the Hills-based muscle model.

## 2.4 Robotic hand ProMain-I

The bio-inspired robotic hand prosthesis ProMain-I <sup>2</sup>, has been developed, tested and manufactured completely in LEME laboratory. It has three fingers disposed to perform precision grasping. Each finger has three joints: Metacarpophalangeal (MP), Proximal interphalangeal (PIP) and distal interphalangeal (DIP).

All joints have one degree of freedom (DoF) to perform flexion and extension. Each finger is controlled by only one servo motor XL-320 Dynamixel™, hence the medial (MP) and distal (DIP) phalanges are driven by the proximal phalanx (PIP) motions. The clockwise rotation of the actuator produces flexion, and the opposite rotation produces extension. The relation between the angles is  $\theta_{j2} = \theta_{j3} = 0.9\theta_{j1}$ , where  $\theta_{j1}$  is the MP joint angle,  $\theta_{j2}$  is the PIP joint angle and  $\theta_{j3}$  is the DIP joint angle. This relation between angles is established manipulating the pulleys ratios and is chosen to mimic the closure of the human hand. Figure 2.9 shows the CAD model and the prototype of the ProMain-I hand performing a grasping gesture



(a) CAD model.

(b) Prototype performing a grasping gesture

Figure 2.9: ProMain-I Hand.

<sup>2</sup>Patent Number: FR1656914[4]

## 2.5 Kinematic model

Due to the tendons introduced in the soft epicyclic mechanism, the designed robotic hand ProMain-I has a flexible behavior in the joint. These soft responses creates a new behavior of the finger which is different from the classical rigid robotic prosthesis presented in section 2.1 and must be analyzed. The modeling of those unpredicted motions requires new considerations regarding kinematic modeling.

Recently, two important approaches have been proposed to model soft robotic hand prostheses. Such as the postural synergies [126] and the adaptive synergies [127]. These synergies are used to formulate grasping forces [128]. Adaptive synergies are particularly referred to the consideration of variable stiffness joints in soft robots, interacting in an adaptive way with the environment and the objects to grasp.

These approaches allow the design of under-actuated robotic hands to accomplish a soft-synergy model, which provides a robust and compliant mechanism [127]. Despite the excellent results to control the internal forces needed to hold an object, the variable stiffness joints state a challenge related to the modeling and handling of unpredicted movements.

Consequently, the synergies approach has been combined with the parameterization of Denavit- Hartenberg (DH) [126]. The DH parameters and its variations were proposed for rigid robots, and new developments are necessary to calculate the kinematic and the dynamic of soft robots. The DH methods use four parameters to describe kinematic chains, two of them are translations ( $d_i$  and  $a_i$ ), and the other two are rotations ( $\theta_i$  and  $\alpha_i$ ). Considering that joint rotations are formulated using the parameters  $\theta_i$ , a joint with multiple DoFs requires several frameworks to describe its complete set of possible rotations. Thus, the main drawback of the DH methods concerns the model size, which increases proportionally to the number of DoFs. Moreover, if rotations are issued from the utilization of soft materials, these are unpredicted and hampers the parameterization of the robot.

An interesting approach of kinematic modelization is presented in [129], where the author proposes a model based on DH parameterization and unit quaternion instead of homogeneous matrices. In the same way, [130] presents a methodology for the geometric design of 3R manipulators using the DH parameterization and quaternions. The DH parameterization and the representation of rotations using quaternions are tested in [131] to express deformation in 3D CAD models. Even so, these methods introduce a real difficulty because they remove totally the homogeneous matrices, and a modelling using only quaternions is not efficient from a computational point of view[132].

For these reasons, in the following section we present a new hybrid model that improves the representation of rotations that arise from soft robotics prosthesis movements. Our model combines the parameterization of DH method with quaternions to formulate soft rotations. This new method allows to: formulate soft robot's rotations even in the neighborhood of rotational singularities, reduce the number of rotation parameters and unify the formulation to describe the kinematic of a soft robot.

### 2.5.1 DHKK parameterization merged With Quaternions Formulation

In order to propose an efficient method to model the kinematic of a soft robot, we propose a hybrid method, that consists in the utilization of the Denhavit-Hartenberg parameterization Modified by Khalil and Kleinfinger (DHKK), and the formulation of soft rotations using quaternions.

For the purpose of formulating the rotations that arise from soft robotics movements, our hybrid method represents the kinematic, using DHKK and homogeneous matrices for rigid rotations, and introduces the formulation of soft rotations using quaternions (SRQ). The SRQ is launched taking into account several parameters as the desired movement precision, the direction of movement vectors, and the stiffness of the joints. Likewise, the SRQ can be launched by sensory feedback.

#### 2.5.1.1 DHKK parameterization

The DHKK convention, allows the representation of open-loop and close-loop kinematic chains, and presents a convenient definition of the axis  $z_i$ , which corresponds to the rotation axe of the  $i - th$  joint. The angle of rotation around  $z_i$  is denoted by  $\theta_i$ , and is applied using a transformation matrix, that is described in equation (2.1), which result of the application of:

1. a rotation  $\alpha_i$  around  $x_{i-1}$ .
2. a translation  $a_i$  along  $x_{i-1}$ .
3. a rotation  $\theta_i$  around  $z_i$ .
4. a translation  $d_i$  along  $z_i$ .

$${}^{i-1}[T]_i = \begin{bmatrix} \cos \theta_i & -\sin \theta_i & 0 & a_i \\ \sin \theta_i \cos \alpha_i & \cos \theta_i \cos \alpha_i & -\sin \alpha_i & -\sin \alpha_i d_i \\ \sin \theta_i \sin \alpha_i & \cos \theta_i \sin \alpha_i & \cos \alpha_i & \cos \alpha_i d_i \\ 0 & 0 & 0 & 1 \end{bmatrix} \quad (2.1)$$

The parameters  $\alpha_i$ ,  $a_i$ ,  $\theta_i$  and  $d_i$ , are known as the DHKK parameters, a graphical representation of the parameters is shown in figure 2.10. Usually, the task of calculation of DHKK parameters is hard. it must be performed manually, and it is more difficult when there are multiple kinematic chains. Even that, a method to automatically generate these parameters is presented in [133], and this methodology is used in the present work.

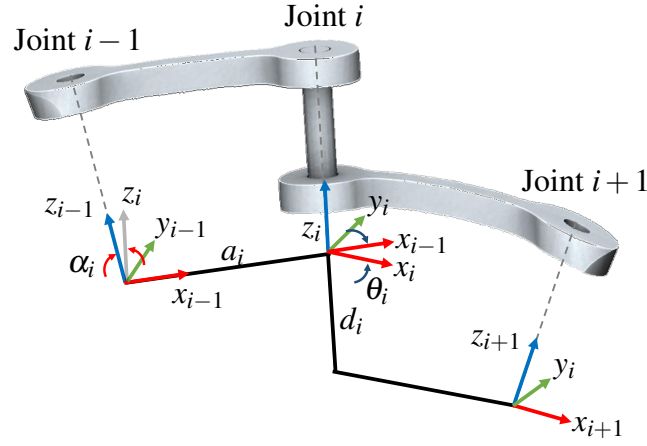


Figure 2.10: Graphical representation of DHKK parameters

Consequently, the kinematic of a robot composed of  $n$  joints is:

$${}^0[T]_n = \prod_{i=1}^n {}^{i-1}[T]_i \quad (2.2)$$

As result the matrix  ${}^0[T]_n$  is a composition of the orientation of the end effector  ${}^0[R]_n$ , and the position vector  $\{{}^0P_n^x, {}^0P_n^y, {}^0P_n^z\}^T$ , as shown in the following expression:

$${}^0[T]_n = \begin{bmatrix} & & & {}^0P_n^x \\ & & & {}^0P_n^y \\ & & & {}^0P_n^z \\ & & & 1 \\ 0 & 0 & 0 & \end{bmatrix} \quad (2.3)$$

### 2.5.1.2 Formulation of Rotations Using Quaternions

The quaternion [134] is a composition of four coefficients, as shown in equation (2.4), usually represented with ordered pairs [135] as  $\mathbb{H} = [[h_0, \vec{h}]]$ , where  $\vec{h} = \{h_1, h_2, h_3\}$ .

$$\mathbb{H} = h_0 + h_1i + h_2j + h_3k \quad (2.4)$$

The components  $i$ ,  $j$ , and  $k$  represent the unit vectors that match the direction of  $\vec{h}$ , and satisfy:

$$i^2 = j^2 = k^2 = ijk = -1 \quad (2.5)$$

The real number  $h_0$  represented as quaternion, is denoted by  $\mathbb{H}_0 = [[h_0, \vec{0}]]$  and the pure quaternion of the vector  $\vec{p}$  is given by  $\mathbb{P} = [[0, \vec{p}]]$ , whose conjugate is  $\bar{\mathbb{P}} = [[0, -\vec{p}]]$ . As presented in [136], two quaternions  $\mathbb{H} = [[h_0, \vec{h}]]$  and  $\mathbb{V} = [[v_0, \vec{v}]]$  can be multiplied as:

$$\mathbb{H}\mathbb{V} = [[h_0v_0 - \vec{h} \cdot \vec{v}, h_0\vec{v} + v_0\vec{h} + \vec{h} \times \vec{v}]] \quad (2.6)$$

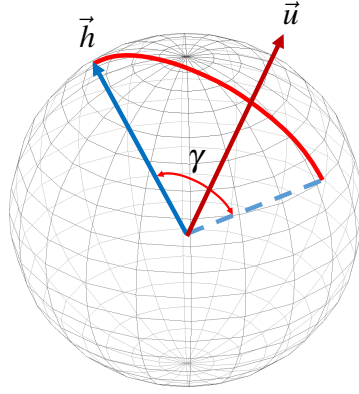


Figure 2.11: Rotation  $\gamma$  applied  $\vec{r}$  to around

In the 3D space, a rotation  $\gamma$  applied to the vector  $\vec{h}$  around the vector  $\vec{u}$ , see figure 2.11, can be formulated using quaternions. For this purpose it is necessary to propose a rotator that is a quaternion  $\mathbb{U}$  as shown in the following equation [134, 135]:

$$\mathbb{U} = [[\cos(\gamma/2), \vec{u} \sin(\gamma/2)]] \quad (2.7)$$

Likewise, it is required to define the pure quaternion  $\mathbb{H}$ , representing the vector to be rotated  $\vec{h}$ , as follows:

$$\mathbb{H} = [[0, \vec{h}]] \quad (2.8)$$

Afterwards, the rotated vector  $\vec{h}'$  is calculated multiplying the rotator  $\mathbb{U}$ , the pure quaternion  $\mathbb{H}$ , and the conjugate of the rotator  $\bar{\mathbb{U}}$ , as follows:

$$[[0, \vec{h}']] = [[\mathbb{U} \mathbb{H} \bar{\mathbb{U}}]] \quad (2.9)$$

Consequently, any combination of three rotations around the axes  $x_i$ ,  $y_i$  and  $z_i$ , can be formulated using three rotators  ${}^x\mathbb{U}_i$ ,  ${}^y\mathbb{U}_i$ , and  ${}^z\mathbb{U}_i$  that are formulated for rotations  $\alpha_i$ ,  $\beta_i$ ,  $\theta_i$  around axes  $x_i$ ,  $y_i$  and  $z_i$  respectively, using unit vectors  $\vec{x}_i$ ,  $\vec{y}_i$ , and  $\vec{z}_i$  in the direction of axes  $x_i$ ,  $y_i$  and  $z_i$ , as follows:

$${}^x\mathbb{U}_i = [[\cos(\alpha_i/2), \vec{x}_i \sin(\alpha_i/2)]] \quad (2.10)$$

$${}^y\mathbb{U}_i = [[\cos(\beta_i/2), \vec{y}_i \sin(\beta_i/2)]] \quad (2.11)$$

$${}^z\mathbb{U}_i = [[\cos(\theta_i/2), \vec{z}_i \sin(\theta_i/2)]] \quad (2.12)$$

Furthermore, it is necessary to define the pure quaternions  ${}^x\mathbb{H}_i$ ,  ${}^y\mathbb{H}_i$ , and  ${}^z\mathbb{H}_i$  using the unit vectors  $\vec{x}_i$ ,  $\vec{y}_i$ , and  $\vec{z}_i$  matching the direction of axes  $x_i$ ,  $y_i$ , and  $z_i$  respectively, as follows:

$${}^x\mathbb{H}_i = [[0, \vec{x}_i]] \quad (2.13)$$

$${}^y\mathbb{H}_i = [[0, \vec{y}_i]] \quad (2.14)$$

$${}^z\mathbb{H}_i = [[0, \vec{z}_i]] \quad (2.15)$$

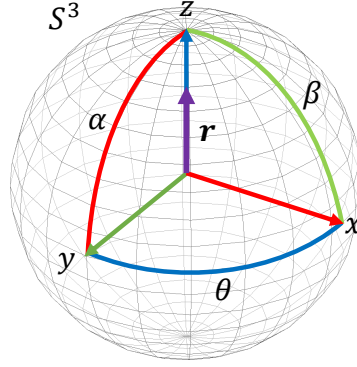


Figure 2.12: Rotation around the axes  $x_i$ ,  $y_i$ , and  $z_i$

Once the rotators and the pure quaternions are defined, we calculate a global rotator  ${}^{xyz}\mathbb{U}_i$ , expressing a rotation around all axes.  ${}^{xyz}\mathbb{U}_i$  is calculated, using the quaternions multiplication introduced in equation (2.6), as shown in the following equation:

$${}^{xyz}\mathbb{U}_i = {}^x\mathbb{U}_i {}^y\mathbb{U}_i {}^z\mathbb{U}_i \quad (2.16)$$

Finally, we formulate rotations following equation (2.9) to calculate unit vectors  $\vec{x}'_i$ ,  $\vec{y}'_i$  and  $\vec{z}'_i$  indicating the orientation of axes after rotation are as:

$$[[0, \vec{x}'_i]] = {}^{xyz}\mathbb{U}_i {}^x\mathbb{H}_i \overline{{}^{xyz}\mathbb{U}_i} \quad (2.17)$$

$$[[0, \vec{y}'_i]] = {}^{xyz}\mathbb{U}_i {}^y\mathbb{H}_i \overline{{}^{xyz}\mathbb{U}_i} \quad (2.18)$$

$$[[0, \vec{z}'_i]] = {}^{xyz}\mathbb{U}_i {}^z\mathbb{H}_i \overline{{}^{xyz}\mathbb{U}_i} \quad (2.19)$$

Those rotators  ${}^x\mathbb{U}_i$ ,  ${}^y\mathbb{U}_i$ , and  ${}^z\mathbb{U}_i$ , which can be considered as points lying a hypersphere  $S^3$  [137] centered at the origin of a joint, can represent any rotation in a 3D space of a rigid-body without singularities[138] and avoiding the addition of extra reference frames. As a result, we can formulate the rotation of any vector  $\vec{h}_i$  represented by the pure quaternion  ${}^h\mathbb{H}_i = [[0, \vec{h}_i]]$ , see figure 2.12, around the axes  $x_i$ ,  $y_i$ , and  $z_i$  as follows:

$$[[0, \vec{h}'_i]] = {}^{xyz}\mathbb{U}_i {}^h\mathbb{H}_i \overline{{}^{xyz}\mathbb{U}_i} \quad (2.20)$$

### 2.5.1.3 Hybrid Model DHKK-SRQ

In the following pages, it will be presented our new hybrid model DHKK-SQR [3] that unifies the DHKK parameters with quaternions using an optimal analysis of the available sensor feedback. This unified formulation allows to express the kinematic of soft robots and reduces the corresponding computational cost.

Each  $i$ th joint (for  $i = 1, \dots, n$  where  $n$  is the number of joints) is considered as an element that has a hybrid (rigid and soft) behavior. In figure 2.13, the  $i$ th joint is modeled, in a first step as a rigid element, and only with the rotation  $\theta_i$  around  $z_i$ ; finally, the rotations  $\alpha_i$  and  $\beta_i$  around

axis  $x_i$  and  $y_i$  are added with the hypersphere  $S_i^3$ . As a result, the model can apply rotations in all axes avoiding to add any extra reference frames.

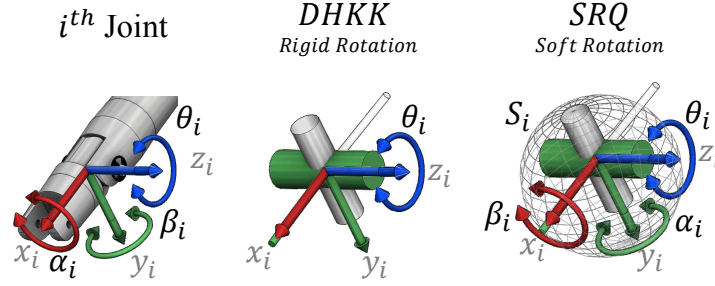


Figure 2.13: Model of hybrid joint using DHKK and SRQ.

The rigid rotations are performed using the homogeneous matrices which are given by equation (2.1) and the kinematics of the rigid joints results from equation (2.2). The orientation and the final position are given by equation (2.3). Using DHKK, the only possible active rotation is  $\theta_i$  around the axes  $z_i$ . Therefore, we formulate the extra rotations (those that appear from the low stiffness joints)  $\alpha_i$  and  $\beta_i$  using SRQ. Additionally, after the SRQ is launched, the rotation  $\theta_i$  is formulated using a quaternion; so that, the set of quaternions for each  $i$ th joint is defined by equation (2.20). To decide when the SRQ is launched, and optimize the extra computational cost, our hybrid method is parameterized in three different cases depending on the available instrumentation:

1. A fully instrumented setting, *i.e.* position and force sensors are available
2. A partially instrumented robot with only position sensors (full or partial measure).
3. No instrumentation available.

For the first case, the model uses equation (2.3) to calculate the final position of the robot. Once the force sensor detects the contact with an object, we apply equation (2.21) to evaluate the absolute position error (Euclidian distance). If the error exceeds the threshold  $\lambda$ , the rotations are performed using equation (2.20), with the measured angles  $\alpha = \{\alpha_1, \dots, \alpha_n\}$ ,  $\beta = \{\beta_1, \dots, \beta_n\}$  and  $\theta = \{\theta_1, \dots, \theta_n\}$  for the  $n$  joints of the robot. The threshold  $\lambda$  depends on the precision requirements of the robot.

$$\sqrt{\sum_{x,y,z} |{}^0\{PM\}_n - {}^0\{P\}_n|^2} \leq \lambda \quad (2.21)$$

Where,  ${}^0\{PM\}_n = \{{}^0PM_n^x, {}^0PM_n^y, {}^0PM_n^z\}^T$  and  ${}^0\{P\}_n = \{{}^0P_n^x, {}^0P_n^y, {}^0P_n^z\}^T$  are the measured and calculated end positions.

For the second case, two scenarios are possible: i) complete angular rotations are measured, *i.e.* angles  $\alpha = \{\alpha_1, \dots, \alpha_n\}$ ,  $\beta = \{\beta_1, \dots, \beta_n\}$  and  $\theta = \{\theta_1, \dots, \theta_n\}$  are available ii) partial measure of angular rotations are measured, *i.e.* only angles  $\theta = \{\theta_1, \dots, \theta_n\}$  are available.

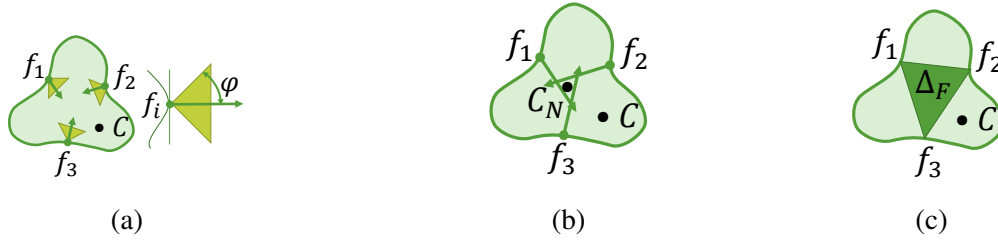


Figure 2.14: Grasp Conditions.

In the first scenario the model use equation (2.3) to calculate the final position of the robot, and the criterion introduced in equation (2.21) is used from the beginning to calculate position error. When the error reaches or exceeds a threshold  $\lambda$  the rotations are formulated using equation (2.20). In the second scenery, we apply equation (2.22) to calculate angles  $\alpha$  and  $\beta$  of each joint, and the rotations are performed using equation (2.20).

$$(\alpha, \beta) = \arg \min_{\alpha, \beta} \left( \sqrt{\sum_{x,y,z} |{}^0\{PM\}_n - {}^0\{P\}_n|^2} \right) \quad (2.22)$$

The last case is proposed for robotic hand applications, where the grasping parameters (size, shape and weight of the object) are known, but the robot doesn't have sensory feedback. So, the known grasping information is used to parametrize our method. To grasp in a steady way an object, it is necessary to consider four conditions [36]:

1. The sum of the applied forces and torques must be equal to zero.
2. The direction of the forces must be orthogonal to the tangential plane of the point of contact with the object, as shown in figure 2.14a. The maximal angle  $\varphi$  of the force depends on the friction coefficient  $\mu$  of the object (cone of force).
3. The center of application of forces  $C_N$  must be as close as possible to the center of mass of the object  $C$ , as shown in figure 2.14b.
4. The area formed by the points where the force is applied  $\Delta_F$ , see figure 2.14c, should be up to  $\xi_o$ , which is a constant defined as a function of the maximal distance between the point of application of force.

The proposed steady grasp conditions, can be expressed as follows:

$$\begin{aligned} \sum_i f_i &= 0 \text{ and } \sum_i \tau_i = 0 \\ \varphi &= \arctan(\mu) \\ |C_N - C| &\rightarrow \varepsilon \\ \Delta_F &\rightarrow \xi_o \end{aligned} \quad (2.23)$$

where,  $f_i$  and  $\tau_i$  are the applied forces and torques with  $i$  fingers and  $\varepsilon$  is the maximal difference between the center of application of forces and the center of mass of the object.

On the basis of the above, we define the following criterion, to calculate the joint values required to position the robot in the desired grasp posture:

$$\begin{aligned} (\alpha, \beta, \theta) &= \arg \max_{\alpha, \beta, \theta} (\Delta_F) \\ \text{s.t } |C_N - C| &< \varepsilon, \Delta_F < \xi_o \end{aligned} \quad (2.24)$$

The rotations are performed using equation (2.1), while the values of  $\alpha$  or  $\beta$  are constant; then the rotations are formulated using SRQ as proposed in equation (2.20).

### 2.5.2 Modeling of the Robotic Hand Prosthesis Promain-I

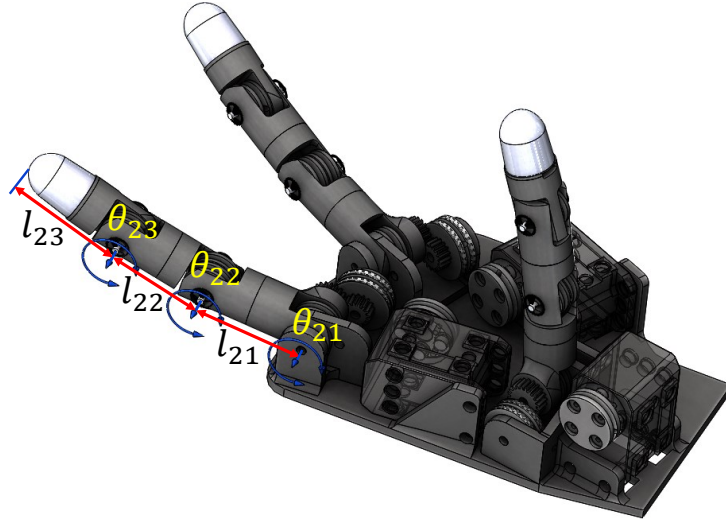
Taking into account that the hand is composed by three fingers, the kinematic model must be adapted. Thus, table 2.7 reports the notation that adapts the DHKK-SRQ model to the ProMain-I hand using a subindex  $i$  for the joints and a subindex  $j$  indicating the finger ( $j = 1$  for the thumb,  $j = 2$  for the index, and  $j = 3$  for the middle).

	Joint's frame	Phalanx length
<b>Finger</b>	MP ( $i = 1$ )	P ( $i = 1$ )
	PIP ( $i = 2$ )	M ( $i = 2$ )
	DIP ( $i = 3$ )	D ( $i = 3$ )
Thumb ( $j = 1$ )	$(x_{1i}, y_{1i}, z_{1i})$	$l_{1i}$
	$(\alpha_{1i}, \beta_{1i}, \theta_{1i})$ $(S_{1i})$	
Index ( $j = 2$ )	$(x_{2i}, y_{2i}, z_{2i})$	$l_{2i}$
	$(\alpha_{2i}, \beta_{2i}, \theta_{2i})$ $(S_{2i})$	
Middle ( $j = 3$ )	$(x_{3i}, y_{3i}, z_{3i})$	$l_{3i}$
	$(\alpha_{3i}, \beta_{3i}, \theta_{3i})$ $(S_{2i})$	

Table 2.7: Adopted notation for ProMain-I hand.

The rotation angles of the PIP and DIP joints are dependent on the rotation angle of the MP joint (under-actuated system). The relation between the angles is  $\theta_{j2} = \theta_{j3} = 0.9\theta_{j1}$ , where  $\theta_{j1}$  is the MP joint angle,  $\theta_{j2}$  is the PIP joint angle and  $\theta_{j3}$  is the DIP joint angle. Furthermore,  $l_{j1}$ ,  $l_{j2}$  and  $l_{j3}$  are the lengths of the proximal, medial and distal phalanges, respectively. Figure 2.15 shows these lengths and the joint angles for the index ( $j = 2$ ).

Before the fingers get in contact with objects, the movement is restricted to flexion-extension, and only rotations  $\theta_{ji}$  are required, in that condition DHKK convention is used. Parameters  $a_{ji}$  are defined as links' lengths, considering that  $a_{j1}$  is located at reference framework, its value is zero. Bearing in mind that each finger performs movements in two dimensions, parameters  $\alpha_{ji}$

Figure 2.15: ProMain-I Hand with angles  $\theta_{ji}$  and lengths  $l_{ji}$ .

and  $d_{ji}$  are zero. Table 2.8 summarizes the DHKK parameters of the ProMain-I hand used to model kinematics before contact.

Joint	Middle Finger				Index Finger				Thumb Finger			
	$\alpha$	$a$	$d$	$\theta$	$\alpha$	$a$	$d$	$\theta$	$\alpha$	$a$	$d$	$\theta$
1	0	0	0	$\theta_{31}$	0	0	0	$\theta_{21}$	0	0	0	$\theta_{11}$
2	0	$l_{31}$	0	$\theta_{32}$	0	$l_{21}$	0	$\theta_{22}$	0	$l_{11}$	0	$\theta_{12}$
3	0	$l_{32}$	0	$\theta_{33}$	0	$l_{22}$	0	$\theta_{23}$	0	$l_{12}$	0	$\theta_{13}$
$f$	0	$l_{33}$	0	0	0	$l_{23}$	0	0	0	$l_{13}$	0	0

Table 2.8: DHKK parameters for the ProMain-I Hand

The index  $f$  is used to describe the fingertip position. Consequently, the kinematics of our robot is entirely defined by the matrix  ${}^0[T]_f^j$ , which is a composition of the orientation  ${}^0[R]_f^j$ , and the position vector  $\{{}^0P_{jf}^x, {}^0P_{jf}^y, {}^0P_{jf}^z\}^T$ , as shown in equation (2.25):

$${}^0[T]_f^j = \prod_{i=1}^f {}^0[T]_i^j = \begin{bmatrix} & & & {}^0P_{jf}^x \\ & & & {}^0P_{jf}^y \\ & & & {}^0P_{jf}^z \\ 0 & 0 & 0 & 1 \end{bmatrix} \quad (2.25)$$

When extra rotations (different of  $\theta_{ji}$ ) are needed, those are formulated using quaternions. Concerning the  $i^{th}$  joint of the finger  $j$ , rotators  ${}^xU_{ji}$ ,  ${}^yU_{ji}$ , and  ${}^zU_{ji}$  are formulated for rotations  $\alpha_{ji}, \beta_{ji}, \theta_{ji}$  around axes  $x_{ji}, y_{ji}$  and  $z_{ji}$  respectively, using unit vectors  $\vec{x}_{ji}, \vec{y}_{ji},$  and  $\vec{z}_{ji}$  in the direction of axes  $x_{ji}, y_{ji}$  and  $z_{ji}$ , as follows:

$${}^xU_{ji} = \llbracket \cos(\alpha_{ji}/2), \vec{x}_{ji} \sin(\alpha_{ji}/2) \rrbracket \quad (2.26)$$

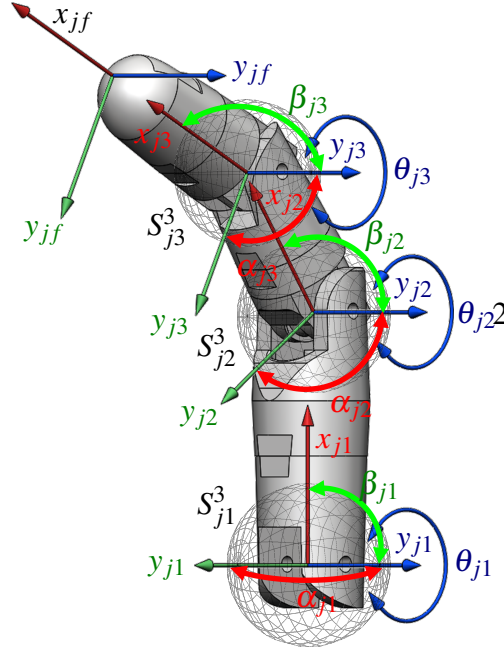


Figure 2.16: Kinematic model of the robotic finger with  $S_{ji}, x_{ji}, y_{ji}, z_{ji}, \alpha_{ji}, \beta_{ji}, \theta_{ji}$ .

$${}^y\mathbb{U}_{ji} = \llbracket \cos(\beta_{ji}/2), \vec{y}_{ji} \sin(\beta_{ji}/2) \rrbracket \quad (2.27)$$

$${}^z\mathbb{U}_{ji} = \llbracket \cos(\theta_{ji}/2), \vec{z}_{ji} \sin(\theta_{ji}/2) \rrbracket \quad (2.28)$$

On the other hand, to model soft rotation, we propose set of vectors  $\vec{r}_{ji} = d_{ji}\vec{x}_{ji}$  and the corresponding pure quaternions  $\mathbb{R}_{ji} = \llbracket 0, \vec{r}_{ji} \rrbracket$  that match direction, orientation, and length of the finger phalanges. The vectors  $\vec{r}_{ji}$  are formulated using the DHKK parameters  $[\alpha_{ji}, a_{ji}, d_{ji}, \theta_{ji}]$ , for the fingers  $j = 1, \dots, 3$  and the joints  $i = 1, \dots, 3$ . Subsequently, we formulate rotation as proposed in equation (2.20) using a global rotator  ${}^{xyz}\mathbb{U}_{ji} = {}^x\mathbb{U}_{ji} {}^y\mathbb{U}_{ji} {}^z\mathbb{U}_{ji}$ . As a result, we have a model where one hypersphere  $S^3_{ji}$  is added to each soft joint. In figure 2.16 the model DHKK-SRQ of one finger  $j$  of the hand is shown. The resulting expression for fingers rotation is as follows:

$$\llbracket 0, \vec{h}'_i \rrbracket = {}^{xyz}\mathbb{U}_i {}^h\mathbb{H}_i \overline{{}^{xyz}\mathbb{U}_i} \quad (2.29)$$

## 2.6 Dynamic model

The proposed dynamic model uses the principle of virtual displacements and virtual work [1]. The equivalent dynamic model of the finger is shown in Figure 2.17, where  $w_{j1}$ ,  $w_{j2}$  and  $w_{j3}$  are respectively the weights of the proximal, medial and distal phalanges of the finger  $j$ , and are placed at the coordinates of the centers of mass  $R_{j1} = (x'_{j1}, y'_{j1})$ ,  $R_{j2} = (x'_{j2}, y'_{j2})$  and  $R_{j3} = (x'_{j3}, y'_{j3})$ .  $F_j$  is the applied force that is equivalent to the reaction force, and  $C_{j1}$  is the input torque.

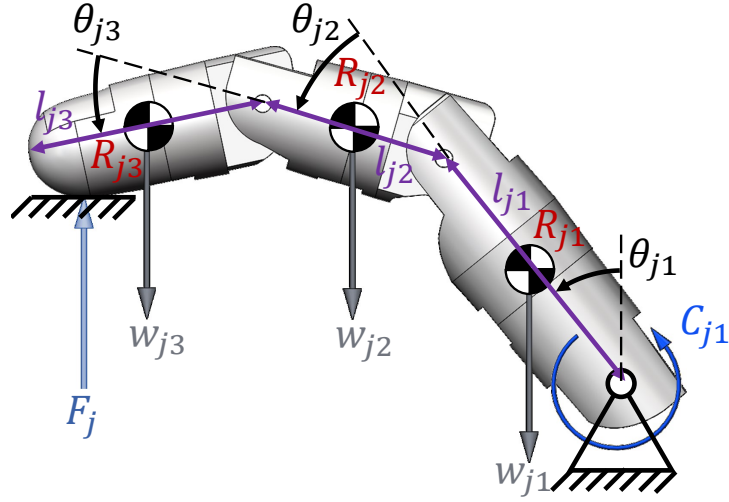


Figure 2.17: Dynamic model of the robotic finger.

The virtual work is calculated for the external forces (*i.e.*, weight, applied force and input torque) in equation (2.30) and the inertial forces (*e.g.*, centrifugal forces) in equation (2.31).

$$\{\delta W_e\} = \{Q_e\}^T \{\delta r_e\} \quad (2.30)$$

Where  $\{Q_e\}^T$  is the transposed external force vector and  $\{\delta r_e\}$  is the virtual displacement vector of the center of masses and the external forces  $F_j$  contact point.

$$\{\delta W_\lambda\} = ([M] \{\ddot{q}\})^T \{\delta r_\lambda\} \quad (2.31)$$

Where  $[M]$  is the diagonal mass matrix composed of the masses  $m_{ji}$  and inertias  $J_{ji}$ ,  $\{\ddot{q}\}$  is the second derivative with respect to time of the coordinates vector  $q$  representing the acceleration vector (see equation (2.32)), and  $\{\delta r_\lambda\}$  is the virtual displacement vector of the inertial frameworks.

$$\{q\} = \{x'_{j1}, y'_{j1}, \theta_{j1}, x'_{j2}, y'_{j2}, \theta_{j2}, x'_{j3}, y'_{j3}, \theta_{j3}\} \quad (2.32)$$

The dynamic equilibrium is given by Eq. (2.33), but as in our model the rigid bodies have movements restrictions, the displacements in the points where forces are applied aren't independent. In order to solve the equilibrium equation, considering the movements restrictions, it is necessary to separate dependent and independent coordinates.

$$\{\delta q\}^T ([M] \{\ddot{q}\} - \{Q_e\}) = 0 \quad (2.33)$$

The equation is simplified because only independent coordinates needs to be recovered. The simplification is performed using the transformation proposed as:

$$\{\delta q\} = [B] \{\delta q_{iu}\}, [B] = \begin{bmatrix} -[C_{qd}]^{-1} [C_{qi}] \\ \hline [I] \end{bmatrix} \quad (2.34)$$

where  $[C_{qd}]$  is the Jacobian of dependent coordinates,  $[C_{qi}]$  is the Jacobian of independent coordinates,  $\{\delta q_{ii}\}$  is the virtual displacement vector of the independent coordinates, and  $[I]$  is the identity matrix. The equilibrium is thus written as follows:

$$\{\delta q_{ii}\}^T [B]^T ([M] \{\ddot{q}\} - \{Q_e\}) = 0 \quad (2.35)$$

Solving equation (2.35), we obtain the input torque  $C_{j1}$  as a function of the force  $F_j$  and the kinematic variables  $\{q\}, \{\dot{q}\}, \{\ddot{q}\}$ . The resulting expression is:

$$C_{j1}(F_j, \{q\}, \{\dot{q}\}, \{\ddot{q}\}) = \frac{H_0 - 4l_{j1} \sin(\theta_{j1}) H_5 + 8(l_{j2} \sin(\theta_{j2}) - 4)(H_6 + H_8)}{8l_{j2} \sin(\theta_{j2}) - 32} \quad (2.36)$$

where

$$H_0 = 2l_{j1}^2 \ddot{\theta}_{j1} \sin(\theta_{j1})^2 [(m_{j1} + m_{j2}) l_{j2} \sin(\theta_{j2}) - 4m_{j1} - 6m_{j2}]$$

$$H_1 = (1/4) l_{j1} l_{j2} m_{j2} \ddot{\theta}_{j1} \cos(\theta_{j1}) \cos(\theta_{j2}) - (1/2) l_{j2}^2 m_{j2} \ddot{\theta}_{j2} \sin(\theta_{j2})^2 - 4gm_{j1}$$

$$H_2 = (1/4) (m_{j2} + 2m_{j3}) l_{j2}^2 \ddot{\theta}_{j2} \cos(\theta_{j2})^2 + 2l_{j3} m_{j3} \ddot{\theta}_{j3} \sin(\theta_{j3}) + 2J_{j2} \ddot{\theta}_{j2}$$

$$H_3 = (1/2) l_{j2} \cos(\theta_{j2}) (l_{j3} m_{j3} \ddot{\theta}_{j3} \cos(\theta_{j3}) + m_{j2} \ddot{y}'_{j1} + 2m_{j3} \ddot{y}'_{j2})$$

$$H_4 = l_{j2} \sin(\theta_{j2}) (gm_{j1} - 2F_j + (2g + 3\ddot{\theta}_{j2} + \ddot{x}'_{j1}) m_{j2} + (g + 2\ddot{\theta}_{j2}) m_{j3})$$

$$H_5 = H_1 + H_2 + H_3 + H_4 + 8F_j + (-6g - 6\ddot{x}'_{j1}) m_{j2} + (-4g - 4\ddot{x}'_{j2}) m_{j3}$$

$$H_6 = (1/4) (m_{j1} + 3/2m_{j2}) l_{j1}^2 \ddot{\theta}_{j1} \cos(\theta_{j1})^2 + J_{j1} \ddot{\theta}_{j1}$$

$$H_7 = (m_{j2} + 2/3m_{j3}) l_{j2} \ddot{\theta}_{j2} \cos(\theta_{j2}) + 2m_{j2} \ddot{y}'_{j1} + 4/3m_{j3} \ddot{y}'_{j2}$$

$$H_8 = (3/8) l_{j1} \cos(\theta_{j1}) ((2/3) l_{j3} m_{j3} \ddot{\theta}_{j3} \cos(\theta_{j3}) + H_7)$$

## 2.7 Discussion

In this chapter, we have introduced the design and modeling of ProMain-I robotic hand prosthesis prototype. The robot aims to perform precision grasping with three fingers and uses a new soft epicyclic driving mechanism. The driving device attempts to mimic the human muscle behavior described by the proposed Hill-based model.

Taking into account that the joints have a low stiffness due to the utilization of tendons, the hand is considered to have a soft behavior. Consequently, we have introduced a new hybrid kinematic model, so-called DHKK-SQR, that is parametrizable according to the available instrumentation. The main advantage of our kinematic model is the ability to formulate several rotations that could or could not be planned. Furthermore, the methodology can be parametrizable including virtual rotation axes that can be inside or outside of the robot's geometry. Moreover, the model is not sensitive to singularities because it is based on the formulation of rotations using quaternions.

On the other hand, we introduce a dynamic model; which is helpful to complete the development of the robot modeling and allows to measure and states the requirements regarding torque consumption of the robot for a specific requirement of force. In the following chapter, we

describe the experiments developed to test the finger and validate the ProMain-I hand grasping capabilities. For those test, both dynamic and kinematic models are used.



## Chapter 3

# Mechatronic assessment of the prosthetic hand

The utilization of smart and soft materials has led to the development of new adaptive devices known as soft robots [5] that use flexible and smart materials to enhance functionalities adding new characteristics up to now not present in robots. The main advantage offered by the soft robotics in the dextrous manipulation is the adaptation capacity, which allows the robotic hand to be used in several uncertain grasping situations. However, it implies to undertake several challenges, *e.g.* concerning the smart materials for artificial muscles, relevant studies are currently being carried out to develop new actuation strategies, even so, technologies are still far from implementation in robotics [111]. Nevertheless, we consider that the current gap between smart materials and robotics can be reduced or eliminated improving mechanic of robots and bounding the problem with the real application requirements.

In the particular case of robotic hands prosthesis, the challenge is to provide a device suitable for daily living and working activities. Thus, the actuation requirements must arise from the following milestones: i) the operating conditions that are drawn from the human hand functionalities and features and ii) the defined actuation specifications that are based on the mechanic assessment of robotic hand. Both elements are crucial to achieve a smart material based actuation solution that satisfies the requirements of a hand prosthesis.

Concerning the first milestone, operating conditions are introduced in chapter 1, in which functionalities and features of the human hand were studied and defined. Regarding the actuation specifications coming from the robotic hand, we need to evaluate the robotic hand ProMain-I (designed to perform the most practiced human precision grasping gestures) that was presented in chapter 2. To define the actuation specifications, we use both experimental results and the kinematic and dynamics models introduced in chapter 2; the kinematic model is the so-called DHKK-SRQ model. The proposed kinematic model takes into account the possible additional degrees of freedom arising from the soft behavior of the robots. Consequently, in the following we present several experiments aiming to: i) validate the DHKK-SRQ model, ii) evaluate mechanical features of the robot, and iii) extract actuation requirements. Figure 3.1 explains the

relationship between the experiments presented in this chapter.

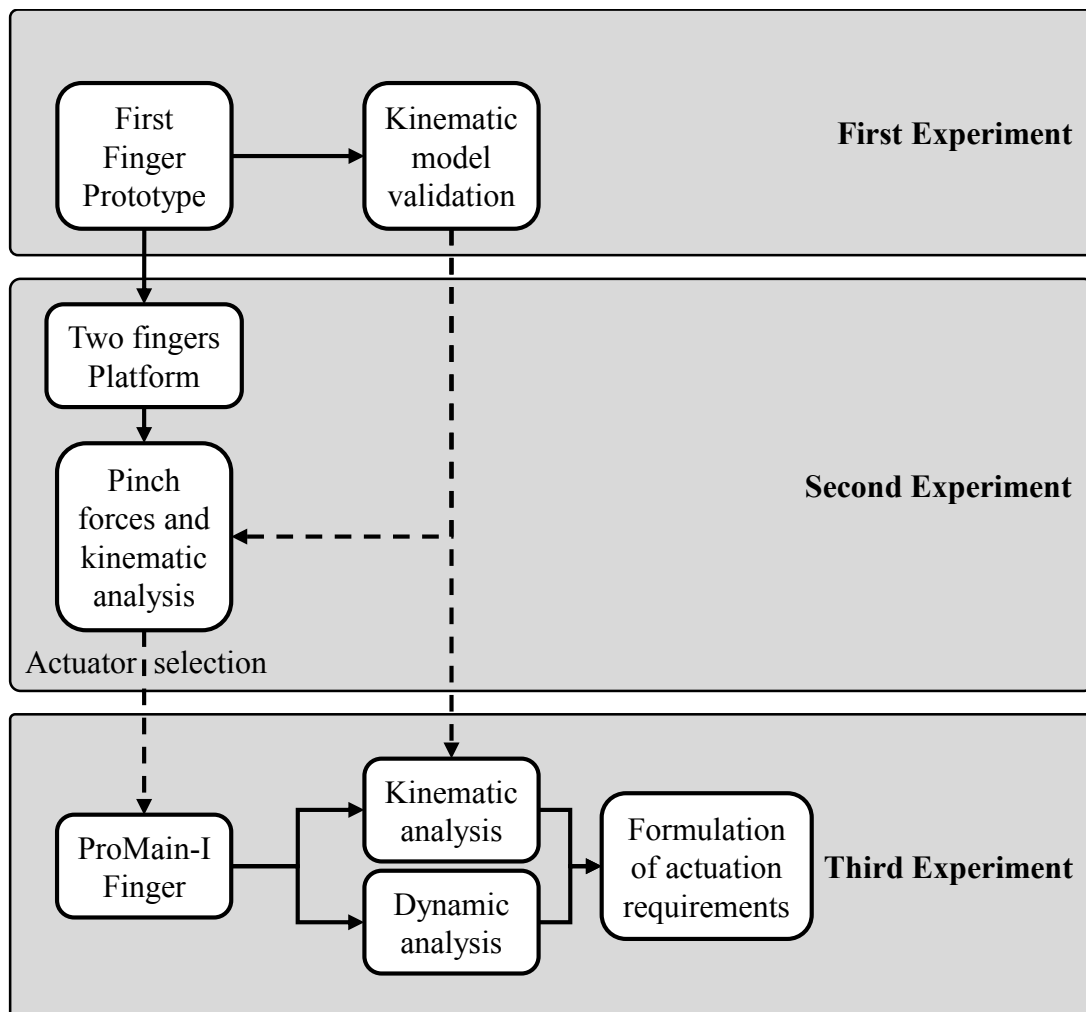


Figure 3.1: Relationship between the experiments

A common experimental set-up is proposed to measure kinematic and forces of the experimental finger prototypes. Thus, in sections 3.1, 3.2, 3.4 and 3.5 we introduce the experimental set-up and the three experiments. Then, we present a generalized methodology to define the requirements of artificial muscles for robotic hands. The method takes into account the human hand capabilities to establish the range and operation limits of the actuator considering the influence of mechanical and functional characteristics of the robotic hand.

### 3.1 General experimental set-up

Considering that the finger prototypes are designed to perform flexion and extension in two dimension, the kinematic is measured using a camera (Canon EOS 600D) to track circular markers placed in finger joints and fingertip. The camera is positioned at 1m from the finger prototype and is adjusted to assure a pixel size of  $0.17 \times 0.17$ mm. The position accuracy

(measured comparing several static images with a known value of length) is 0.51mm.

Images coming from the camera are processed to automatically recognize circular markers. The image analysis follows these Four main steps: (i.) Crop image to extract the finger working area, see 3.2a (ii.) transform image into a gray scale, see Figure 3.2b, (iii.) shift image into a black and white scale, see Figure 3.2c, (iv.) detect image edges, see Figure 3.2d, and (v.) apply Hough transform [139] to find the circles positions in the image, see Figure 3.2e.

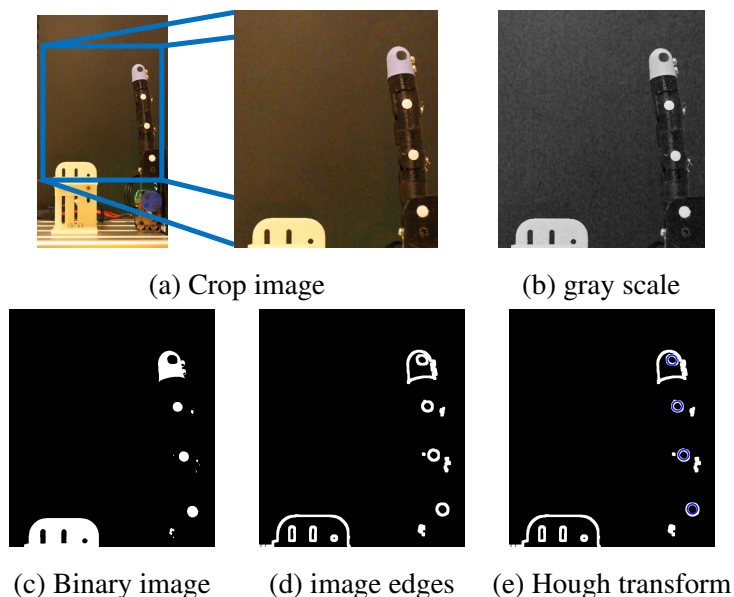


Figure 3.2: Automatic detection of finger joints and fingertip position

Taking into account that digital images are composed by pixels, which are formed by a combination of primary colors organized in three channels red ( $R$ ), green ( $G$ ), and blue ( $B$ ), the gray scale  $L$  channel of the image is calculated as the average of the color components. However, both  $R$  and  $G$  channels are brighter than  $B$ , so that, using a simple average the resulting  $L$  will appear to be too dark in the red and green areas and too bright in the blue ones. Therefore, a weighted sum of the color components is used to compute the gray scale equivalent as presented below in equation (3.1). The coefficients that multiply  $R$ ,  $G$ , and  $B$  were originally proposed for encoding analog color television signals and are chosen to avoid information saturation (due to bright) while the image is transformed into black and white scale.

$$L = 0.2989R + 0.5870G + 0.1140B \quad (3.1)$$

Thereafter, the gray scale image is binarized to obtain a black and white image, which is processed using a Canny filter [140] to automatically detect image borders; in this step the markers appear to be circles with white borders, see figure 3.2d. Finally, the circular Hough's transform is applied to obtain the coordinates of each circle in the image, circles positions correspond to the joint and fingertip coordinates. The image analysis is repeated for the sequence of images stored during flexion and extension tests. Figure 3.3 shows four sample images of a flexion cycle.

The image analysis delivers the position vectors of the joints, *i.e.* the vectors  $\{^0P_{j1}^x, ^0P_{j1}^y, 0\}^T$  for the MCP joint of the finger  $j$ ,  $\{^0P_{j2}^x, ^0P_{j2}^y, 0\}^T$  for the PIP joint and  $\{^0P_{j3}^x, ^0P_{j3}^y, 0\}^T$  for the DIP joint. Likewise the vectors  $\{^0P_{jf}^x, ^0P_{jf}^y, 0\}$  correspond to the fingertip positions. Considering that the movement is performed in the  $xy$ -plane,  $^0P_{ji}^z$  is always zero. The angles are measured as shown in figure 3.4, following the DHKK parameterization.

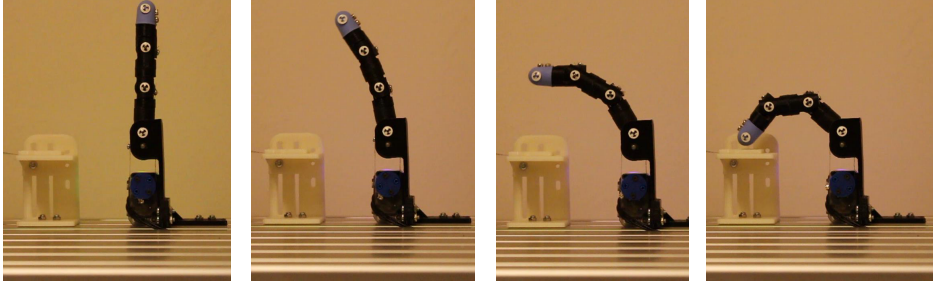


Figure 3.3: Positions of the robotic finger articulations during flexion

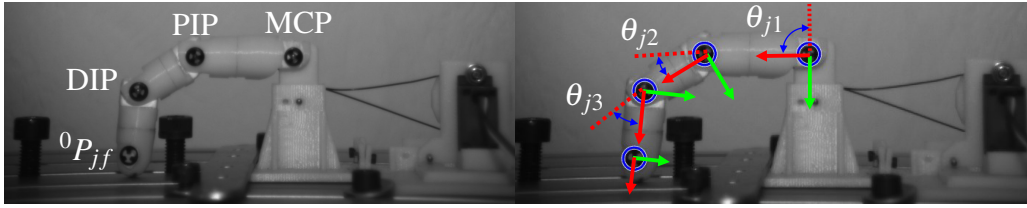


Figure 3.4: Angles and final position measure

Thereafter, the following three vectors linking joints are defined: i) vector  $\vec{r}_{j1}$  between the MCP and PIP joints, ii) vector  $\vec{r}_{j2}$  between the PIP and DIP joints, and iii) vector  $\vec{r}_{j3}$  between the DIP joint and fingertip. These vectors are used to calculate rotation angles  $\theta_{ji}$  as:

$$\theta_{ji} = \arccos \left( \frac{\vec{r}_{ji} \cdot \vec{r}_{ji-1}}{\|\vec{r}_{ji}\| \|\vec{r}_{ji-1}\|} \right) \quad (3.2)$$

The first angle  $\theta_{j1}$  is calculated with respect to a reference positive vertical unitary vector  $\vec{r}_{j0} = 0, 1, 0$ , figure 3.5 shows the vectors  $\vec{r}_{ji}$ , the joints and fingertip position, and the location of  $\theta_{ji}$ .

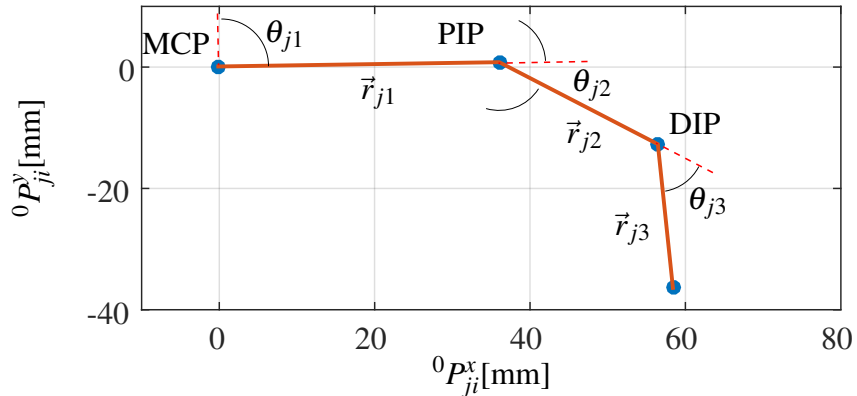


Figure 3.5: Interpretation of measured kinematic data.

Moreover, the force applied on the fingertip is evaluated using a resistive-based force sensor Flexiforce®, that measures up to 5N, connected to a circuit that uses an inverting operational amplifier arrangement to produce an analog output based on the sensor resistance, the output voltage is registered with a digital oscilloscope. The sensor was calibrated in the range 0.6N to 4.8N, and placed on a support (platform) which is located in the trajectory of the fingertip. Furthermore, We developed software that controls the finger's position and speed. Force and kinematic data of prototypes are synchronized and stored during the desired number of flexion and extension trials. The global setup of the experiment is shown in figure 3.6.

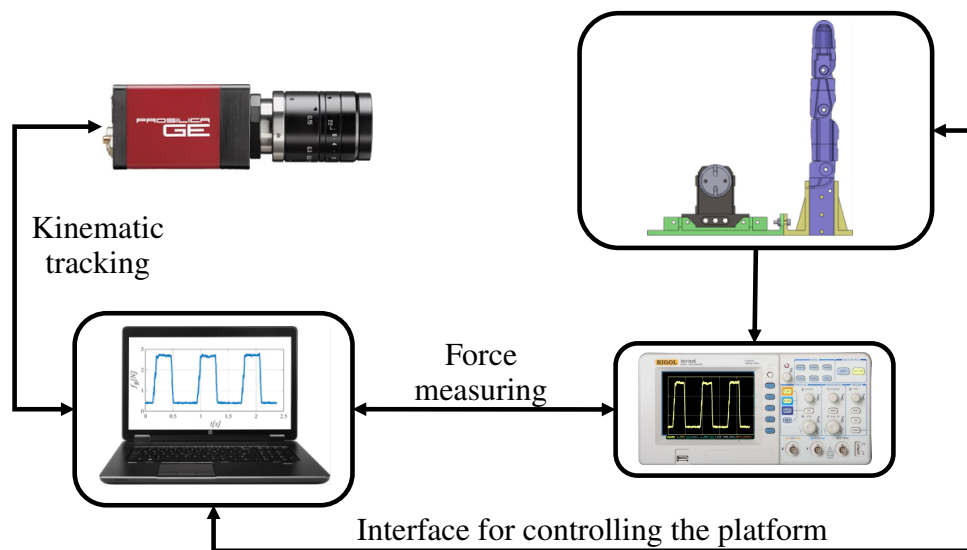


Figure 3.6: Experiment Set-up

## 3.2 Validation of kinematic model DHKK-SRQ

In the first stage, we carried out a test with the first tendon driven finger prototype, introduced in section 2.3, which has three phalanges and is actuated by only one servomotor. The finger has rigid joints but due to the soft driving mechanism, it mechanically self-adjusts the articulation when is needed, this behavior can be considered as soft.

The aim of the test is to implement and try out our hybrid modeling method DHKK-SRQ. Therefore, we design a platform aiming to: i) measure the kinematics of the finger, and ii) measure the robotic fingertip force.

Furthermore, the experiment is performed using several servomotors to evaluate the influence of actuator in the mechanism performance. The experiment is carried out using an experimental platform that allows to swap actuators. For that purpose, the position of the finger can be vertically adjusted guaranteeing that the actuator is aligned with finger's MCP joint. The CAD model of the test platforms are shown in figure 3.7.

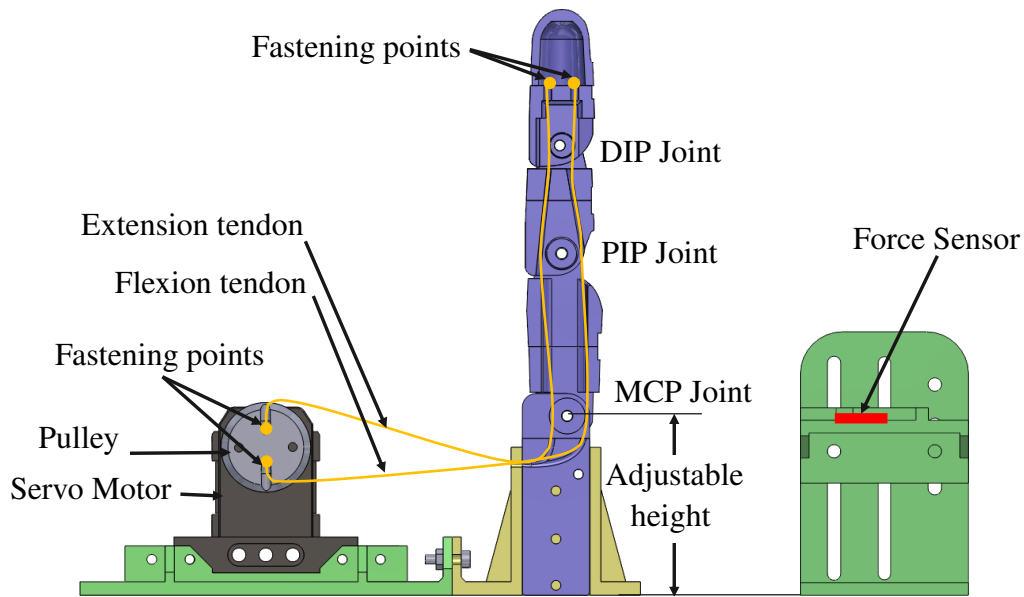


Figure 3.7: CAD Model of the test platform

The measured kinematic data is computed to calculate the joint angles  $\theta_{ji}$  as explained in equation (3.2). The angles are used to feed DHKK and DHKK-SRQ methods and compute fingertip position through direct kinematic analysis. The data issued from both kinematic methods is compared with the measure of fingertip position and the absolute error is computed. In DHKK-SRQ, the measured force is used as a flag indicating when quaternions must be used to formulate rotations. Figure 3.8 shows the work flow of the experimental validation

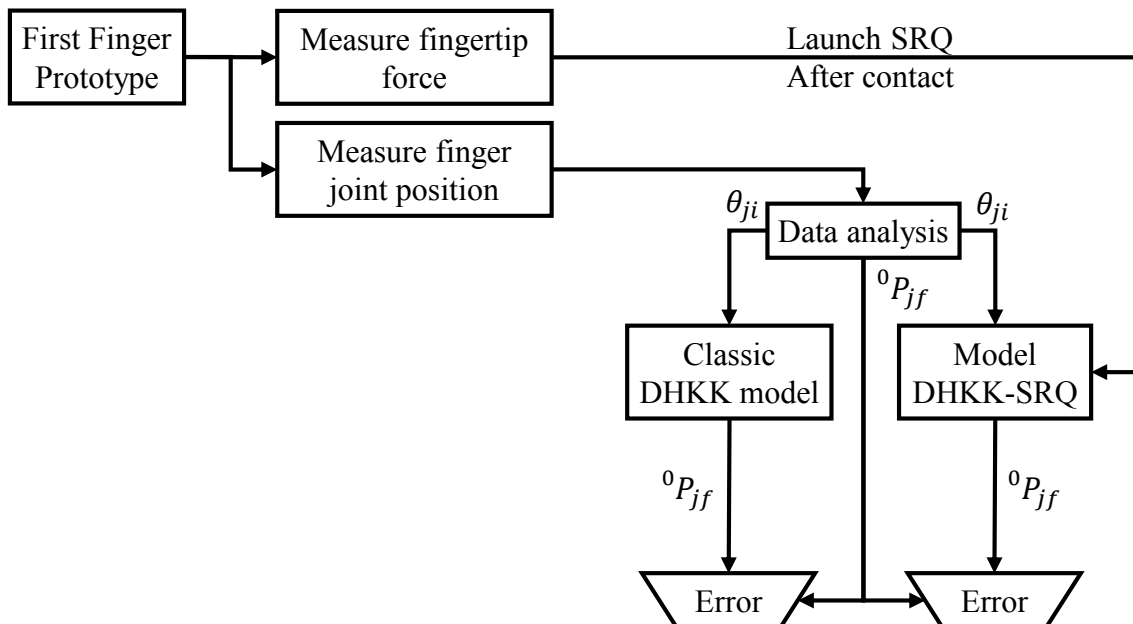


Figure 3.8: Work flow of the kinematic method error estimation.

The experiments are performed using two standard servo motors HS-422 and Traxxas 2065 with torques of  $0.324Nm$  and  $0.225Nm$  respectively, and three serial servo motors Dynamixel

XL-320 and AX-12a with torques of  $0.390Nm$  and  $1.50Nm$  respectively. The finger is configured to perform five trials of flexion-extension movements for each servomotor. Figure 3.9 shows an example of the kinematic data measured using the HS-422 servo motor.

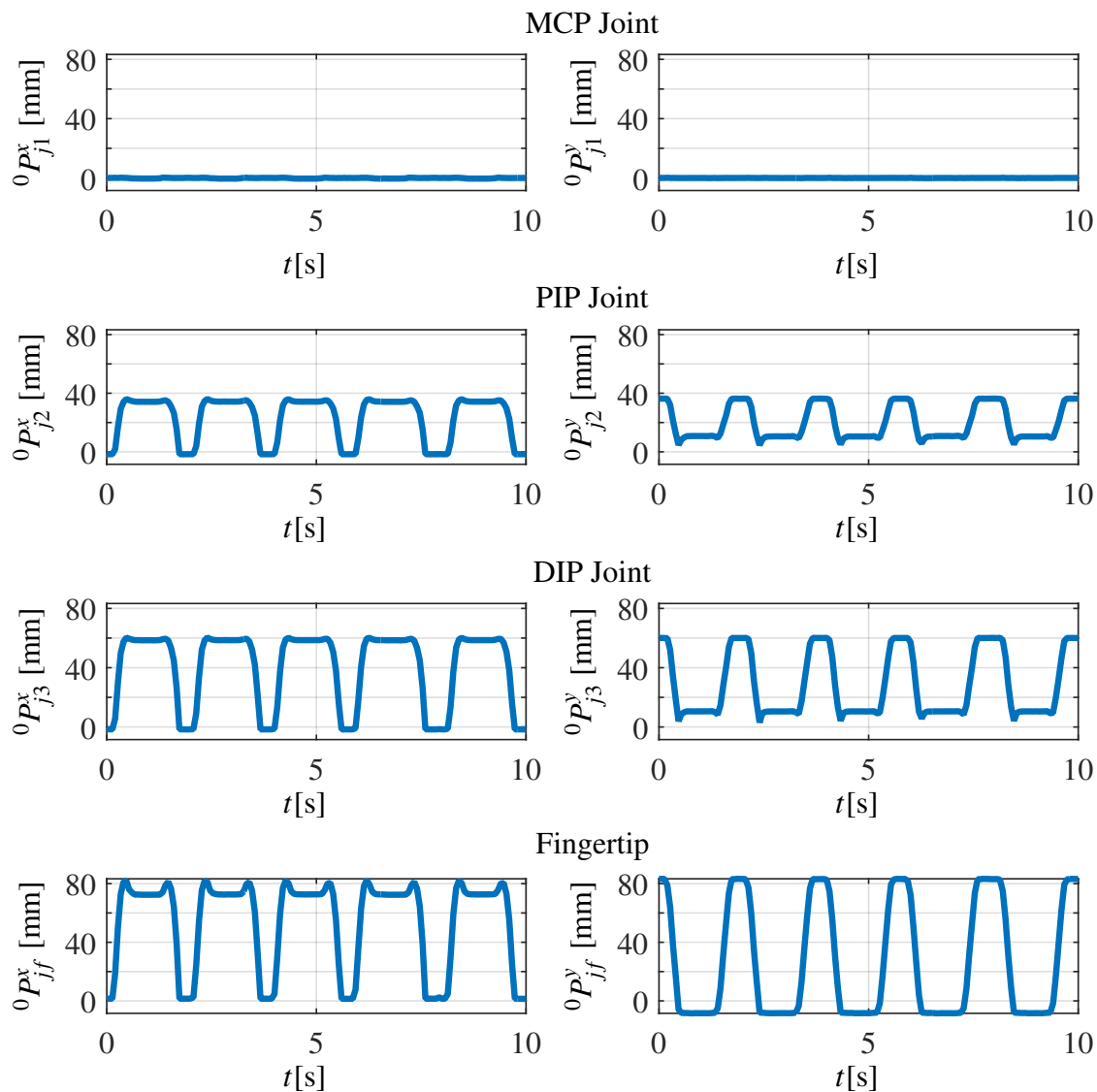


Figure 3.9: Results of the position tracking using the HS-422 servo motor.

The error comparison is summarized in table 3.1. Our kinematic model (DHKK-SRQ) presents better result than the DHKK model, as it produces smaller errors (even if the difference is not huge). The error of our method is lower because after getting in contact with the object, the DHKK-SRQ is launched and the mechanical slack of the finger is modeled as angles  $\alpha_{ji}$  and  $\beta_{ji}$ . The error reduction is more important for the final model of the ProMain-I hand, which is subject to unexpected rotations ( $\alpha$  and  $\beta$ ) due to the soft epicyclic mechanism.

Actuator	DHKK-Error [mm]	DHSKK-SRQ-Error [mm]	Fingertip force [N]
HS-422	2.0438	1.7927	2.19
Traxxas 2065	0.6929	0.4206	1.19
AX-12a	1.8032	1.3900	3.21
XL-320	2.2647	2.2300	2.10

Table 3.1: Mean absolute position error and fingertip force.

Moreover, this experiments allow us to compare forces performed by different actuators under the same conditions (actuators' rotation and angular speed are fixed to be the same). Concerning the force to size ratio, the best actuator is the TR-2065 followed by the XL-320, the HS-422 and the AX-12a. However, the amount of force produced by the TR-2065 is low making the HS-422 and the XL-320 servomotors the best option to actuate the hand.

### 3.3 Robotic finger pinch force

With the objective of establishing the actuation requirements to mimic the human precision grasping with a robotic hand, we design a test platform. The platform consists of two fingers whose tips are brought together, and is used to measure kinematic and pinch force applied by the robotic fingers. The CAD model of the test platform is shown in Figure 3.10. Considering that the goal is to estimate the performance of a robotic finger mechanism regarding pinch force during grasping, the experiment can be executed using any actuator. Therefore, we use a standard servo motor HS-422 whose maximal torque is  $\tau = 0.324Nm$ .

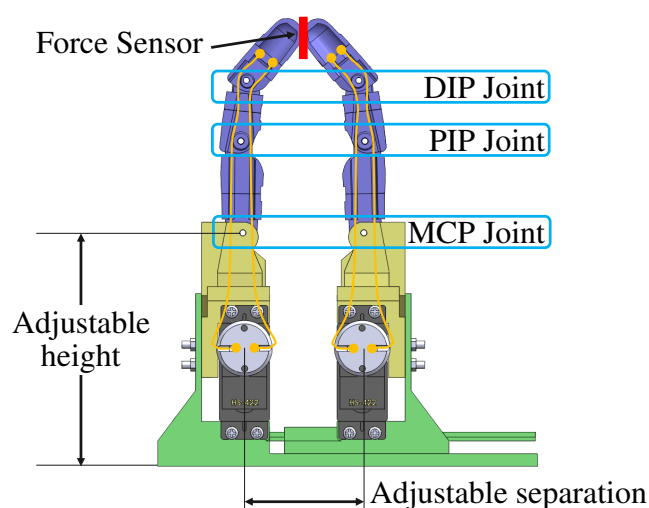


Figure 3.10: CAD Model of the pinch force test platform.

The same experimental setup presented in section 3.1 is used, but the force sensor is placed on the trajectory of the fingertip, see figure 3.10. To evaluate the influence of the finger location

during grasping, The tests are conducted increasing distances between fingers (50, 55, 60 and 65mm). For each distance the test is carried out five times. Table 3.2 shows the measured grip force.

Distance [mm]	Mean pinch Force [N]	Standard deviation [N]
50	4.02	0.02
55	4.62	0.08
60	4.70	0.05
65	3.54	0.06

Table 3.2: Mean pinch force (two-finger platform).

The results show that the applied force changes in function of the fingers position. The higher pinch forces is measured when the distance between fingers is set to 5.5 and 6.0 cm. Furthermore, the amount of force, performed during the pinch experiment, is close to the lower limit of the human pinch force. As a consequence, both the HS-422 and XL-320 actuators (which has similar torque capacity) are suitable to be used in precision grasping applications in a robotic hand. Consequently, the XL-320 servo motor is chosen as actuator for the ProMain-I finger mechanism.

### 3.4 Kinematic and force of the ProMain-I finger

The experiment carried out with the ProMain-I finger aims to measure displacement and force. The information obtained experimentally is used to feed the kinematic and the dynamic models to define actuation requirements. Furthermore, we compare the expected rotation relations fixed in the soft epicyclic mechanism and the measured ones to verify the behavior of the finger. We follow the same experimental protocol introduced in section 3.1. The position vectors  ${}^0P_{ji}^x$ ,  ${}^0P_{ji}^y$  and  $\theta_{ji}$  are measured using a single-finger platform shown in Figure 3.11.

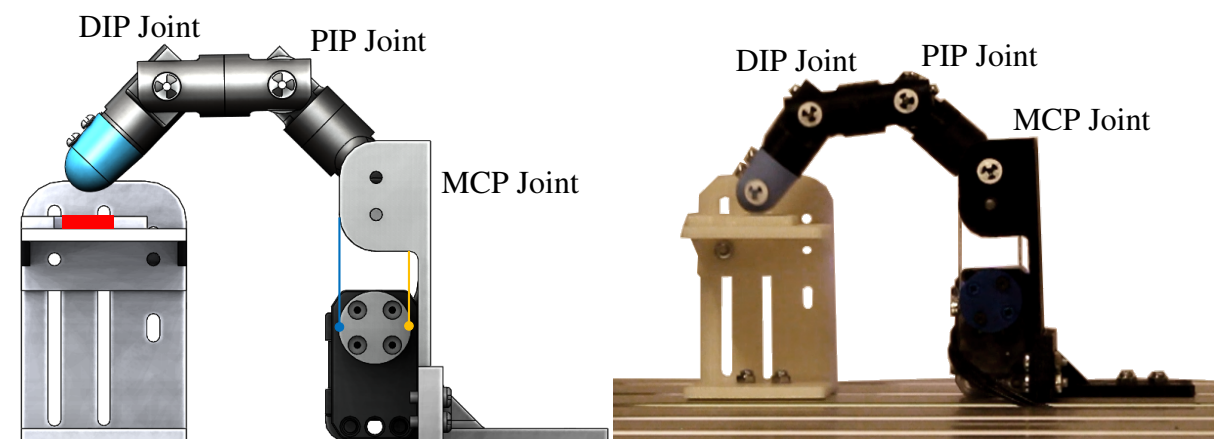


Figure 3.11: ProMain-I finger test platform.

The kinematic measured using ProMain-I fingers is presented in figure 3.12, the MCP joint was expected to be at zero because it is considered fixed to frame. Even that, standard deviation of the MCP joint position is  $0.4733mm$  due to the flexibility of actuator support. Likewise, the standard deviation of the PIP and DIP joints measures are  $0.1848mm$  and  $0.5598mm$  respectively. The standard deviation of the fingertip measures is  $1.6069mm$ .

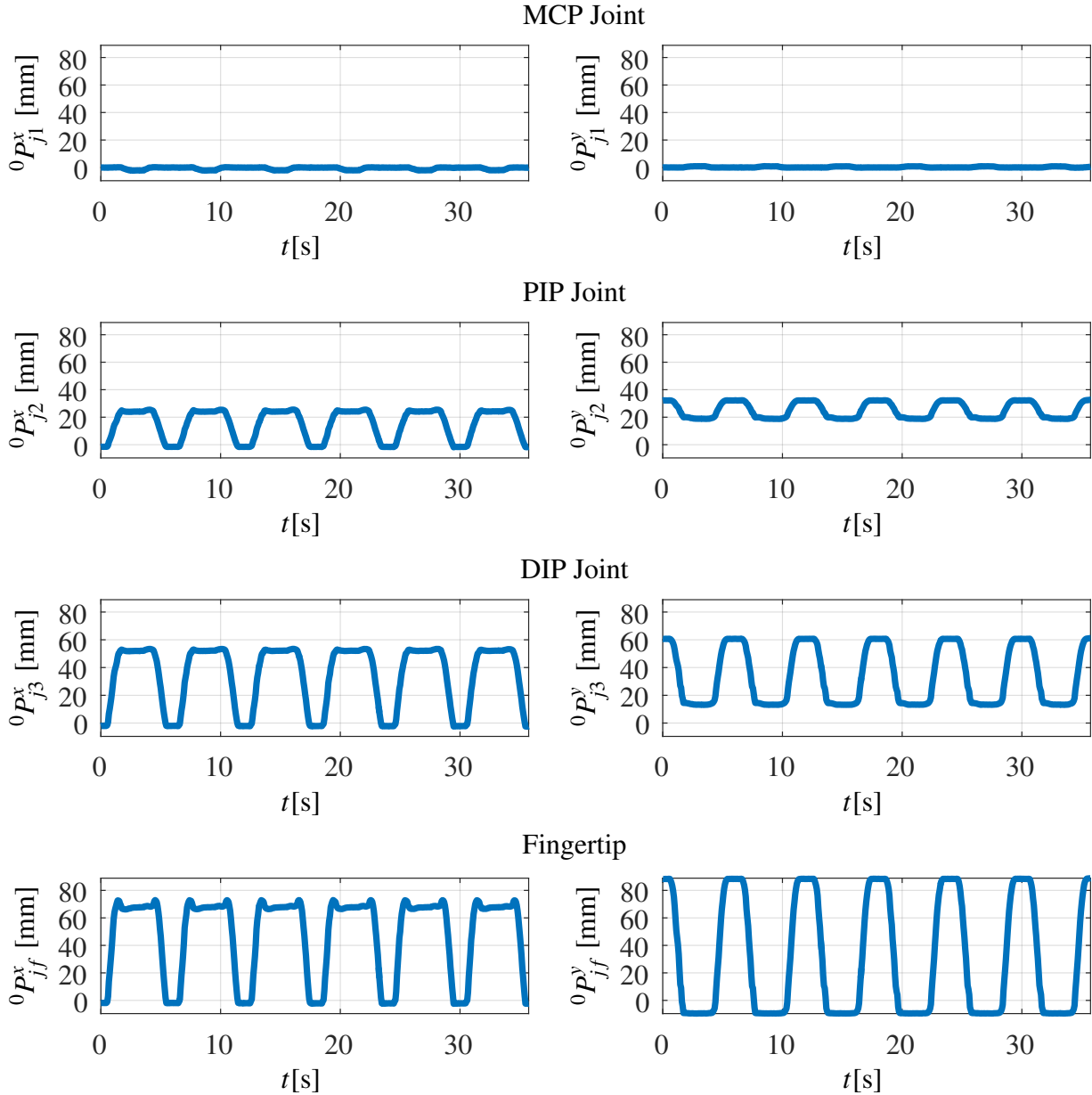


Figure 3.12: Results of the position tracking of ProMain-I finger.

The calculated PIP and DIP joint angles, see figure 3.13, shows a under-damped behavior for the PIP and the DIP joints when the finger gets in contact with the platform where the force sensor is placed. To evaluate the mean absolute error of the PIP and DIP joint angles, we compare the angle value obtained from the kinematic measure with the calculated angle value issued from the relation  $\theta_{j2} = \theta_{j3} = 0.9 \theta_{j1}$  formulated in section 2.4.

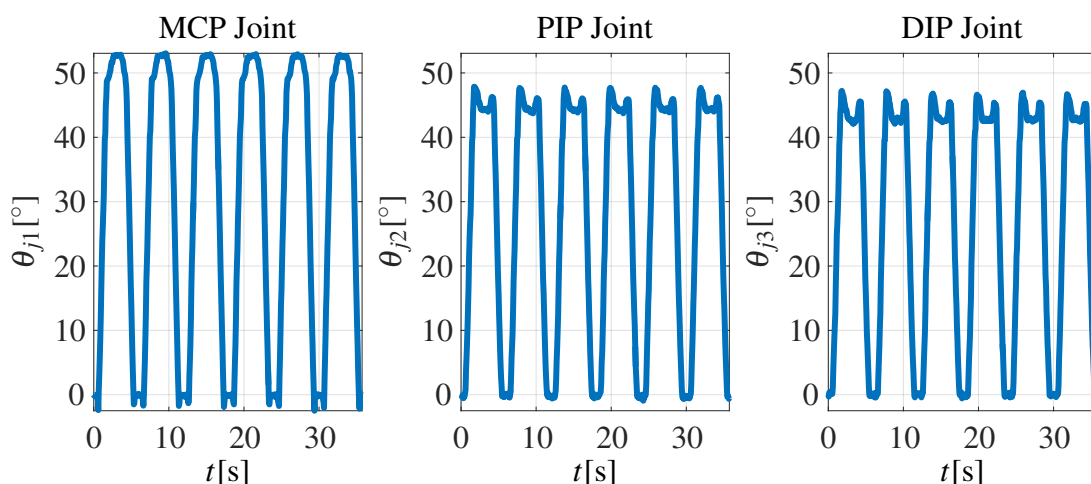


Figure 3.13: Results of the position tracking of ProMain-I finger.

As a result, we find that the mean absolute error of the angle  $\theta_{j_2}$  is  $2.21^\circ$ , and the standard deviations is  $1.2206^\circ$ . With respect to the angle  $\theta_{j_3}$  of the DIP joint, the mean absolute error is  $2.6235^\circ$ , and the standard deviations is  $1.6370^\circ$ . Moreover, the probability density function of PIP joint's absolute error presents two peaks values; the first shows a concentration around zero degrees that correspond to the error during free movement, and the second is the error when the finger gets in contact with the object. Likewise, the probability density function of DIP joint's absolute error presents three peaks values the first around zero degrees during free movement and the two others during the contact phase. Both probability density functions are presented in figures 3.14 and 3.15, in which red lines represent median, cross is mean, a blue box represent the 25% and 75% quartiles and whiskers bound 9% and 91%.

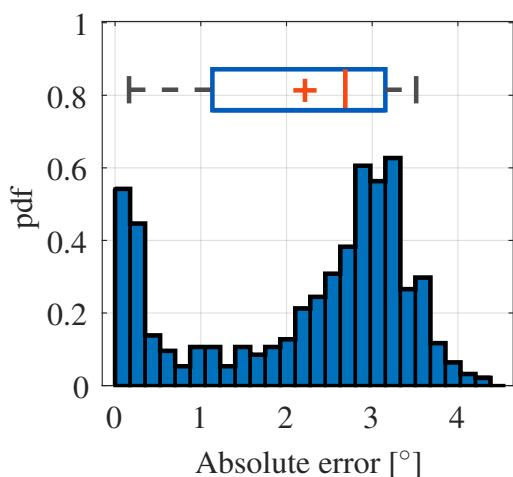


Figure 3.14: Probability density function of  $\theta_{j_2}$  absolute error.

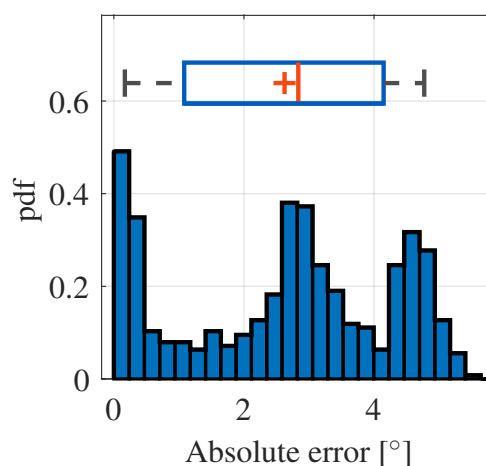


Figure 3.15: Probability density function of  $\theta_{j_3}$  absolute error.

These errors present in the articular joint values  $\theta_{j_2}$  and  $\theta_{j_3}$  is the result of the self adaptability of the finger to objects during grasping. This effect is the result of the low stiffness

of tendons used in the soft epicyclic mechanism. Another important analysis of the kinematic data consists in obtaining the position of the finger's center of masses. This information is further required to process the dynamic of the finger. The proposed dynamic model, requires the vector  $q$ , which corresponds to the dependent and independent coordinates of the robot and is composed as shown in Eq. (2.32). Taking into account that the orientation of the framework  $(x_i, y_i)$  is the same of the center of masses  $(x'_i, y'_i)$ , we use the relations  $x'_i = x_i + l_i \cos \theta_i/2$  and  $y'_i = y_i + l_i \sin \theta_i/2$  to calculate the vector  $q$ . Figure 3.17 shows the position of  $R_{j2}$  with respect to the framework  $(x_{j2}, y_{j2}, z_{j2})$ . Figure 3.16 show the calculated position of center masses  $R_{ji} = (x'_{ji}, y'_{ji})$ , in which clearly the two upper plots are not more zero because corresponds to the position of center of mass of proximal phalanx (PP). Likewise, the under-damped behavior is still present in the DIP joint and fingertip positions.

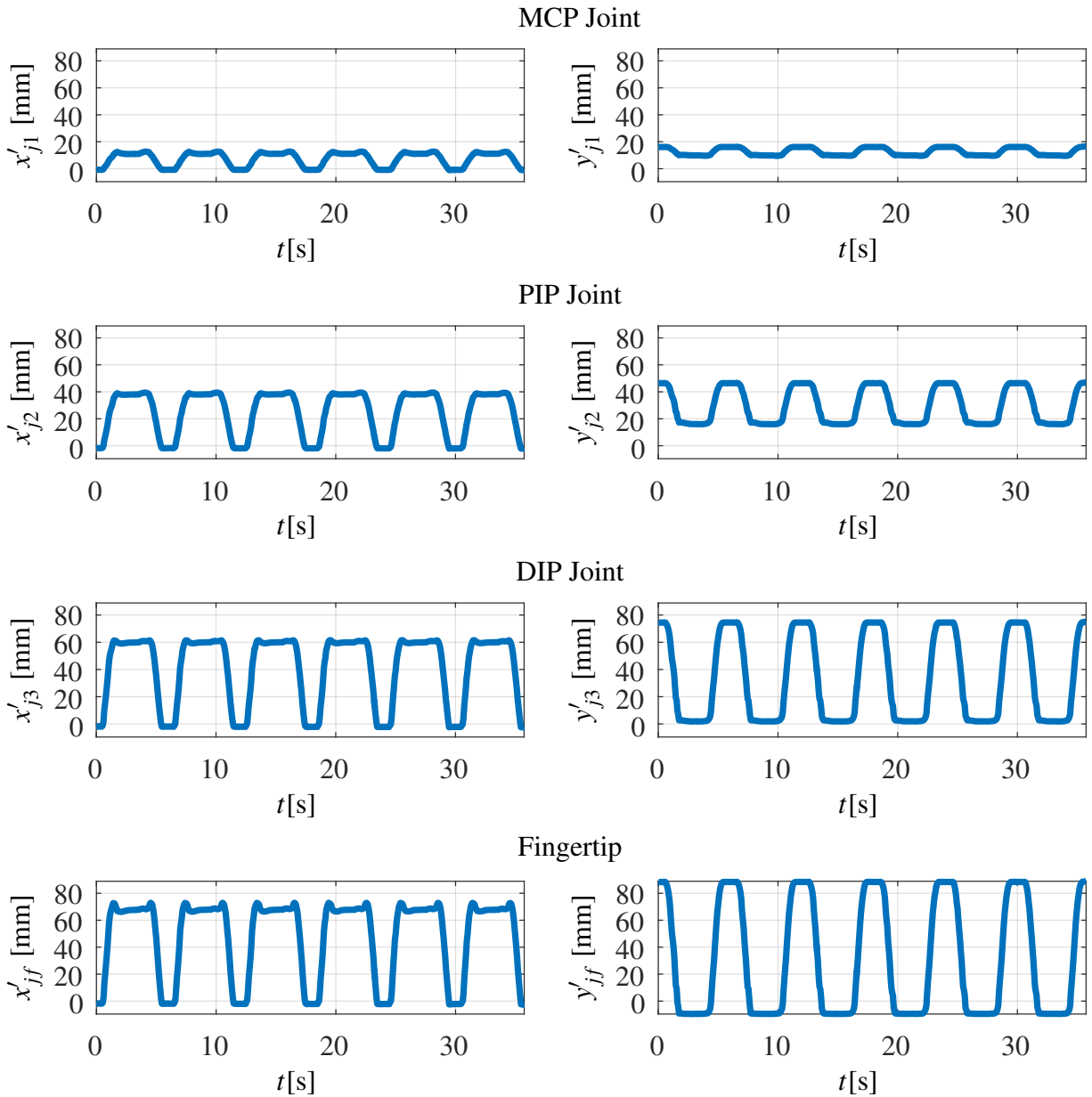


Figure 3.16: Calculated position of center masses  $R_{ji} = (x'_{ji}, y'_{ji})$ .

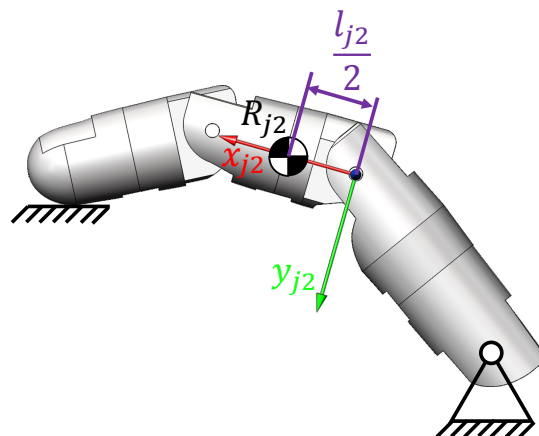


Figure 3.17: Position of  $R_{j2}$  with respect to the framework  $(x_{j2}, y_{j2}, z_{j2})$ .

Regarding the force, the measured mean value is 1.3289N with a standard deviation of 0.0671N. It is important to note that a under-damped behavior appears during all the trials. Thus a maximal overshoot of 1.4284N was reported during the experiments. Figure 3.18 shows the absolute frequencies of the measured forces during contact with the measure platform.

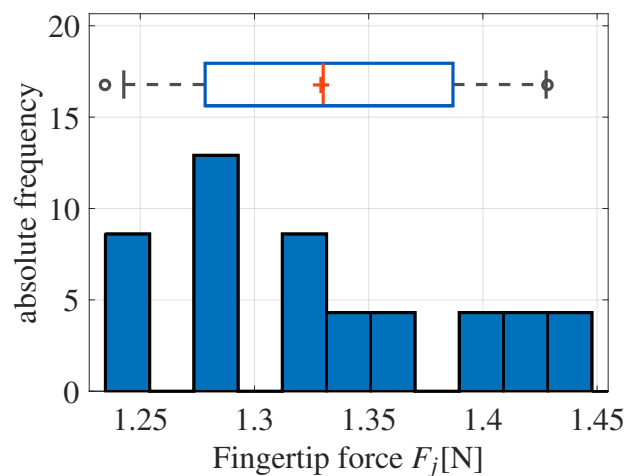


Figure 3.18: Measured fingertip force  $F_j$  during contact.

### 3.5 Artificial muscle design methodology

The main features of a smart material based actuator are the force  $f_a$ , the active strain  $\varepsilon$  and the frequency  $\omega_n$ . Thus, we need to define these characteristics for the artificial muscle. Considering that our goal is to design a robotic hand that will be able to mimic human precision grasping movement, the actuator features can be established from measures and analysis of the human hand, introduced in chapter 1. However, it is important to take into account that the robotic finger mechanism can modify the actuator requirements. Consequently, the proposed approach, to identify the artificial muscle requirements, is defined by three types of measures:

i) the human pinch force introduced in section 1.3.3, ii) the settling time of the human force also introduced in section 1.3.3, and iii) the kinematic and dynamic behavior of the robotic finger ProMain-I, measured in section 3.4. We propose a general methodology which aims at designing smart material based actuators for particular applications. This methodology is based on the following four stages:

1. **Application requirements modeling:** in this phase the main parameters and the relationships between them are modeled, allowing to establish the operating conditions of the actuators.
2. **Experimental identification of parameters:** once the key parameters and their relationships have been modeled, it is necessary to carry out an experiment. The experimental protocol is designed in agreement with proposed models, to measure the required parameters.
3. **Parameters quantification:** Experimental data must be analyzed using the defined models to characterize the artificial muscle and quantify operational limits of the actuator.
4. **Material selection:** finally, the retrieved information is used to approximate the actuator dynamic behavior, allowing the selection of a smart material that fits the application requirements.

### 3.5.1 Particularized methodology for robotic fingers

In our case we are focused in artificial muscles that can be considered as smart materials based actuators with operational similarity to biological muscles. Consequently, it is important to take into account the human hand muscles capabilities and the robotic finger mechanisms that also impact the actuator requirements.

#### Application requirements modeling:

Considering that the artificial muscle will drive a robotic hand, the operating conditions and actuator parameters active strain  $\varepsilon$ , force  $f_a$ , and frequency  $\omega_n$  are influenced by the mechanism of the robot. Consequently, the kinematic and the dynamic data must be analyzed to define operating conditions.

Parameters  $\varepsilon$  and  $f_a$  are obtained regarding the amount of rotation  $\theta_{j1}$  and torque  $C_{j1}$  needed to move the finger and apply a force  $F_j$  on an object. Likewise, frequency  $\omega_n$  is obtained based on the dynamic behavior of the mechanism. Consequently, in section 3.5.3.2 we use the proposed models (kinematic and dynamic) to identify relationships between parameters regarding the mechanism.

**Experimental parameters identification:**

Considering that the target is to mimic human precision grasping, we carry out an experiment to measure maximal and minimal values of human pinch force (pinch force should correspond to  $F_j$ ). To measure parameters  $\theta_{j1}$  and  $C_{j1}$  (needed to identify  $\varepsilon$ ,  $f_a$ , and  $\omega_n$ ) we perform an experiment with the robotic finger using a test platform.

**Parameters quantification:**

Experiments provide dynamic and steady-state values of  $\theta_{j1}$  and  $F_j$ , these experimental data are combined with the kinematic and dynamic models allowing the quantification of  $\varepsilon$ ,  $f_a$ , and  $\omega_n$ . The quantification procedure is detailed in section 3.5.3.

**Material selection:**

The retrieved data allows the proposition of a dynamic behavior permitting the selection of the smart material that best fits the application requirements. The selection will be introduced in the following chapter 4, even that, in the discussion we address a first approach to choose a smart material.

**3.5.2 Characteristics issued from the human hand**

Pinch force requirements: to define a reference value of the human pinch force, we have collected multiple samples from all subjects and computed a mean force value for each one, as shown in Table 1.5, section 1.3.3. Summarizing the obtained results, we can state that if we attempt to reproduce the human precision grasping, the actuator must fulfill the following features:

1. the force  $f_R$  applied by the robotic finger must be inside the human pinch force interval  $[4.78N, 6.70N]$ . Thus, the torque should be enough to produce at least a fingertip force  $f_R = 4.78$ .
2. Settling time must be in the range  $0.18s < t_s < 0.45s$ .

The measured human pinch force has an exponential behavior. Thus, the transient phenomena can be approximated by a first order transfer function, whose output (pinch force) is the result of a step input (muscular activation). Thus, the settling time  $t_s$  is defined as the required time to settle the output to the steady state amplitude, within a 2% margin. Moreover, for a first order behavior, the frequency is calculated as  $\omega = 4/t_s$ , see Lu *et al.*, [100]. As a result,  $\omega$  is in the interval  $[8.89\text{Hz}, 22.2\text{Hz}]$ .

### 3.5.3 Characteristics issued from ProMain-I hand

#### 3.5.3.1 Required active strain

The active strain of smart materials can be defined in different manners depending on the working principle of the actuator, see Fig. 3.19. An extension-based actuator (Fig. 3.19a) undergoes an unidirectional elongation  $\Delta l$ , for initial length  $l_0$ , that can be directly linked to the active strain  $\varepsilon_a$  as:

$$\varepsilon_a = \frac{\Delta l}{l_0} \quad (3.3)$$

The active strain  $\varepsilon_b$  of a bending-based actuator (Fig. 3.19b) can be defined from the transverse deflection  $\Delta l_h$  according to [141] as:

$$\varepsilon_b = \frac{\Delta l_h}{l_0} \quad (3.4)$$

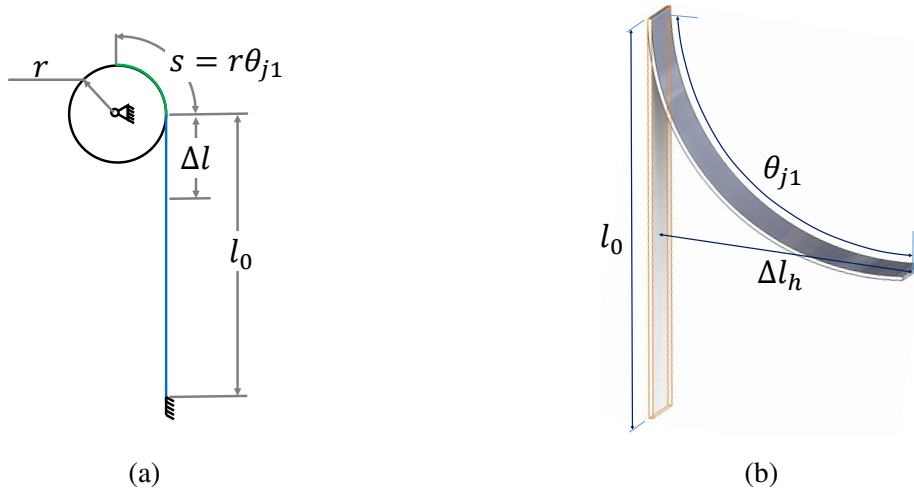


Figure 3.19: Actuator displacements: (a) Extension-based (b) Bending-based.

Concerning the ProMain-I hand, the required active strain is defined in terms of the input rotation  $\theta_{j1}$ . Considering that complete finger flexion occurs when joint angles  $\theta_{j2}$  and  $\theta_{j3}$  reach values of  $80^\circ$ , and taking into account the relationship between angles ( $\theta_{j2} = \theta_{j3} = 0.9\theta_{j1}$ ), we can state that the input rotation must be in the interval  $0^\circ < \theta_{j1} < 90^\circ$ .

So, the elongation  $\Delta l$  of an extension-based actuator for the ProMain-I hand requires a kinematic conversion into the rotation  $\theta_{j1}$  through opportune transmission mechanisms such as rack-pinions or pulleys, i.e.,  $\Delta l = r \theta_{j1}$  where  $r$  is the wheel's radius, see Fig. 3.19a. The required active strain is then obtained from Equation (3.3) as  $\varepsilon_a = \Delta l/l_0 = s/l_0 = r \theta_{j1}/l_0$ . The pulley of the proposed ProMain-I configuration has a radius  $r = 7\text{mm}$  and a maximum initial length of  $l_0 = 200\text{mm}$ . The required active strain for obtaining a rotation of  $\theta_{j1} = 90^\circ$  results thus to be 5.5%.

For a cantilever bending-based actuator, the required deflection  $\Delta l_h$  that corresponds to a  $90^\circ$  rotation is  $0.6l_0$  [141], see Fig. 3.19b. Therefore, according to the definition given in Equation (3.4), the required active strain for such a bending-based actuator is 60%.

### 3.5.3.2 Required actuator force

The force of the bending based actuators is measured as the force applied by the material during flexion when is mechanically blocked and is named blocking force. It is evident that the blocking force of a bending-based actuator must be equivalent to the required fingertip force, *i.e.*, it has to match the interval [4.78N, 6.70N]. However, for an extension-based actuator, the blocking force must be expressed in terms of the equivalent torque that acts on the pulley. The way of converting the required fingertip force into the corresponding active torque is described in the following.

To calculate the required torque using the proposed dynamic model, it is necessary to know the vector  $\{q\}$ , which corresponds to the dependent and independent coordinates of the robotic finger. The values  $x'_{ji}$  and  $y'_{ji}$  correspond to the position of the center of masses  $R_{ji}$ , and are calculated during the experiment described in section 3.4, the work flow to calculate the input torque to apply a force  $F_j = 4.78N$  is shown in figure 3.20.

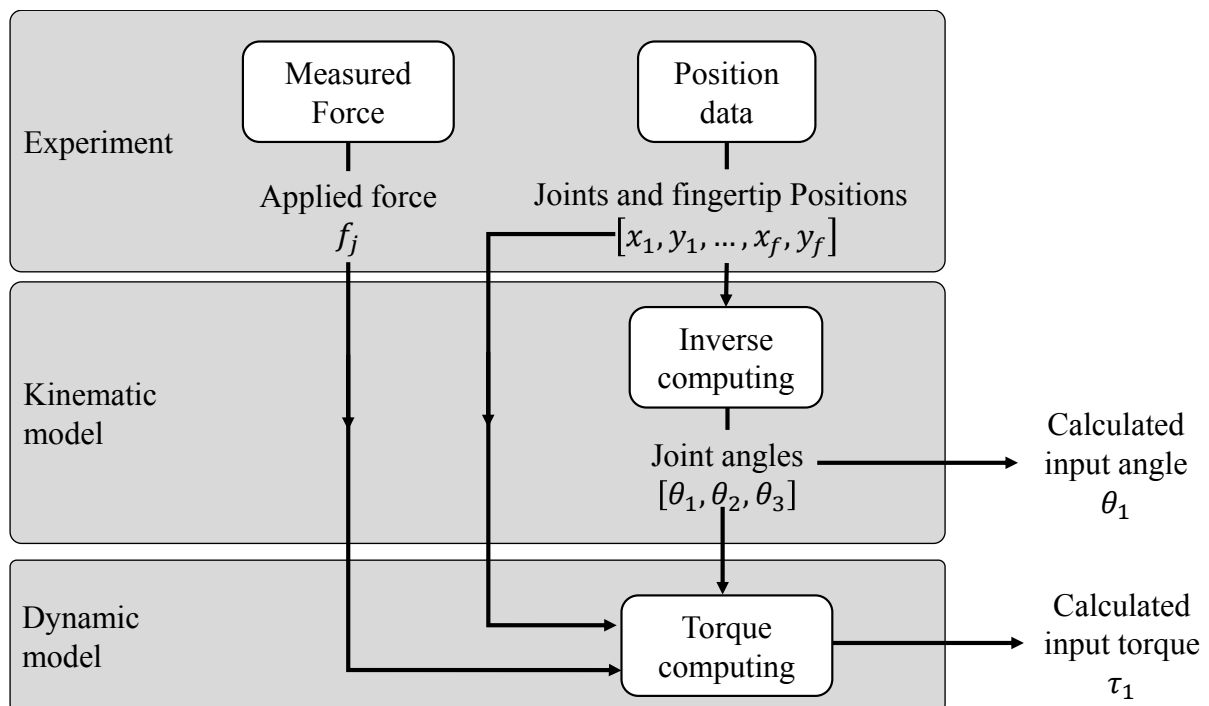


Figure 3.20: Parameter quantification workflow.

Finally, applying the dynamic and kinematic models, we calculate the required input torque for a force in the range  $4.78N \leq F_j \leq 6.70N$ . The input torque  $C_{j1}(F_j, \{q\}, \{\dot{q}\}, \{\ddot{q}\})$  must be in the interval [124.7Nmm, 175.8Nmm]. Taking into account that the ProMain-I Finger radius is

7mm, the required force of the actuator must be in the interval [17.81N, 25.11N], for extension-based actuation.

### 3.6 Smart actuator characteristics

According to the performed analysis, the actuator must provide a rotation of  $\pi/2$ rad and a torque in the interval [124.7Nmm, 175.8Nmm]. There are different kind of smart materials *e.g.* ionic polymer metal composites (IPMC), hydrogels, conductive polymers (CP), piezoelectric ceramics (PC), electronic electroactive polymers (electronic EAP), and shape memory alloys (SMAs). Regarding the main characteristics of our application, the material that best fits the requirements is SMAs [2]. Moreover, in the following chapter 4 we introduce a detailed review comparing several smart materials to justify that selection.

#### Shape memory alloys (SMAs):

SMAs are a kind of materials that can recover a shape. The shape recovery effect is the result of a change in the internal material structure, *i.e.* the crystalline structure is transformed from martensite phase to austenite phase when the temperature increases. Considering that the Young's modulus is lower in the martensite phase than in the austenite phase. During the austenite phase, the material can recover strain produced by external loads. The required temperature for changing phase is known as austenite start temperature.

Martensitic and austenitic transformations are reversible, and thus, the material deformation can be controlled by an external stimulus. Strain-temperature relation is different during heating (martensite-austenite transformation) and cooling (austenite-martensite transformation), this hysteresis is shown in Figure 3.21, for a nickel-titanium (NiTi) based SMA.

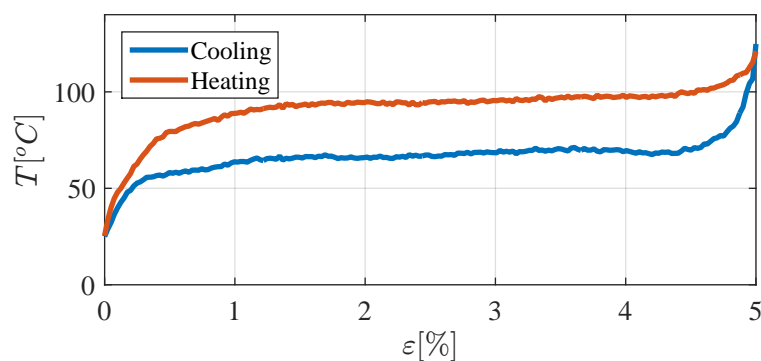


Figure 3.21: Temperature vs strain for NiTi SMAs.

For our application, the actuator will be composed by a NiTi SMA wire fastened to a pulley, see Figure 3.22. Therefore the active strain must rotate the pulley  $\pi/2$ rad, applying a torque of 124.7Nmm. Considering the maximal active strain  $\epsilon = 5\%$ <sup>1</sup>, we can calculate the wire length

<sup>1</sup>Typical maximal strain of the NiTi SMA

variation  $\Delta l$  needed to produce a rotation of  $\pi/2$ rad. Then using  $\Delta l$ , we can calculate the pulley radius  $r = 2\Delta l/\pi$ . Likewise the required force  $f_a$  is obtained as  $f_a = C_{j1}/r$ , where  $C_{j1}$  is the input torque.

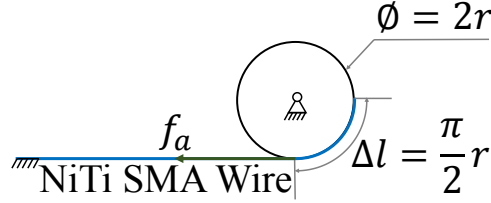


Figure 3.22: Schema of the SMA-based actuator.

Considering a wire length  $l = 200$ mm, length variation  $\Delta l = 0.05l = 10$ mm. The pulley radius  $r = 2\Delta l/\pi = 6.35$ mm. The force based on the required input torque  $C_{j1} = 124.7$ Nmm must be  $f_a \geq 124.7$ Nmm/ $r \geq 19.6$ N. Summarizing we need a NiTi SMA wire with the following conditions: i) length  $l = 200$ mm, ii) active strain  $\varepsilon = 5\%$ , and iii) force  $f_a \geq 19.6$ N. These conditions are fulfilled by a NiTi SMA wire with a diameter of 0.38mm, which has a force  $f_a = 20.04$ N.

For the selected wire, the austenite start temperature of  $90^\circ\text{C}$  is produced by an electric current  $i = 2.25$ A applied to the SMA wire. Considering the electric resistance of the material  $R = 1.66\Omega$ , we need apply a voltage  $u = 3.72$ V. Furthermore, and taking into account the behavior of the NiTi SMAs, the active strain can be modeled with respect to the electrical current through a second order transfer function as:

$$\frac{\varepsilon_n(s)}{i_n(s)} = \frac{\omega_n^2}{s^2 + 2\zeta\omega_n s + \omega_n^2} \quad (3.5)$$

Where  $\varepsilon_n = \varepsilon/\varepsilon_{max}$  is the normalized active strain,  $\zeta$  is the damping coefficient,  $\omega_n$  is the frequency, and  $i_n = i/2.25$ A is the normalized electric current.

With the objective of identifying the SMA wire transfer function, we carried out an experimental observation (see [2]), measuring the active strain produced during the excitation with an applied step of electric current. The obtained results, see Figure 3.23, show that overshoot is zero and consequently the damping coefficient is  $\zeta = 1$ . The frequency  $\omega_n$ , can be calculated as the inverse of the time constant  $1/\tau$  [100], which for a critically damped response is considered the time to reach 26.42% of the steady state value, thus, from the measured time constant  $\omega_n = 13.02$ Hz. As a result the SMA wire transfer function is:

$$\varepsilon_n(s) = \frac{169.5}{s^2 + 26.04s + 169.5} \quad (3.6)$$

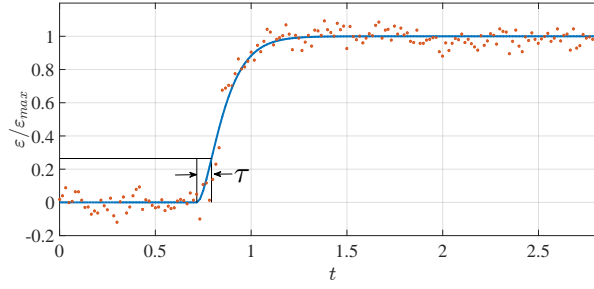


Figure 3.23: Identified transfer function of the normalized strain (based on the strain of NiTi SMA wire in response to a current step input).

Comparing the SMA-based actuator characteristics with the actuation requirements of the ProMain-I hand, see table 3.3, we can see that the rotation and torque and frequency, fulfill the requirements of the robotic hand to achieve human-like precision grasping movements.

Parameter	ProMain-I Hand	SMA-based Actuator
	Requirements	$r = 6.35mm, F_a = 20.04N$ and $l = 200mm$
$\theta[rad]$	$\pi/2$	$\pi/2$
$\tau[Nmm]$	[124.7, 175.8]	127.3
$\omega[Hz]$	[8.89, 22.2]	13.02

Table 3.3: Comparison of ProMain-I hand requirements and actuator characteristics.

The presented actuator analysis shows that smart material based actuators are suitable for grasping application. In the following chapter a more deep study of smart materials is introduced and the last version of the soft epicyclic mechanism is described.

### 3.7 Discussion

We have presented a methodology to design artificial muscles based on four steps: 1) Application requirements modeling, 2) Experimental parameter identification, 3) Parameters quantification, and 4) Material selection. The methodology was applied to design an artificial muscle for a robotic finger.

The used finger is the Promain-I, which is anthropomorphic, under-actuated, and driven by flexible wires to produce more adaptive grasping movements. The proposed kinematic and dynamic models allow to calculate the torque requirement to mimic human finger force. Experiments allow to identify and quantify the main actuator parameters. According to the obtained results and the performed analysis, we identify that shape memory alloys (SMAs) can fulfill the requirements of artificial muscles for robotic finger.

## Chapter 4

# Development of an artificial muscle based on smart materials

In this chapter, we investigate further the study of smart materials that we have started in the last part of the previous chapter. In the first section, we present a review of different smart materials following key actuation features that were introduced regarding actuation requirements. This study takes into account material features reported in the literature and applies, when is required, a mechanic, physic or mathematic analysis to transform data into comparable values. The study is centered on the smart materials whose characteristics are suitable for grasping applications.

In the second section, we propose an evolution of the hand prosthesis ProMain-I, and we present a new prototype called ProMain-II. Based on the analysis of the performed review, a smart material is chosen to improve the ProMain-I hand mechanism adding the possibility to control the stiffness of the soft epicyclic mechanism. This evolution is proposed based on the behavior of the SMA issued from the model and experiments proposed in section two. The elements of the new soft epicyclic tendon-driven mechanism based on controllable stiffness wires are introduced and detailed. Furthermore, an additional modification is added to the robotic hand prosthesis, consisting in a flexible link that substitutes the DIP joint to append an elastic behavior to the finger. The effect of the soft link added to the hand prosthesis is presented.

In section three, a constitutive model that uses thermo-mechanical formulation to describe SMAs behavior is presented. The formulation is suitable to characterize the material and also to complement the dynamic modeling of an actuator. Furthermore, a one dimension particularization is introduced, the model is used to approximate the behavior of the SMA wires in the context of a rotary actuator. Three experiments are presented in order to: i) Identify the Young's modulus of SMA in martensite and austenite phases, ii) Identify thermal SMA characteristics, and iii) Kinematic evaluation of a SMA rotary actuator. The final identification of the SMA parameters uses optimization techniques for fitting the model to the real material behavior.

## 4.1 Smart materials review and comparison

We have introduced three critical parameters defining the requirements of artificial muscles for robotic hands: the strain (obtained from the robot features), the frequency (based on the human settling time) and the force (estimated from experiments on human hand combined with kinematics and dynamics of the robot). The requirements, summarized in Table 4.1, can be fulfilled by classical actuators, as it has been shown previously [2]. In the following, we assess several smart materials against the stated requirements by referring to state-of-the-art data gathered from an extensive bibliographic research. The aim is to identify potential candidates to be used as artificial muscles for the ProMain hand.

Actuation	Extension	Bending
Parameter		
Min active strain [%]	5.5	60
Frequency [Hz]	[8.89, 22.2]	
Force [N]	[17.81, 25.11]	[4.8, 6.74]

Table 4.1: summary of requirements of artificial muscles for robotic hands.

Smart materials have one or more properties that can be significantly changed in a controlled way by an externally applied excitation. Their behavior is reversible, and consequently these materials could fulfill actuation and/or sensing requirements [142]. In the state of the art, we find several types of smart materials. Considering operation and control of the robotic hand, we select those that are activated by an electrical stimulus as follows:

1. Ionic polymer metal composite (IPMC)
2. Hydrogels
3. Conductive polymers (CPs)
4. Piezoelectric ceramics (PCs)
5. Rheological fluids
6. Electronic electroactive polymers (electronic EAP)

Furthermore, we are interested on shape memory alloys (SMAs) due to their characteristics such as blocking force and active strain. SMAs require a thermal stimulus that can be produced by an electric current [143]. The result of the bibliographic research is summarized in Table 4.2: for each smart material we report the values for the 3 key features along with the reference from which the state-of-the-art characteristics have been extracted. Equations (3.3) and (3.4) are used to recalculate active strain  $\varepsilon$  for comparison proposals. Frequency  $\omega$  and force  $F$  were obtained

directly from authors. The reported force  $F$  for the active bending materials is measured as the force applied by the material during flexion when is mechanically blocked and is named blocking force. For the active extension materials, The reported force  $F$  is the pulling force exerted by the material when the external stimulus is applied.

Material	Frequency $\omega$ [Hz]	Active strain $\epsilon$ [%]	Force $F$ [N]	Reference
IPMC (B)	[0.6, 10]	[10, 60]	[0.001, 0.1]	$\omega$ ([144, 145]) $\epsilon$ ([141, 146]) $F$ ([147])
Electrolyte gels (B, E)	[0, 0.2]	[0, 50]	[0.001, 6]	$\omega$ ([148]) $\epsilon$ ([148, 149]) $F$ ([150])
CPs (B)	[0.01, 1]	[0, 60]	[0, $200 \times 10^{-9}$ ]	$\omega$ ([151]) $\epsilon$ ([152]) $F$ ([151])
PCs (B)	[100, 600]	[0.002, 1.5]	0.25	[153]
Rheological Fluid (B)	[25, 100]	[1.8, 1.9]	[0.5, 3]	$\omega$ ([154]) $\epsilon, F$ ([155])
Electronic EAP (B, E)	[1, 4]	[10, 200]	[0, 0.4]	$\omega$ ([156]) $\epsilon$ ([157]) $F$ ([156])
SMA (B, E)	[0.23, 22.2]	[3, 110]	[0.032, 34.9]	[158]

Table 4.2: Main characteristics of smart materials (B: Bending, E: Extension).

It can be seen that concerning active strain, IPMC, CPs, electronic EAP, and SMA satisfy grasping requirements. Regarding frequency, IPMC, PCs, Rheological fluid and SMA fulfill grasping requirements. Concerning the force, only the electrolyte gels and SMA can achieve the range of the human hand pinch force. Furthermore, the implementation of smart materials in prostheses is bounded by other factors, *e.g.* the excitation voltages (see Table 4.3) can impact the device autonomy. Thus, an excitation voltage in the range kV can not be used.

Taking into account available state of the art regarding smart materials, we have compared the main actuator's features with the requirements of artificial muscles for the ProMain-I hand.

As a result, we find out that two kinds of materials, namely ionic polymer metal composites (IPMCs) and shape memory alloys (SMAs), match at least two of the three requirements of artificial muscles for robotic hand hands presented in table 4.1. The IPMCs constitute an interesting smart material to drive prosthetic fingers, due to their attractive active strain and settling time, nevertheless, their blocking force is below the requirements. Consequently, the SMAs are chosen for the design of the smart material based actuation system for the evolution of the ProMain-I hand.

Material	Stiffness $k$ [MPa]	Applied voltage $u$ [V]	Ref.
IPMC	[10, 50]	[0, 5]	$k$ ([159]) $u$ ([145])
Electrolyte gels	[0.001, 0.04]	[0, 21]	$k$ ([150]) $u$ ([149])
CPs	[80, 440]	1	[152]
PCs	$210 \times 10^3$	[30, 220]	$k$ ([160]) $u$ ([161])
Rheological Fluid	$[100 \times 10^3, 650 \times 10^3]$	$[3 \times 10^3, 120 \times 10^3]$	[154]
Electronic EAP	$[20 \times 10^{-6}, 120 \times 10^{-6}]$	$[0, 6 \times 10^3]$	[156]
SMA	103	[1.72, 6.41]	[158]

Table 4.3: Stiffness and voltage excitation of smart materials.

In summary, We have introduced a methodology to identify the requirements and specifications of artificial muscles for robotic hand prostheses. Our methodology combines experimental data with the kinematics and dynamics model of the robotic hand to define actuator requirements. The methodology is applied to the robotic hand ProMain-I, and the requirements for the hand are defined as follows: (i) Minimum active strain 5.5% for extension-based actuation or 60% bending-based actuation, (ii) Frequency [8.89Hz, 22.2Hz], and (iii) Force [4.78N, 6.70N] for bending-based actuation or Force [17.81N, 25.11N] for extension-based actuation .

Consequently, the shape memory alloys (SMAs) is chosen as it fulfill all actuation requirements for precision grasping. Thus, in the following we introduce: i) a SMA-based rotary actuator modeled and identified with a constitutive model of the SMA and an experimental approach, and ii) a new prototype of robotic hand prosthesis using artificial muscles based on SMA.

## 4.2 Modeling of a SMA-based actuator

Shape memory alloys (SMAs) are of high interest in research due to their outstanding features such as high energy density and silent operation among others. Those features make SMAs suitable for actuation application [162] and in case of robotic hand prostheses they could constitute a key solution to several unsolved issues *e.g.* actuator noise, compliance, weight, and adaptability.

Nevertheless, despite scientific advances in the understanding of material behavior [163–169], SMAs are not available to be implemented as actuator due to the lack of linkages between the models, the problematic of robotic hand prosthesis, and the automatic control. Consequently, in this study, we introduce a SMA-based actuator. Furthermore, the SMAs behavior modeling is addressed, taking into account the actuator configuration and automatic control theory.

### 4.2.1 SMA-based actuator

The actuation requirements that must fulfill the SMA based actuator are summarized in table 4.4. These requirements are defined to mimic the human precision grasping as presented in chapter 1 (see also Ramírez *et al.*, [2]).

Description	Parameter	Required value
Rotation	$\theta$ [rad]	$\pi/2$
Torque	$\tau$ [Nmm]	124.7
Frequency	$\omega$ [Hz]	16.36

Table 4.4: ProMain-I hand actuation requirements

The actuator is composed of a NiTi SMA wire fastened to a pulley and a bias spring to reset the wire in its original shape, see figure 4.1. The NiTi SMA maximal active strain  $\epsilon^{max}$  is 4.55% [170] and thus wire elongation is calculated as  $\Delta l = 0.045l$  for a wire of length  $l$ . Furthermore, the wire elongation is linked with pulley's ratio  $r$ , and required rotation  $\theta$  through the relation  $\Delta l = \theta r$ . Thus, the wire length is calculated as  $l = \theta r / 0.045$ .

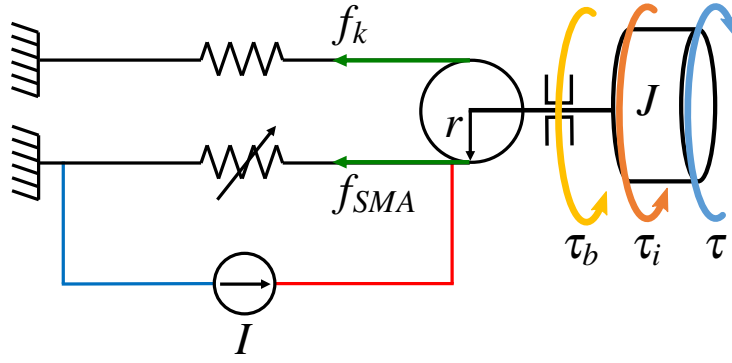


Figure 4.1: Schematic representation of the SMA-based actuator.

The torque  $\tau$  is calculated as function of the difference between the SMA's pulling force  $f_{SMA}$  and the bias spring force  $f_k$ , and the pulley's ratio  $r$  as shown in equation (4.1) below:

$$\tau = (f_{SMA} - f_k) r \quad (4.1)$$

The spring force can be considered as the stiffness constant  $k$  times the wire elongation  $\Delta l$ , hence, equation (4.1) can be rewritten as:

$$\tau = (f_{SMA} - k \overbrace{\theta r}^{\Delta l}) r \quad (4.2)$$

The actuator's inertial and frictional forces can be respectively modeled as  $\tau_i = J\ddot{\theta}$  and  $\tau_b = b\dot{\theta}$ , where  $J$  is the moment of inertia of the rotor and  $b$  is the motor viscous constant. Consequently, we can derive the following governing equation based on Newton's second law:

$$J\ddot{\theta} + b\dot{\theta} = \tau \quad (4.3)$$

Replacing equation (4.2) in equation (4.3), we obtain:

$$\frac{J}{r}\ddot{\theta} + \frac{b}{r}\dot{\theta} + kr\theta = f_{SMA} \quad (4.4)$$

The governing equation (4.4) shows that the temporal response of the actuator position depends on the SMA's pulling force produced during wire contraction. The contraction of the wire is due to heating and the relaxation to cooling. Both contraction and relaxation are virtually instantaneous with the temperature of the wire [170]. Thus, the SMA's pulling force changes instantaneously as a consequence of the variation of the applied temperature  $T$ .

Taking into account that the wire is a current-conducting filament, the temperature can be induced by an electrical current flowing through the wire. Hence, it is necessary to propose an additional governing equation to describe the temperature as function of the electrical current.

The SMA wire can be considered as a closed system exchanging heat and work (in the form of power) with the environment, when exposing it to an electrical current (see figure 4.2). Since the wire is in an isobaric environment, and considering the first law of thermodynamics, it is clear that the sum of heats is equal to the enthalpy variation.

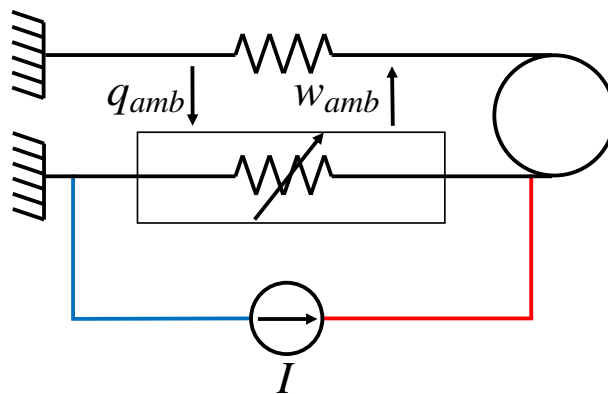


Figure 4.2: Schematic representation of the SMA-based actuator.

$$\dot{H} = q_{amb} + q_G \quad (4.5)$$

Where  $H$  is the enthalpy,  $q_{amb}$  is the ambient heat, and  $q_G$  is the generated heating power. Furthermore, considering the SMA as a solid with mass  $m$  and specific heat  $c$  the following equation is proposed.

$$mc\dot{T} = q_{amb} + q_G \quad (4.6)$$

The wire is in contact with air, thus, the chosen heat transfer mechanism is convection. In the other hand, the generated heating power  $q_G$  is equal to the electric power, which according to the Ohm's law is the product of the square of the current  $I^2$  times the electrical resistance  $R$ . Furthermore, as the wire is in contact with air, the chosen heat transfer mechanism is convection. Thus, the additional govern equation to describe the temperature as function of the electrical current is written as follows:

$$mc\dot{T} = hA(T_0 - T) + I^2R \quad (4.7)$$

where  $h$  is the convection coefficient,  $A$  is the external surface of the SMA wire, and  $T_0$  is the ambient temperature.

The governing equations (4.4) and (4.7) describes the dynamic behavior of the SMA based actuator. Nevertheless, the value of the pulling force  $f_{SMA}$  and of the electrical resistance  $R$  changes depending on the material state, so it is necessary to introduce a constitutive model, in order to describe material influence. This constitutive model is described in the following section.

#### 4.2.2 SMA constitutive model

In the state of the art, the modeling of SMAs is addressed through the analysis of free energy balance using the convex potential [163], the Helmholtz free energy  $\Psi$  [167], or Gibbs free energy  $G$  [169]. furthermore, the small strain formalism can be adopted because the maximal

macroscopic reversible strain is lower than 6%. Both, Helmholtz  $\Psi$  and Gibbs  $G$  specific<sup>1</sup> free energies, whose physical parameters are introduced in table 4.5, are presented in equations (4.8) and (4.9) as follows:

$$\Psi(\boldsymbol{\varepsilon}, T, \boldsymbol{\varepsilon}^t, \zeta) = \frac{1}{2\rho} \boldsymbol{\varepsilon} : (\mathbf{C} \times \boldsymbol{\varepsilon}) - \frac{1}{\rho} \boldsymbol{\varepsilon} : (\mathbf{C} \times [\boldsymbol{\alpha}(T - T_0) + \boldsymbol{\varepsilon}^t]) + c \left[ (T - T_0) - T \ln \left( \frac{T}{T_0} \right) \right] + u_0 - s_0 T + \frac{1}{\rho} f(\zeta) \quad (4.8)$$

$$\mathbf{G}(\boldsymbol{\sigma}, T, \boldsymbol{\varepsilon}^t, \zeta) = -\frac{1}{2\rho} \boldsymbol{\sigma} : (\mathbf{S} \times \boldsymbol{\sigma}) - \frac{1}{\rho} \boldsymbol{\sigma} : [\boldsymbol{\alpha}(T - T_0) + \boldsymbol{\varepsilon}^t] + c \left[ (T - T_0) - T \ln \left( \frac{T}{T_0} \right) \right] + u_0 - s_0 T + \frac{1}{\rho} f(\zeta) \quad (4.9)$$

Parameter	Description
$\mathbf{C}$	Stiffness tensor
$\mathbf{S}$	Softness tensor
$\boldsymbol{\varepsilon}$	Strain (2 <sup>nd</sup> -order symmetric tensor)
$\boldsymbol{\sigma}$	Stress tensor(2 <sup>nd</sup> -order symmetric tensor)
$\rho$	Material density
$\boldsymbol{\alpha}$	2 <sup>nd</sup> -order effective thermal expansion tensor
$T$	Temperature
$T_0$	Reference temperature
$\boldsymbol{\varepsilon}^t$	Transformation strain
$c$	Effective specific heat
$u_0$	Effective specific internal energy at reference state
$s_0$	Effective specific entropy at reference state
$\zeta$	Martensitic volume fraction
$f(\zeta)$	Function of hardness

Table 4.5: Physical parameters description of Helmholtz  $\Psi$  and Gibbs  $G$  specific free energies

The choice between  $\Psi$  or  $G$  is done regarding the variable to control during measures [171]. Taking into account that the target of the present study is to perform force and position control, we use Gibbs free energy  $G(\boldsymbol{\sigma}, T, \boldsymbol{\varepsilon}^t, \zeta)$  to estimate the strain, and the Helmholtz free energy  $\Psi(\boldsymbol{\varepsilon}, T, \boldsymbol{\varepsilon}^t, \zeta)$  to estimate stress.

<sup>1</sup>as specific quantities all defined per unit mass

The first law of thermodynamics states that  $\rho\dot{U} - \boldsymbol{\sigma} : \dot{\boldsymbol{\varepsilon}} = \rho r - \nabla q$ , where  $r$  are the heat sources,  $U$  is the internal energy, and  $q$  is the heat flux. Moreover, taking into account that: i) the internal entropy production is always greater than or equal to zero and ii) heat only flows from a hotter material point to a colder one, the second law of thermodynamics can be expressed through the Clausius-Duhem inequality as  $\rho s\dot{T} \geq \rho r - \nabla q$ , where  $s$  is the specific entropy. Thus, combining the first law of thermodynamic with the Clausius-Duhem inequality we obtain  $\rho s\dot{T} \geq \rho\dot{U} - \boldsymbol{\sigma} : \dot{\boldsymbol{\varepsilon}}$  that is known as the Clausius-Planck inequality.

The Gibbs  $\mathbf{G}$  and the Helmholtz free energies  $\Psi$  can be written as function of the internal energy using the Legendre transformation as  $\Psi = U - sT$  and  $G = U - (1/\rho)\boldsymbol{\sigma} : \boldsymbol{\varepsilon} - sT$ . Thus, the Clausius-Planck inequality can be written for the Gibbs (see equation (4.10)) and the Helmholtz (see equation (4.11)) free energies as follows:

$$-\dot{\boldsymbol{\sigma}} : \boldsymbol{\varepsilon} - \rho\dot{\mathbf{G}} - \rho s\dot{T} \geq 0 \quad (4.10)$$

$$\boldsymbol{\sigma} : \dot{\boldsymbol{\varepsilon}} - \rho\dot{\Psi} - \rho s\dot{T} \geq 0 \quad (4.11)$$

The derivative with respect to the time of the Gibbs  $\mathbf{G}$  and the Helmholtz  $\Psi$  free energies can be performed using the chain rule as follows:

$$\dot{\mathbf{G}} = \frac{\partial \mathbf{G}}{\partial \boldsymbol{\sigma}} : \dot{\boldsymbol{\sigma}} + \frac{\partial \mathbf{G}}{\partial T} \dot{T} + \frac{\partial \mathbf{G}}{\partial \boldsymbol{\varepsilon}^t} \dot{\boldsymbol{\varepsilon}}^t + \frac{\partial \mathbf{G}}{\partial \zeta} \dot{\zeta} \quad (4.12)$$

$$\dot{\Psi} = \frac{\partial \Psi}{\partial \boldsymbol{\varepsilon}} : \dot{\boldsymbol{\varepsilon}} + \frac{\partial \Psi}{\partial T} \dot{T} + \frac{\partial \Psi}{\partial \boldsymbol{\varepsilon}^t} \dot{\boldsymbol{\varepsilon}}^t + \frac{\partial \Psi}{\partial \zeta} \dot{\zeta} \quad (4.13)$$

From equations (4.8) to (4.13) the following relations are obtained.

$$\boldsymbol{\varepsilon} = -\rho \frac{\partial \mathbf{G}}{\partial \boldsymbol{\sigma}} = \frac{1}{2} \boldsymbol{\sigma} : \mathbf{S} + [\boldsymbol{\alpha}(T - T_0) + \boldsymbol{\varepsilon}^t] \quad (4.14)$$

$$\boldsymbol{\sigma} = \rho \frac{\partial \Psi}{\partial \boldsymbol{\varepsilon}} = \frac{1}{2} \mathbf{C} : \boldsymbol{\varepsilon} - \mathbf{C} : [\boldsymbol{\alpha}(T - T_0) + \boldsymbol{\varepsilon}^t] \quad (4.15)$$

$$s = -\frac{\partial \mathbf{G}}{\partial T} = -\frac{\partial \Psi}{\partial T} = \frac{1}{\rho} \boldsymbol{\sigma} : \boldsymbol{\alpha} + c \ln \left( \frac{T}{T_0} \right) + s_0 \quad (4.16)$$

$$\left( -\rho \frac{\partial \mathbf{G}}{\partial \boldsymbol{\varepsilon}^t} \right) : \dot{\boldsymbol{\varepsilon}}^t + \left( -\rho \frac{\partial \mathbf{G}}{\partial \zeta} \right) \dot{\zeta} \geq 0 \quad (4.17)$$

As can be seen in equations (4.14) and (4.15), the transformation strain  $\boldsymbol{\varepsilon}^t$  is necessary to calculate total strain  $\boldsymbol{\varepsilon}^t$  and stress. Thus, in the following the relation between martensitic volume fraction  $\zeta$  and transformation strain  $\boldsymbol{\varepsilon}^t$  is introduced.

The total strain of SMAs  $\boldsymbol{\varepsilon}$  is considered as an additive composition of the thermoelastic  $\boldsymbol{\varepsilon}^{el}$  and inelastic strains. Considering that plastic strain is negligible with respect to the transformation strain  $\boldsymbol{\varepsilon}^t$ , the inelastic strain is composed only by the  $\boldsymbol{\varepsilon}^t$ . Thus the total strain is given by:

$$\boldsymbol{\varepsilon} = \boldsymbol{\varepsilon}^{el} + \boldsymbol{\varepsilon}^t \quad (4.18)$$

Typically the transformation strain  $\boldsymbol{\varepsilon}^t$  is bounded by the maximal strain  $\boldsymbol{\varepsilon}^{max}$ , whose value is between 4.5% [170] and 6% [164], in such a way that:

$$0 \leq \boldsymbol{\varepsilon} \leq \boldsymbol{\varepsilon}^{max} \quad (4.19)$$

In addition, as Machado and Lagoudas [171] pointed out, changes in the SMAs state are a result of variation in the martensitic volume fraction. Thus, the Stiffness  $\mathbf{C}$ , the Softness  $\mathbf{S}$ , the effective thermal expansion  $\boldsymbol{\alpha}$ , the effective specific internal energy  $u_0$ , and the effective specific entropy  $s_0$ , can be written as function of the martensitic volume fraction  $\zeta$  as follows:

$$\mathbf{C} = \mathbf{C}^A + \zeta(\mathbf{C}^M - \mathbf{C}^A) = \mathbf{C}^A + \zeta\Delta\mathbf{C} \quad (4.20)$$

$$\mathbf{S} = \mathbf{S}^A + \zeta(\mathbf{S}^M - \mathbf{S}^A) = \mathbf{S}^A + \zeta\Delta\mathbf{S} \quad (4.21)$$

$$\boldsymbol{\alpha} = \boldsymbol{\alpha}^A + \zeta(\boldsymbol{\alpha}^M - \boldsymbol{\alpha}^A) = \boldsymbol{\alpha}^A + \zeta\Delta\boldsymbol{\alpha} \quad (4.22)$$

$$u_0 = u_0^A + \zeta(u_0^M - u_0^A) = u_0^A + \zeta\Delta u_0 \quad (4.23)$$

$$s_0 = s_0^A + \zeta(s_0^M - s_0^A) = s_0^A + \zeta\Delta s_0 \quad (4.24)$$

where the super index  $A$  and  $M$  denote the austenite and martensite phases respectively, e.g.  $\mathbf{C}^A$  is the stiffness in pure austenite phase and  $\mathbf{C}^M$  is the stiffness in pure martensite phase.

The temporal variation of the transformation strain is proportional to the temporal variation of the martensitic volume fraction during forward and reverse transformation, and the following relation can be proposed:

$$\dot{\boldsymbol{\varepsilon}}^t = \left( \frac{3}{2} \boldsymbol{\varepsilon}^{max} \frac{\boldsymbol{\sigma}'}{\bar{\boldsymbol{\sigma}}} \right) \dot{\zeta} = \boldsymbol{\Gamma} \dot{\zeta} \quad (4.25)$$

where  $\boldsymbol{\sigma}'$  is the deviatoric stress,  $\bar{\boldsymbol{\sigma}}$  is the effective stress, and  $\boldsymbol{\Gamma}$  is a transformation tensor that describes the relation between the martensitic volume fraction variation and transformation strain variation. The above assumption is done because the transformation strain is supposed to be in the direction of the deviatoric stress [172]. Substituting equation (4.25) on equation (4.17), and taking into account that  $\rho \partial \mathbf{G} / \partial \boldsymbol{\varepsilon}^t = -\boldsymbol{\sigma}$ , the following flow rule is obtained:

$$\left( \boldsymbol{\sigma} : \boldsymbol{\Gamma} - \rho \frac{\partial \mathbf{G}}{\partial \zeta} \right) \dot{\zeta} = \varphi \dot{\zeta} \geq 0 \quad (4.26)$$

Where  $\varphi$  is the thermodynamic force conjugated to the martensitic volume fraction  $\zeta$  [172]. Taking into account the relations proposed in equations (4.20) to (4.24), the term  $-\rho \partial \mathbf{G} / \partial \zeta$ , needed to compute the thermodynamic force  $\varphi$ , is calculated as follows:

$$\begin{aligned} -\rho \frac{\partial \mathbf{G}}{\partial \zeta} &= \frac{1}{2} \boldsymbol{\sigma} : (\Delta \mathbf{S} \times \boldsymbol{\sigma}) + \boldsymbol{\sigma} : \Delta \boldsymbol{\alpha} (T - T_0) \\ &\quad - \rho \Delta u_0 + \rho \Delta s_0 T - \frac{\partial f(\zeta)}{\partial \zeta} \end{aligned} \quad (4.27)$$

Then, operating equations (4.26) and (4.27), the thermodynamic force  $\varphi$  is calculated as follows:

$$\varphi = \boldsymbol{\sigma} : \boldsymbol{\Gamma} + \overbrace{\frac{1}{2} \boldsymbol{\sigma} : (\Delta \mathbf{S} \times \boldsymbol{\sigma}) + \boldsymbol{\sigma} : \Delta \boldsymbol{\alpha} (T - T_0)}^{\varphi_{te}} - \rho \Delta u_0 + \rho \Delta s_0 T - \frac{\partial f(\zeta)}{\partial \zeta} \quad (4.28)$$

The parameter  $\varphi_{te}$  can be considered as the thermoelastic part of the thermodynamic force, and is introduced only to simplify the equation.

When the martensitic volume fraction  $\zeta$  is increasing ( $\dot{\zeta} > 0$ ), the thermodynamic force must be greater than zero  $\varphi > 0$  to fulfill the flow rule proposed in equation (4.26). Likewise, applying the same analysis, when the martensitic volume fraction  $\zeta$  is decreasing ( $\dot{\zeta} < 0$ ), the thermodynamic force must be lower than zero  $\varphi < 0$ .

Furthermore, when the martensitic volume fraction reaches its maximum value 1, the thermodynamic force gets saturated to a threshold value  $Y$ . Similarly when the martensitic volume fraction reach its minimum value 0, the thermodynamic force gets saturated to a threshold value  $-Y$ .

Additionally, it is necessary to define the function of hardness  $f(\zeta)$  and the threshold  $Y$ . We choose the second-order polynomial representation introduced by Machado and Lagoudas [171] as follows:

$$f(\zeta) = \begin{cases} \frac{1}{2} \rho b^M \zeta^2 + (\mu_1 + \mu_2) \zeta & \text{for } \dot{\zeta} > 0 \\ \frac{1}{2} \rho b^A \zeta^2 + (\mu_1 - \mu_2) \zeta & \text{for } \dot{\zeta} < 0 \end{cases} \quad (4.29)$$

Where  $b^M$ ,  $b^A$ ,  $\mu_1$ , and  $\mu_2$  are model parameters to be identified experimentally. Those terms and the threshold  $Y$ , are related to the material parameters as follows[172]:

$$Y = \frac{1}{4} \rho \Delta s_0 (M_s + M_f - A_f - A_s) \quad (4.30)$$

$$b^A = -\Delta s_0 (A_f - A_s) \quad (4.31)$$

$$b^M = -\Delta s_0 (M_s - M_f) \quad (4.32)$$

$$\mu_1 = \frac{1}{2} \rho \Delta s_0 (M_s + A_f) - \rho \Delta u_0 \quad (4.33)$$

$$\mu_2 = \frac{1}{4} \rho \Delta s_0 (M_f - A_s - A_f - M_f + M_s) \quad (4.34)$$

Where  $M_s$  is the martensite start temperature,  $M_f$  is the martensite finish temperature,  $A_s$  is the austenite start temperature, and  $A_f$  is the austenite finish temperature.

Taking into account the following two considerations: i)  $\varphi - Y = 0$  for  $\dot{\zeta} > 0$  and ii)  $-\varphi - Y = 0$  for  $\dot{\zeta} < 0$ , an explicit solution for the martensitic volume fraction  $\zeta$  can be obtained, during the forward and reverse transformation of the material.

$$\zeta = \begin{cases} \frac{\boldsymbol{\sigma}:\boldsymbol{\Gamma} + \varphi_{te} + \rho\Delta s_0(T - M_s)}{\rho\Delta s_0(M_f - M_s)} & \text{for } \dot{\zeta} > 0 \\ \frac{\boldsymbol{\sigma}:\boldsymbol{\Gamma} + \varphi_{te} + \rho\Delta s_0(T - A_f)}{\rho\Delta s_0(A_s - A_f)} & \text{for } \dot{\zeta} < 0 \end{cases} \quad (4.35)$$

By integrating equation (4.25), we obtain the following expression for the transformation strain:

$$\boldsymbol{\varepsilon}^t = \boldsymbol{\Gamma}\zeta \quad (4.36)$$

In summary, we have one equation for the total strain, one for the stress and one for the transformation strain. Top part of Table 4.6 shows the equations and parameters of the models.

Response functions	Equation	Variables	Parameters
Strain $\boldsymbol{\varepsilon}$	(4.14)	$\boldsymbol{\sigma}, \boldsymbol{\varepsilon}^t, T, \boldsymbol{S}, \boldsymbol{\alpha}, \zeta$	$\boldsymbol{S}^A, \boldsymbol{S}^M, \boldsymbol{\alpha}^A, \boldsymbol{\alpha}^M$
Stress $\boldsymbol{\sigma}$	(4.15)	$\boldsymbol{\varepsilon}, \boldsymbol{\varepsilon}^t, T, \boldsymbol{C}, \boldsymbol{\alpha}, \zeta$	$\boldsymbol{C}^A, \boldsymbol{C}^M, \boldsymbol{\alpha}^A, \boldsymbol{\alpha}^M$
Martensitic volume fraction $\zeta$	(4.35)	$T, \boldsymbol{\sigma}, \boldsymbol{\Gamma}$	$\rho, \Delta s_0, M_s, M_f, A_s, A_f, \boldsymbol{S}^A, \boldsymbol{S}^M, \boldsymbol{\alpha}^A, \boldsymbol{\alpha}^M, \boldsymbol{\varepsilon}^{max}$
Transformation Strain $\boldsymbol{\varepsilon}^t$	(4.36)	$\zeta, \boldsymbol{\sigma}, \boldsymbol{\Gamma}$	$\boldsymbol{\varepsilon}^{max}$

Table 4.6: General constitutive model equations and parameters

#### 4.2.2.1 1D constitutive model of SMA

Bearing in mind that the SMA wire is under uniaxial stress for the proposed actuator, the model can be simplified through a 1D approach, using the following considerations:

1. Considering uniaxial load, the stress tensor is formulated as presented in equation (4.37). Therefore, the components  $\varepsilon_{12}$ ,  $\varepsilon_{13}$ , and  $\varepsilon_{23}$  of the strain tensor are zero.

$$\boldsymbol{\sigma} = \begin{bmatrix} \sigma_{11} & 0 & 0 \\ 0 & 0 & 0 \\ 0 & 0 & 0 \end{bmatrix} \quad (4.37)$$

2. Given that the stress tensor is composed only by  $\sigma_{11}$ , the softness and the thermal expansion tensors ( $\boldsymbol{S}$  and  $\boldsymbol{\alpha}$ ) are reduced to scalar values, see equations (4.38) and (4.39) below:

$$S = S^A + \zeta \overbrace{(S^M - S^A)}^{\Delta S} \quad (4.38)$$

$$\boldsymbol{\alpha} = \boldsymbol{\alpha}^A + \zeta \overbrace{(\boldsymbol{\alpha}^M - \boldsymbol{\alpha}^A)}^{\Delta \boldsymbol{\alpha}} \quad (4.39)$$

where  $S^M, S^A, \boldsymbol{\alpha}^M$ , and  $\boldsymbol{\alpha}^A$  are the scalar reduction of  $\boldsymbol{S}^M, \boldsymbol{S}^A, \boldsymbol{\alpha}^M$ , and  $\boldsymbol{\alpha}^A$ .

3. Following the same reasoning, the stiffness tensor  $\mathbf{C}$  can be substituted by the Young's modulus, which depends on the martensitic volume fraction and is defined as follows:

$$E = E^A + \zeta \overbrace{(E^M - E^A)}^{\Delta E} \quad (4.40)$$

4. The transformation tensor  $\mathbf{\Gamma}$  is calculated based on equation (4.25) considering the stress  $\sigma_{11}$  as follows:

$$\mathbf{\Gamma} = \begin{bmatrix} \frac{\varepsilon^{max} \sigma_{11}}{\sqrt{\sigma_{11}^2}} & 0 & 0 \\ 0 & -\frac{\varepsilon^{max} \sigma_{11}}{2\sqrt{\sigma_{11}^2}} & 0 \\ 0 & 0 & -\frac{\varepsilon^{max} \sigma_{11}}{2\sqrt{\sigma_{11}^2}} \end{bmatrix} \quad (4.41)$$

Thus, the double dot product  $\boldsymbol{\sigma} : \mathbf{\Gamma}$ , required in equation (4.35), becomes:

$$\boldsymbol{\sigma} : \mathbf{\Gamma} = \gamma = \frac{\varepsilon^{max} \sigma_{11}}{\sqrt{\sigma_{11}^2}} \sigma_{11} \quad (4.42)$$

5. Likewise, The thermoelastic part  $\varphi_{te}$  of the thermodynamic force becomes:

$$\varphi_{te} = \frac{1}{2} \Delta S \sigma_{11}^2 + \sigma_{11} \Delta \alpha (T - T_0) \quad (4.43)$$

Given the above conditions, equations (4.14), (4.15), (4.35) and (4.36) are reformulated for the SMA one-dimensional constitutive model (whose variables and parameters are summarized in bottom part of table 4.6) as follows:

$$\varepsilon = \frac{1}{2} \sigma_{11} S + \alpha (T - T_0) + \varepsilon^t \quad (4.44)$$

$$\sigma_{11} = \frac{1}{2} E \varepsilon - E \alpha (T - T_0) - E \varepsilon^t \quad (4.45)$$

$$\zeta = \begin{cases} \frac{\gamma + \varphi_{te} + \rho \Delta s_0 (T - M_s)}{\rho \Delta s_0 (M_f - M_s)} & \text{for } \dot{\zeta} > 0 \\ \frac{\gamma + \varphi_{te} + \rho \Delta s_0 (T - A_f)}{\rho \Delta s_0 (A_s - A_f)} & \text{for } \dot{\zeta} < 0 \end{cases} \quad (4.46)$$

$$\varepsilon^t = \frac{\varepsilon^{max} \sigma_{11}}{\sqrt{\sigma_{11}^2}} \zeta \quad (4.47)$$

Response functions	Equation	Variables	Parameters
Strain $\varepsilon$	(4.44)	$\sigma_{11}, \varepsilon^t, T, S, \alpha,$ $\zeta$	$S^A, S^M, \alpha^A, \alpha^M$
Stress $\sigma_{11}$	(4.45)	$\varepsilon, \varepsilon^t, T, E, \alpha, \zeta$	$E^A, E^M, \alpha^A, \alpha^M$
Martensitic volume fraction $\zeta$	(4.46)	$T, \sigma_{11}$	$\rho, \Delta s_0, M_s, M_f, A_s, A_f,$ $S^A, S^M, \alpha^A, \alpha^M, \varepsilon^{max}$
Transformation Strain $\varepsilon^t$	(4.47)	$\zeta, \sigma_{11},$	$\varepsilon^{max}$

Table 4.7: 1-D Constitutive model equations and parameters

### 4.2.3 Parametric identification of SMA based actuator

The material properties, required to feed the SMA's governing equations, are obtained from three experiments: i) a uniaxial test to identify martensite and austenite Young's modulus, ii) a strain recovery test to identify transformation temperatures and reference entropy difference, and iii) a double effect actuation test to characterize the complete actuator. Furthermore, informations furnished by the manufacturer, as austenite start temperature and the typical temperature vs strain characteristics, are used to complement the characterization. Table 4.8 summarizes the source and procedure used for the material's parameters identification.

Parameter	Description	Source	Method
$\rho$	Material density	Manufacturer	–
$\alpha^A$	Austenite thermal expansion coefficient	Manufacturer	–
$\alpha^M$	Austenite thermal expansion coefficient	Manufacturer	–
$\varepsilon^{max}$	Maximal strain	Manufacturer	–
$A_s$	Austenite start temperature	Manufacturer	–
$c$	Specific Heat	Manufacturer	–
$\Delta s_0$	Reference entropy difference	Manufacturer	Strain recovery test
$M_s$	Martensite start temperature	Manufacturer	Strain recovery test
$M_f$	Martensite finish temperature	Manufacturer	Strain recovery test
$A_f$	Austenite finish temperature	Manufacturer	Strain recovery test
$E^A$	Martensite Young's Modulus	Experiments	Uniaxial test
$E^M$	Austenite Young's Modulus	Experiments	Uniaxial test

Table 4.8: Sources and methods used to identify material parameters

### Experimental Estimation of SMA Young's modulus (uniaxial test)

The identification of the Young's Modulus during full austenite and martensite phases is performed through an experiment using a test machine. Seven specimens of an SMA wires are tested in uniaxial tension: i) first the wires are tested with thermal stimulus to measure the Young's modulus in full austenite phase and ii) then a thermal stimuli is removed to measure the Young's modulus in full martensite phase. The thermal stimuli is generated using a DC source in which voltage and current are controlled, then the temperature is measured and when it exceeds the reported max temperature of  $120^{\circ}\text{C}$  [170] the measure of the Young's Modulus in full austenite phase is performed.

In order to measure the Young's Modulus in both austenite and martensite phases, the machine is controlled in position. Taking into account that the material can change phase from austenite to martensite increasing the tensional stress, we apply a strain of 0.45% (corresponding to 10% of maximal strain) granting a axial stress lower than 172Mpa, in which material remains in austenite phase at a temperature of  $120^{\circ}$ .

During the test, force and displacement are measured and reordered using the LabView software from National Instruments, the cDAQ-9174 rack and and NI 9215 analog input module. Figure 4.3 shows the experimental set-up used to measure the Young's Modulus in both martensite and austenite phases.

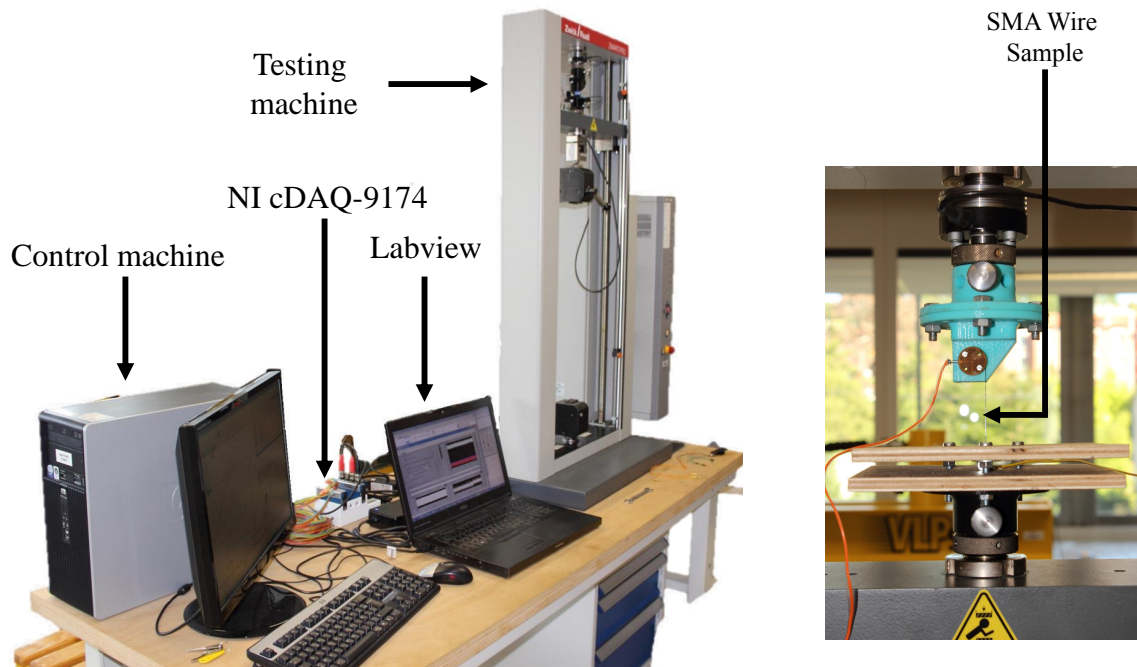


Figure 4.3: Experimental set-up to measure Young's Modulus

Figure 4.4: Placement of SMA wire specimen

Figure 4.4 shows a SMA wire specimen, which is fixed to the machine using a 3D printed support to isolate the wire from the machine. the specimens are Flexinol wires with diameter 0.38mm, the initial length  $l_0$  is 72mm. The Young's modulus are calculated using equa-

tion (4.48), in which  $F_m$  is the measured force,  $\varepsilon_m$  is the applied strain, and  $A$  is the cross section of the wire. The results are reported in table 4.9.

$$E = \frac{\sigma_m}{\varepsilon_m} = \frac{F_m}{A\varepsilon_m} \quad (4.48)$$

Phase	Measured force [N]	Standard deviation [N]	Young's modulus [GPa]
Austenite	16.33	0.77	$E^A = 31.8$
Martensite	6.00	0.39	$E^M = 11.7$

Table 4.9: Measured Young's modulus in martensite and austenite phases

#### Identification of transformation temperatures and reference entropy difference (strain recovery test)

The identification of the transformation temperatures  $M_s$ ,  $M_f$ ,  $A_s$ ,  $A_f$  and the reference entropy difference  $\Delta s_0$  is proposed as an optimization problem in which we seek to fit our model result to the temperature vs strain (see figure 4.5) response of the SMA wire, which is given by the manufacturer [170].

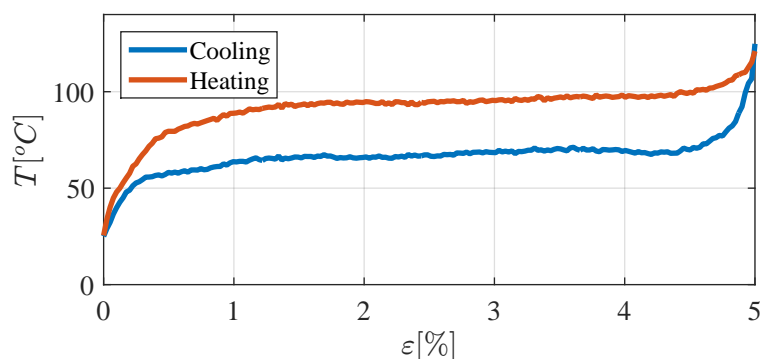


Figure 4.5: Temperature vs strain for NiTi SMAs at constant stress  $\sigma_{11} = 172\text{Mpa}$ .

The 1-D model, summarized in table 4.7 is used to simulate the strain in the following conditions: i) temperature changing from  $20^\circ\text{C}$  until  $120^\circ\text{C}$ , ii) stress  $\sigma_{11} = 172\text{Mpa}$ , iii) initial values of transformation temperatures and reference entropy difference as presented in table 4.10.

		Parameter	Value
Given parameters	Young's Modulus	$E^A$	3.18 GPa
		$E^M$	1.17 GPa
	Thermal Expansion Coefficient	$\alpha^A$	6.09E-06 K <sup>-1</sup>
		$\alpha^M$	1.09E-05 K <sup>-1</sup>
	Poisson Ratio	$\nu$	0.33
	Density	$\rho$	6450 kg/m <sup>3</sup>
	Specific Heat	$c$	837.36 J/Kg K
	Max Transformation Strain	$\epsilon^{max}$	0.045
Austenite Start Temperature	$A_s$	343.15 K	
Calculated parameters	Reference entropy difference	$\Delta s_0$	-17.91 J/m <sup>3</sup> K
	Finish Temperatures	$M_f$	313.15 K
		$A_f$	353.15 K
	Martensite Start Temperature	$M_s$	323.15 K

Table 4.10: Initial parameter values for 1-D model simulation.

The strain  $\epsilon$  resulting from the simulation is compared with the strain ( $\epsilon_g$ ) obtained from figure 4.5, to calculate a mean square error that is used as an objective function. Thus, we calculate the transformation temperatures  $M_s$ ,  $M_f$ ,  $A_s$ ,  $A_f$  and the reference entropy difference  $\Delta s_0$  to minimize the mean square error as follows:

$$\begin{aligned}
 & \arg \min_{M_s, M_f, A_s, A_f, \Delta s_0} \frac{1}{N_s} (\epsilon_i^2 - \epsilon_g^2) \\
 & \text{subject to } [A] \{ \Delta s_0 \ M_f \ A_f \ M_s \ A_s \}^T < \{0\} \\
 & A_s = 70^\circ\text{C}
 \end{aligned} \tag{4.49}$$

Where  $[A]$  guarantee that  $M_f < M_s < A_s < A_f$  and are formulated as follows:

$$[A] = \begin{bmatrix} 0 & 0 & -1 & 0 & 1 \\ 0 & 0 & 0 & 1 & -1 \\ 0 & 1 & 0 & -1 & 0 \end{bmatrix} \tag{4.50}$$

The optimization results to find the transformation temperatures  $M_s$ ,  $M_f$ ,  $A_s$ ,  $A_f$  and the reference entropy difference  $\Delta s_0$  are presented in figure 4.6, in which the blue and red circles represents the manufacturer SMA wire data and the continuous line are the model result. Clearly, the model has differences with respect to the manufacturer data at start and finish temperatures, this is because the chosen hardening function is a linear approximation of the phenomena. Even

that, the model solution is enough accurate to describe the material behavior. Furthermore, the parameters obtained from optimization are presented in table 4.11.

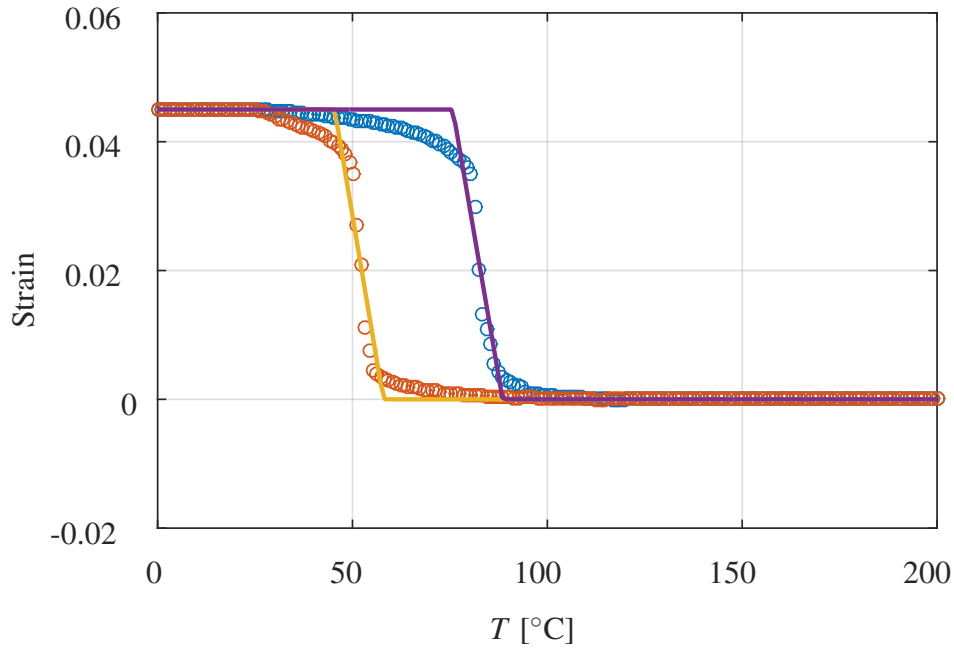


Figure 4.6: Optimization results.

Parameter	Value
Reference entropy difference	$\Delta s_0$ -923.80 J/m <sup>3</sup> K
Finish Temperature	$M_f$ 39.77°C
	$A_f$ 85.30°C
Start Temperature	$M_s$ 54.79°C
	$A_s$ 70.00°C

Table 4.11: Optimized parameter values for 1–D model simulation.

### Identification of the actuator model (double effect actuation test)

Finally, an experiment to identify the parameters of the complete model of the actuator is proposed. The experiment consists in a set-up following the characteristics of the SMA based motor introduced in figure 4.1, for the sake of simplicity, we use another SMA wire to produce a bidirectional rotation. Table 4.12 summarizes the source and procedure for the actuator parameter identification.

	Parameter	Description	Source	Method
Equation (4.4)	$J$	Rotor's inertial moment	CAD model	Measured
	$b$	Roller viscous friction coefficient	Experiments	Estimated
	$r$	Rotor pulley's ratio	CAD model	Measured
	$k$	Stiffness spring constant	Experiments	Estimated
Equation (4.7)	$m$	SMA wire mass	Manufacturer	Calculated
	$c$	SMA's specific heat	Manufacturer	–
	$h$	Convection coefficient	Experiments	Estimated
	$A$	External surface of SMA wire	CAD model	Calculated
	$R$	Electrical resistance of SMA wire	Manufacturer	–

Table 4.12: Sources and methods used to identify parameters for governing equations (4.4) and (4.7).



Figure 4.7: Experiment to identify and test the SMA-based actuator.

Figure 4.7 shows the experimental set-up used for the actuator identification. Four trials of clockwise and counter-clockwise rotation are performed (see figure 4.8), then the results are used to identify the required model parameters, that are reported in table 4.13.

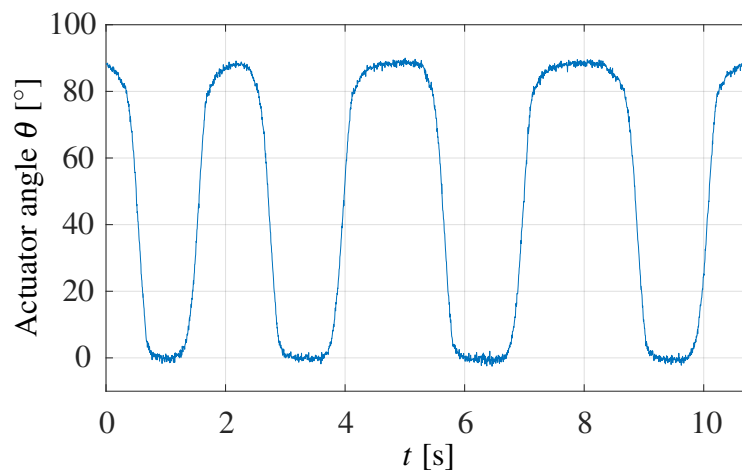


Figure 4.8: Angular position tracking of the actuator.

Parameter	Description	value
$J$	Rotor's inertial moment	$1.88 \times 10^{-8} \text{Kg m}^2$
$b$	Roller viscous friction coefficient	$0.019 \text{ N m s}$
$r$	Rotor pulley's ratio	$0.007 \text{ m}$
$h$	Convection coefficient	$555.6 \text{ W m}^{-2} \text{ K}^{-1}$
$k$	Stiffness spring constant	$1.24 \times 10^3 \text{ N m}^{-1}$

Table 4.13: Actuator parameters obtained using Matlab Ident toolbox.

The identified model is simulated using Matlab Simulink in which the one-dimensional constitutive model of the SMA is assembled with the two governing Equations (4.4) and (4.7) (see figure 4.9). Each block of the diagram corresponds to a part of the model, taking into account, kinematic and dynamics of the actuator.

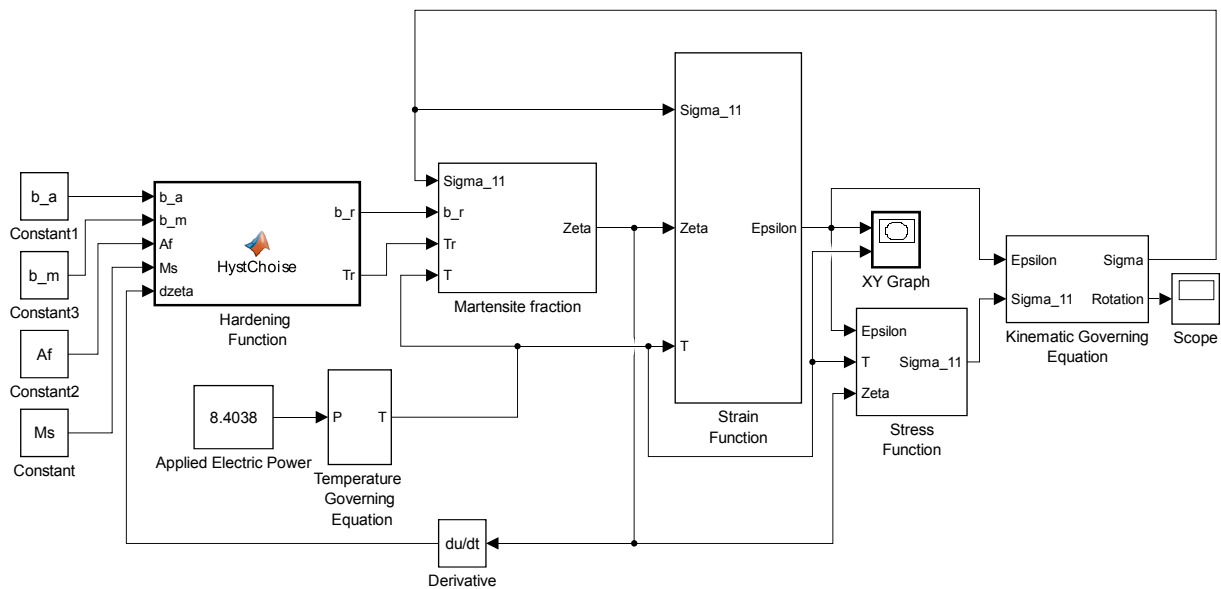


Figure 4.9: Simulink simulation of the complete proposed model.

The tracking of actuator's angular position is compared with the simulation results issued from the Simulink model. Figure 4.10 shows the simulated result represented by a blue line and the experimental data represented as red points. Certainly, both experimental and simulation results are highly coincident in steady state. In transient state a difference appear that could be explained by the behavior of the chosen hardening functions. Even the difference in the transient state, the proposed model is accurate enough to describe the behavior of the proposed SMA actuator.

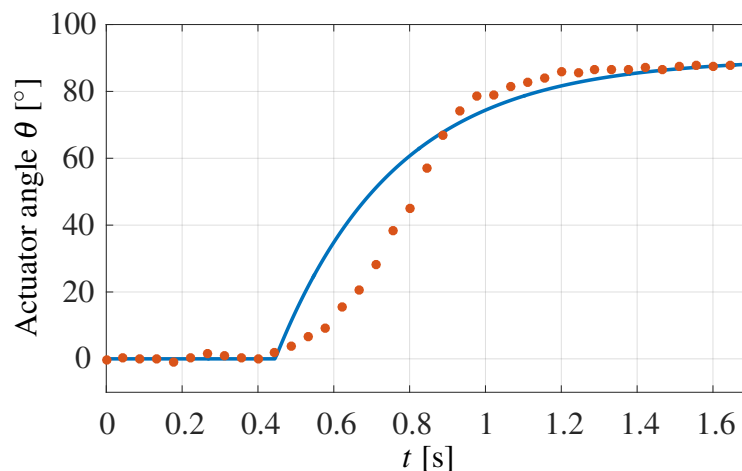


Figure 4.10: Simulation an experimental result of the SMA actuator.

### 4.3 Smart material based mechanism of Promain-II Hand

The bio-inspired soft robotic hand prosthesis ProMain-II has been designed, developed, and produced in the LEME laboratory, see Figure 4.11. It uses the virtues of the soft robotics, considering: i) soft epicyclic tendon-driven mechanism based on smart materials, which replicates functionally of human tendon-muscle mechanism, and ii) flexible bodies, which increases compliance and self adaptability with unknown objects and reduces the contact forces.

The soft prosthesis has three fingers, each of them has three phalanges<sup>2</sup>: proximal, medial and distal. And also three joints: Metacarpophalangeal (MCP), Proximal interphalangeal (PIP) and distal interphalangeal (DIP). MP and PIP has one DoF to perform flexion-extension, and DIP joints are endowed with high number of DoF, due to their flexible material. The fingers are assembled separately and then integrated to a support chassis with the same configuration of the ProMain-I hand, described in section 2.2. The support chassis offers the ideal configuration to perform the selected prehension patterns.

Each finger is controlled by only one servo motor XL-320 Dynamixel; hence PIP phalanx is driven by the MP phalanx. The clockwise rotation of the actuator produces the flexion and the opposite produces the extension. Thus, the angles of PIP joints depend on the rotation angle of MCP joints, which are linked to servomotor. Joints are identified by subindex  $i$ , where MP and PIP joint are  $i = 1$ ,  $i = 2$  respectively and the DIP bending joint is represented by  $i = 3$ . Moreover, each finger is represented by  $j$ , in which thumb, index and middle are  $j = 1$ ,  $j = 2$ ,  $j = 3$ , respectively. The relation between angles is established as  $\theta_2 = 0,9\theta_1$  and the bending angle formed by DIP joint depends on the object to grasp. Figure 4.11 illustrates the ProMain-II Hand architecture, in which disposition of the three fingers is highlighted. Furthermore, each finger has a force sensor in the fingertip.

<sup>2</sup>The hand and fingers architecture follows the same concept introduced in chapter 2 for the ProMain-I hand

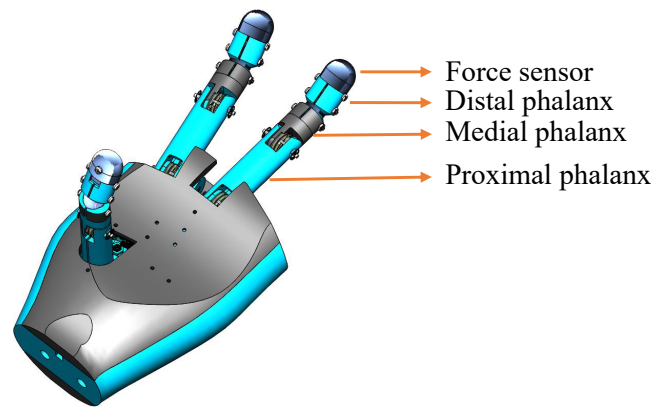


Figure 4.11: Promain Hand-II

In section 3.4 we have shown that the absence of damping in the tendons increases angular joint errors. Furthermore, under some particular conditions, the flexibility of the tendons requires being adapted to grasp objects in a more steady way. Taking into account that the addition of damper element in the tendon adds extra constraints to the soft behavior of the epicyclic mechanism, we modify the driving mechanism introduced in section 2.3 adding an SMA wire in parallel to flexible tendons to control joint stiffness during grasping. As a result, a new soft epicyclic tendon-driven actuation system based on SMA is proposed. The choice of SMA wires follows the study introduced in section 4.1.

The soft epicyclic tendon-driven actuation system is also based on the proposed hill's muscle model (see section 1.3.2), but the damper is substituted by a SMA wire in order to control the mechanism's stiffness. As can be seen figure 4.12, the SMA wire  $k_{Tce}$  is placed in parallel to the elastic tendon  $k_{Tee}$ . During the operation, when the tendon is under a tension  $F_T$  a control stimulus (Temperature increment) shift the SMA wire to austenite phase increasing the stiffness to recover the produced strain.

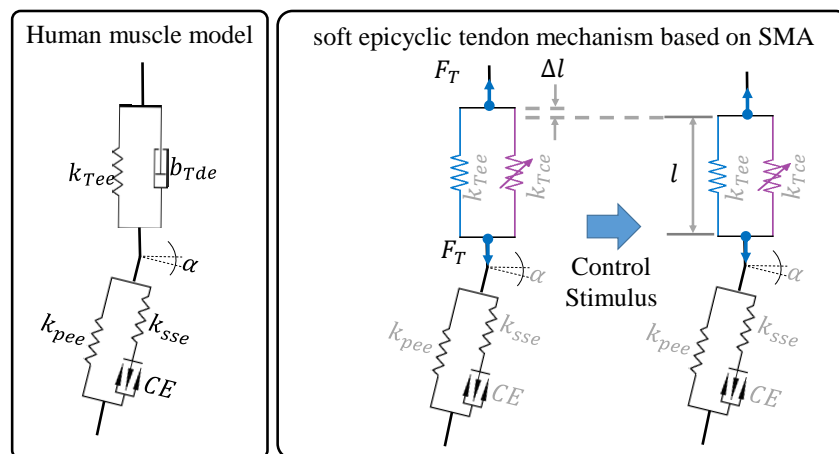


Figure 4.12: Schematic representation of the ProMain Hand-II's soft epicyclic tendon-driven actuation system based on SMA

Finger motion is produced by the soft epicyclic tendon-driven mechanism based on smart materials, which is shown in figures 4.13 and 4.14, and is mainly composed of: i) a servomotor (3), which is fixed to the pulley (6), see figure 4.13 ii) a pulley (7) that is fixed to the proximal phalange, iii) a pulley (22), that is fixed to the medial phalange, iv) a pulley (12), that is fixed to the finger framework v) two group of wires *WB*, each group, contains two wires placed in parallel, one is made of an elastic material, illustrated with a yellow line in figure 4.14, and the other wire is fabricated of shape memory alloy, which is represented by purple line in the same figure, and vi) two group of wires *WA*, composed only of flexible wires in parallel.

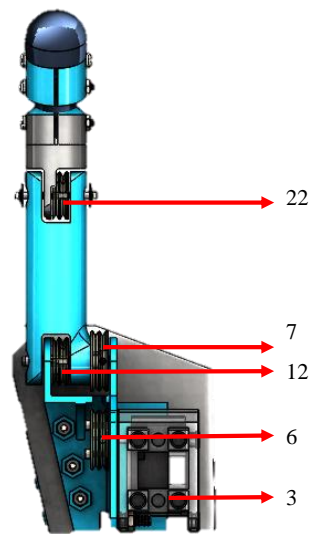


Figure 4.13: Promain Hand-II

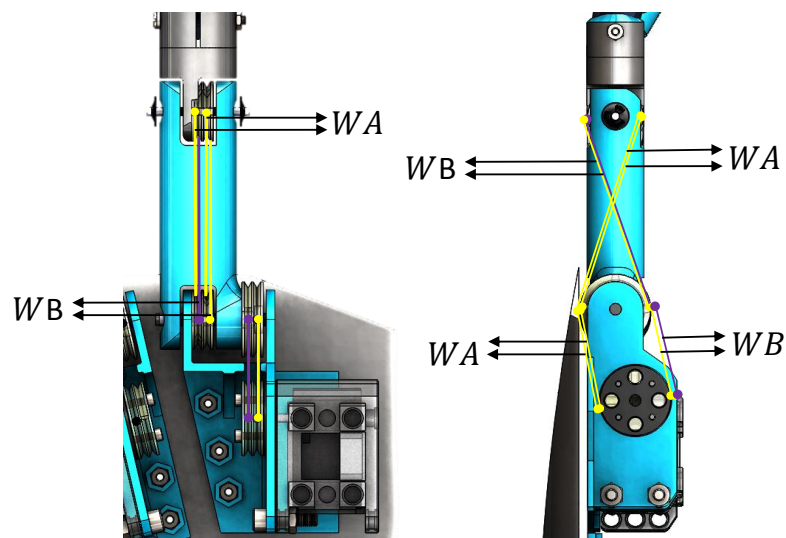


Figure 4.14: Promain Hand-II

The pulley (7) is linked to the pulley (6), through a group of wires *WA* and *WB*. The *WA* group is positioned in parallel with *WA* group. The pulley (12) is coupled to the pulley (22), by *WA* and *WB* group, but each group is crossed, see figure 4.14 right side. Group *WB* causes robotic finger flexion and the *WA* produces the extension motion. The flexible tendon and the parallel SMA wire are shown in figure 4.15 for the MCP Joint, and the assembly of the ProMain-II finger prototype is shown in figure 4.16.

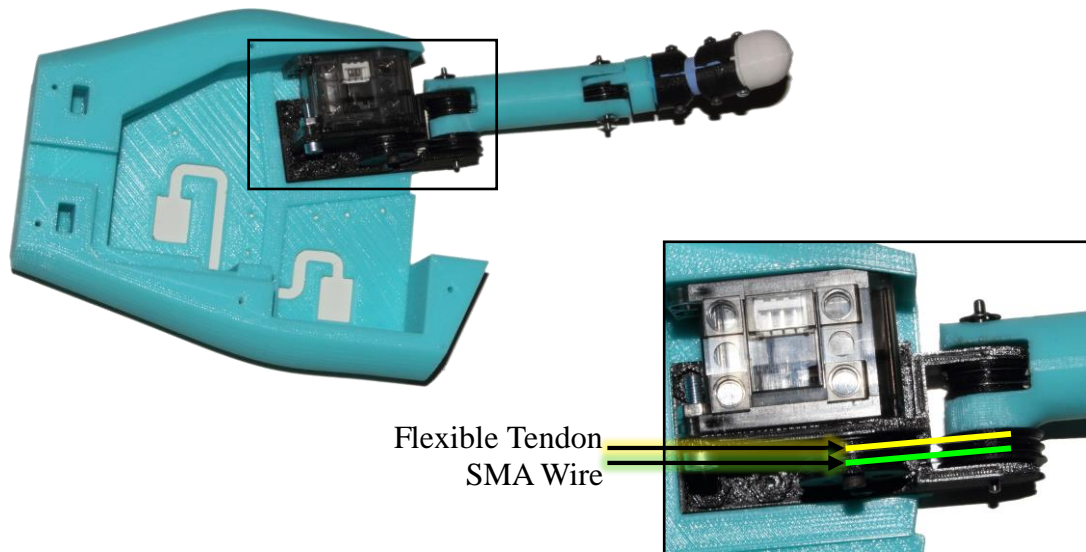


Figure 4.15: Parallel disposition of the flexible tendon and the SMA wire in the MCP joint



Figure 4.16: ProMain-II finger prototype

The flexion of the finger is produced when the servomotor turns in clockwise direction, see figure 4.17 causing that the pulley (6) and (7) turn in the same direction to the motor rotation.

It generates that the proximal phalange and the pulley (22) turn. The motion of the pulley (22) provides motion to the PIP phalange.

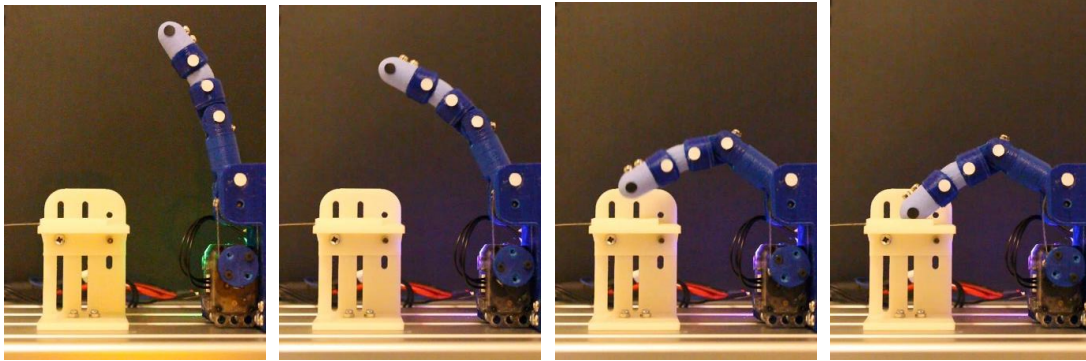


Figure 4.17: ProMain-II finger flexion cycle

Once the finger is in contact with the grasped object, the DIP joint is bended depending on the size and shape of the grasped object. Then, the shape memory alloy wire is activated with the goal of:

1. Changing the stiffness of the driving mechanism and
2. Increases stability in grasping task.

Once the grasping task is finished, the extension movement begins, in which the servomotor turns in the counter-clockwise direction. It causes that all the mechanism rotates in the opposite way to the flexion motion.

## 4.4 Discussion

In summary, we have introduced three main contributions in this chapter: 1. a review of state of the art regarding smart materials, which allows us to identify two materials as possible candidates to be used as artificial muscles, 2. a model of a complete actuator using SMA as main actuation system, the model allows us to simulate the whole behavior of the SMA taking into account the main material parameters, and 3. a new soft epicyclic tendon-driven mechanism based on smart materials that use an SMA-based tendon.

The proposed review considered the actuation requirements issued from the human precision grasping conditions merged with the experimental data released from the tests of the ProMain-I robotic hand prosthesis. These requirements are summarized into three main parameters: actuation force, active strain, and frequency. Then, the smart materials that could fit the proposed requirements were studied and compared. As a result, we identify that the only one that meets all the requirements is the shape memory alloy.

A constitutive model to study the SMAs behavior is proposed, the model is simplified to one dimension to model the Flexinol wires used in the rotary SMA-based prototype of the actuator.

---

Moreover, the SMA constitutive model is merged with two governing equations that describe the dynamic of rotation and the dynamics of the temperature applied to the SMA wire using an electrical current as input. The obtained results show that the SMA fulfill the precision grasping requirements and the experiment allows us to validate the proposed constitutive model of SMA. The solution of the SMA model is issued from experimental analysis performed using a testing machine and the actuator set-up.

Finally, we introduce the design of a new version of the soft epicyclic mechanism using an SMA wire in parallel to the flexible tendon for the ProMain-II soft robotic prosthesis hand. This actuation system allows controlling the stiffness of the actuated joints controlling the damping effect evidenced during the experiments performed with the ProMain-I finger.

# Chapter 5

## Conclusions

The synergy between the mechanism, the actuation, and the functionality has been taken into account to formulate the requirements for a prosthetic hand. For that purpose, we studied: i) the hand anatomy and the joint limits during movements to propose an equivalent biomechanic model of the human hand. ii) the grasping gestures, taking into account the frequency of utilization of movements and the most used grasping gestures in daily living and working activities, to choose the group of movements that a hand prosthesis should perform. iii) the human force during precision grasping considering two approaches: a Hill's equivalent model suitable to qualify the muscle's behavior through the comparison with mechanical elements, and an experimental assessment of the human pinch force. As a result, we define the most used grasping gestures, which at the same time are the movements that a hand prosthesis must perform and the requirements needed to develop a robotic hand prosthesis that is actuated using smart materials.

The most used grasping gestures are: i) medium wrap, ii) light tool, iii) prismatic four fingers, iv) prismatic three fingers, v) prismatic two fingers, vi) precision disk, and vii) tripod. We have shown that these seven grasping movements can be merged in single hand gestures using three fingers, if the prosthetic hand have enough compliance to be adapted to different objects. Thus, a robotic prosthetic hand fitted with three fingers can fulfill six of the seven most used hand gestures, restoring 85.7% of the daily working necessities regarding hand usage of an amputated person.

With respect to requirements needed to develop a robotic hand prosthesis we find that: i) The active flexion of the MCP, PIP, and DIP joints must be in the range  $[60, 90]$  degrees. ii) The adduction and abduction movements are important to prepare the hand for grasping, but not during the grasping, in which the most important movement is flexion. iii) The behavior of the actuators must follow a viscoelastic schema as proposed in the Hill-based model. iv) The necessary force range is in the interval  $[4.78\text{N}, 6.70\text{N}]$ . v) The operating frequency must be in the interval  $[8.89\text{Hz}, 22.2\text{Hz}]$ .

Following the proposed considerations based on the human grasping requirements, a new actuation system, so-called soft epicyclic tendon-based mechanism, is developed to add a soft behavior to the robotic hand joints. The mechanism actuates the soft robotic hand prosthesis

ProMain-I hand, which has three fingers, is under-actuated, and has a support designed to hold the fingers in an ideal position to perform the selected precision grasping gestures. The driving mechanism is able to accurately fix the joint angles relations during free movement. A new kinematic model DHKK-SRQ is introduced, the approach combines the parameterization of Denavit-Hartenberg DH with the formulation of rotations using quaternions. The DHKK-SRQ allows accurately modeling the rotations that arise with the soft behavior of the ProMain-I hand.

An alpha prototype of the robotic finger is introduced and tested to validate the DHKK-SRQ model experimentally. The obtained results show that the kinematic model (DHKK-SRQ) presents better result than the DHKK model, as it produces smaller errors. The error of our method is lower because after getting in contact with the object, the DHKK-SRQ is launched and the mechanical slack of the finger is modeled as angles  $\alpha_{ji}$  and  $\beta_{ji}$ . The error reduction is more important for the final model of the ProMain-I hand, which is subject to inspected rotations ( $\alpha$  and  $\beta$ ) that arise with the utilization of the soft epicyclic mechanism.

Furthermore, we use the alpha finger to identify key design considerations for the ProMain-I finger. The tests are conducted using two fingers placed to perform pinch movements, and are conducted increasing distances between fingers (50, 55, 60 and 65mm) to evaluate the influence of finger placement in the applied fingertip force. The results show that the force changes in function of the fingers position. The higher pinch forces are measured when the distance between fingers is set to 5.5 and 6.0 cm. Furthermore, the amount of force, performed during the pinch experiment, is close to the lower limit of the human pinch force using the actuators HS-422 and XL-320.

The designed ProMain-I finger is also assessed experimentally with the aim of validating its performance in terms of displacement and force. The PIP and DIP joint angles show a under-damped behavior for the PIP and the DIP joints when the finger gets in contact with the platform where the force sensor is placed. We compare the angle value obtained from the kinematic measure with the calculated angle value issued from fixed transmission relation of the soft epicyclic mechanism. As a result, we find that the mean absolute error of the PIP angle is  $2.2139^\circ$ , and the standard deviation is  $1.2206^\circ$ . With respect to the angle of the DIP joint, the mean absolute error is  $2.6235^\circ$ , and the standard deviation is  $1.6370^\circ$ . This error is coherent with the softness of the driving mechanism.

Moreover, a design methodology for smart material based actuators is introduced. The method considers three main features to design smart material based actuator, which are the force  $f_a$ , the active strain  $\varepsilon$  and the frequency  $\omega_n$ . The strain is obtained from the robot features, the frequency is based on the human settling time and the force is estimated from experiments on human hand combined with kinematics and dynamics of the robot. The parameters are defined for extension and bending based smart materials as: i) Minimum active strain 5.5% for extension-based actuation or 60% bending-based actuation, ii) Frequency [8.89Hz, 22.2Hz], and iii) Force [4.78N, 6.70N] for bending-based actuation or Force [17.81N, 25.11N] for extension-based actuation .

---

A study of state of the art regarding smart materials is introduced. The study evaluates and compares the smart materials features with ProMain-I actuation requirements. As a result, we chose the shape memory alloys (SMA) for the actuation solutions considering that it fits all the actuation needs. Moreover, this study allows us to point out that the precision grasping movements can be achieved using smart material based actuators. A double effect rotary actuator based on SMA is introduced. Also, a constitutive model for the SMA is presented with two governing equations to define the dynamic behavior of the actuator. The model is experimentally identified, and we prove that during the steady state the error is close to zero. Furthermore, we validate that the proposed actuator is suitable to be implemented in a robotic hand prosthesis designed for precision applications.

Finally, an evolution of the soft epicyclic mechanism is proposed in which an SMA wire is placed in parallel with the soft tendon allowing joint stiffness control. This improvement allows to increase or reduced the damping effect according to the grasping requirements. The preliminary tests performed with the ProMain-II finger prototype have shown a better adaptability to variable conditions, and a reduction of the joint angle error during contact when the SMA wire is activated.

This progress is encouraging and permits to follow new directions in the research of smart materials for artificial muscles in robotic hands.



# Chapter 6

## Perspectives

In this thesis dissertation, we have introduced: i) the development of two prototypes of the robotic hand prostheses ProMain, ii) the design and modeling of an SMA-based actuator, iii) the development of a soft epicyclic driving mechanism, and iv) the evolution of the soft epicyclic driving mechanism including a parallel SMA wire to control the joints stiffness during grasping movements. These contributions are based on the functionality of the human hand, the biomechanical assessment of the human musculoskeletal system, and the mechanic constraints of the designed robotic hand. Furthermore, our research opens the scope to new questions, *e.g.* the assessment of the soft epicyclic driving mechanism to test the efficiency controlling soft joints stiffness, the test in a three-dimensional working space of the DHKK-SRQ kinematic model, and the development of other new actuation technology merging the advantages of various smart materials.

The soft epicyclic driving mechanism has been assembled in the prototype of the ProMain-II soft robotic hand prosthesis. The preliminary tests have shown that the combination of the variable stiffness joints (in which SMA wires control the stiffness) and the flexible link (introduced in the patent FR1656673 [173]) furnishes a desirable soft behavior to grasp objects in a smooth and steady way. Thus, we envision the development of a set of tests aiming to highlight and prove the advantage offered by the combination of those two elements.

The DHKK-SRQ model has shown to be suitable to accurately formulate soft rotations while the grasping task is performed considering hand-object interaction. Moreover, the integration of a soft link in the ProMain-II robotic hand prosthesis has reinforced the need to model soft rotations in an accurate way. Thus, we foresee the development of an experimental set-up in a motion capture laboratory to evaluate the performance of the robotic hand and quantify the accuracy of the DHKK-SRQ model in the three-dimensional working space.

Concerning the application of smart materials for robotic hand prosthesis, we have proved that the SMA is a suitable solution for actuation during grasping. Moreover, our review of smart materials allows us to identify that the Ionic Polymer Metal Composites IPMCs fulfill two (strain and frequency) of the three primary actuation requirements. We have also carried a preliminary work concerning the modeling and identification of this kind of materials for grasp-

ing applications. This preliminary work allows us to establish that the IPMCs have the potential to fulfill precision grasping requirements. For that purpose, additional research concerning the modeling and assessment of this material is required. Consequently, we consider that an important perspective concerns the improvement of the hand mechanism and the development of a hybrid actuation system using IPCMs.

# Bibliography

- [1] J.L. Ramírez, A. Rubiano, N. Jouandeau, L. Gallimard, and O. Polit. *New Trends in Medical and Service Robots: Human Centered Analysis, Control and Design*, chapter Morphological optimization of prosthesis' finger for precision grasping, pages 249–263. Springer International Publishing, Nantes, FR, jul 2016. ISBN 978-3-319-30674-2. doi: 10.1007/978-3-319-30674-2\_19. URL [http://dx.doi.org/10.1007/978-3-319-30674-2\\_19](http://dx.doi.org/10.1007/978-3-319-30674-2_19).
- [2] J.L. Ramírez, A. Rubiano, N. Jouandeau, L. Gallimard, and O. Polit. *Smart structures and materials*, chapter Artificial muscles design methodology applied to robotic fingers, pages 1–17. Springer, 2015.
- [3] J.L. Ramírez, A. Rubiano, N. Jouandeau, M.N. El Korso, L. Gallimard, and O. Polit. Hybrid kinematic model applied to the under-actuated robotic hand prosthesis ProMain-I and experimental evaluation. In *Proceedings of 14th IEEE/RAS-EMBS International Conference in rehabilitation robotics (ICORR)*, pages 301–306, Singapore, SGP, aug 2015. IEEE.
- [4] A. Rubiano, J. L. Ramirez, L. Gallimard, O. Polit, and N. Jouandeau. Chaîne articulée comprenant un unique actionneur et ensemble de chaînes articulées associées FR1656914, Jul. 2016.
- [5] S.G. Nurzaman, F. Iida, C. Laschi, A. Ishiguro, and R. Wood. Soft robotics [tc spotlight]. *IEEE Robotics Automation Magazine*, 20(3):24–95, sep 2013. ISSN 1070-9932.
- [6] Ottobock HealthCare. *SensorHand Speed VariPlus Speed*. Deutschland GmbH, Max-Näder-Straße 15, 37115 Duderstadt/Germany, 2013.
- [7] *Bebionic Technical Manual*. Steeper, 3619 Paesanos Parkway, Suite 200, San Antonio TX 78231 USA, 2 edition, 2015.
- [8] *i-limb<sup>TM</sup> ultra Clinician Manual*. touch bionics, 35 Hampden Road Mansfield MA 02048 USA, 2 edition, Mar 2013.
- [9] *The Michelangelo® Hand in Practice*. Ottobock, Max-Näder-Straße 15, 37115 Duderstadt/Germany.

- [10] S. Kim, C. Laschi, and B. Trimmer. Soft robotics: a bioinspired evolution in robotics. *Trends in biotechnology*, 31(5):287–294, 2013.
- [11] G. Schlesinger. *Ersatzglieder und Arbeitshilfen: Für Kriegsbeschädigte und Unfallverletzte*, chapter Der mechanische Aufbau der künstlichen Glieder, pages 321–661. Springer Berlin Heidelberg, Berlin, Heidelberg, 1919. ISBN 978-3-662-33009-8. doi: 10.1007/978-3-662-33009-8\_13. URL [http://dx.doi.org/10.1007/978-3-662-33009-8\\_13](http://dx.doi.org/10.1007/978-3-662-33009-8_13).
- [12] Donald B. Slocum and Donald R. Pratt. Disability evaluation for the hand. *The Journal of Bone & Joint Surgery*, 28(3):491–495, 1946. ISSN 0375-9229. URL <http://jbjs.org/content/28/3/491>.
- [13] C. L. Taylor and R. J. Schwarz. The anatomy and mechanics of the human hand. *Artificial limbs*, 2(2):22–35, 1955.
- [14] J. R. Napier. The prehensile movements of the human hand. *Bone & Joint Journal*, 38(4):902–913, 1956.
- [15] D. Lyons. A simple set of grasps for a dextrous hand. In *Proceedings of IEEE International Conference on Robotics and Automation*, volume 2, pages 588–593, mar 1985. doi: 10.1109/ROBOT.1985.1087226.
- [16] M. A. Arbib, T. Iberall, and D.M. Lyons. Coordinated control programs for movements of the hand. *Hand function and the neocortex*, pages 111–129, 1985.
- [17] T. Feix, J. Romero, H. B. Schmiebmayer, A. M. Dollar, and D. Kragic. The grasp taxonomy of human grasp types. *IEEE Transactions on Human-Machine Systems*, 46(1):66–77, feb 2016. ISSN 2168-2291. doi: 10.1109/THMS.2015.2470657.
- [18] WP Cooney and EY Chao. Biomechanical analysis of static forces in the thumb during hand function. *The Journal of Bone & Joint Surgery*, 59(1):27–36, 1977. ISSN 0021-9355. URL <http://jbjs.org/content/59/1/27>.
- [19] N. Kamakura, M. Matsuo, H. Ishii, F. Mitsuboshi, and Y. Miura. Patterns of static prehension in normal hands. *American Journal of Occupational Therapy*, 34(7):437–445, 1980.
- [20] J. M. Elliott and K. J. Connolly. A classification of manipulative hand movements. *Developmental Medicine & Child Neurology*, 26(3):283–296, 1984.
- [21] M. Cutkosky and P. Wright. Modeling manufacturing grips and correlations with the design of robotic hands. In *Robotics and Automation. Proceedings. 1986 IEEE International Conference on*, volume 3, pages 1533–1539, Apr 1986. doi: 10.1109/ROBOT.1986.1087525.

## BIBLIOGRAPHY

---

- [22] T. Feix, R. Pawlik, H. Schmiedmayer, J. Romero, and D. Kragic. A comprehensive grasp taxonomy. In *Proceedings of Robotics, Science and Systems: Workshop on Understanding the Human Hand for Advancing Robotic Manipulation*, pages 1–2, jun 2009. URL <http://grasp.xief.net>.
- [23] M. Vergara, J.L. Sancho-Bru, V. Gracia-Ibáñez, and A. Pérez-González. An introductory study of common grasps used by adults during performance of activities of daily living. *Journal of Hand Therapy*, 27(3):225–234, July 2014. ISSN 08941130. doi: 10.1016/j.jht.2014.04.002. URL <http://linkinghub.elsevier.com/retrieve/pii/S0894113014000520>.
- [24] Y. Yang, C. Fermüller, Y. Li, and Y. Aloimonos. Grasp type revisited: A modern perspective on a classical feature for vision. In *2015 IEEE Conference on Computer Vision and Pattern Recognition (CVPR)*, pages 400–408, June 2015. doi: 10.1109/CVPR.2015.7298637.
- [25] K. Wolf, A. Naumann, M. Rohs, and J. Müller. A Taxonomy of Microinteractions: Defining Microgestures Based on Ergonomic and Scenario-Dependent Requirements. In *Human-Computer Interaction - INTERACT 2011*, volume 6946, pages 559–575. Springer Berlin Heidelberg, Berlin, Heidelberg, 2011. ISBN 978-3-642-23773-7 978-3-642-23774-4. URL [http://link.springer.com/10.1007/978-3-642-23774-4\\_45](http://link.springer.com/10.1007/978-3-642-23774-4_45).
- [26] R. Wimmer and S. Boring. Handsense: Discriminating different ways of grasping and holding a tangible user interface. In *Proceedings of the 3rd International Conference on Tangible and Embedded Interaction*, pages 359–362. ACM, 2009.
- [27] R. F. Weir and J. W. Sensinger. *Design of artificial arms and hands for prosthetic applications*. McGraw Hill, New York, 2003.
- [28] L. Villani, F. Ficuciello, V. Lippiello, G. Palli, F. Ruggiero, and B. Siciliano. Grasping and Control of Multi-Fingered Hands. In Bruno Siciliano, editor, *Advanced Bimanual Manipulation*, volume 80, pages 219–266. Springer Berlin Heidelberg, Berlin, Heidelberg, 2012. ISBN 978-3-642-29040-4 978-3-642-29041-1. URL [http://link.springer.com/10.1007/978-3-642-29041-1\\_5](http://link.springer.com/10.1007/978-3-642-29041-1_5).
- [29] K. M. Varadarajan and M. Vincze. Knowledge Representation and Inference for Grasp Affordances. In *Computer Vision Systems*, volume 6962, pages 173–182. Springer Berlin Heidelberg, Berlin, Heidelberg, 2011. ISBN 978-3-642-23967-0 978-3-642-23968-7. URL [http://link.springer.com/10.1007/978-3-642-23968-7\\_18](http://link.springer.com/10.1007/978-3-642-23968-7_18).
- [30] R. Tomovic, G. Bekey, and W. Karplus. A strategy for grasp synthesis with multifingered robot hands. In *Proceedings of IEEE International Conference on Robotics and Automation*, volume 4, pages 83–89, mar 1987. doi: 10.1109/ROBOT.1987.1087842.

- [31] G. Tessitore, C. Sinigaglia, and R. Prevede. Hierarchical and multiple hand action representation using temporal postural synergies. *Experimental Brain Research*, 225(1): 11–36, March 2013. ISSN 0014-4819, 1432-1106. doi: 10.1007/s00221-012-3344-9. URL <http://link.springer.com/10.1007/s00221-012-3344-9>.
- [32] P. Sung. Biomechanical assessment of muscle forces of thumb and fingers for simulated glovebox tasks with three commonly used hand tools. *International Journal of Applied Science and Engineering*, 9(2):83–98, 2011.
- [33] C. Sollerman and A. Ejeskär. Sollerman Hand Function Test: A Standardised Method and its Use in Tetraplegic Patients. *Scandinavian Journal of Plastic and Reconstructive Surgery and Hand Surgery*, 29(2):167–176, January 1995. ISSN 0284-4311. doi: 10.3109/02844319509034334. URL <http://www.tandfonline.com/doi/full/10.3109/02844319509034334>.
- [34] C. Rosales, L. Ros, J. M. Porta, and R. Suárez. Synthesizing grasp configurations with specified contact regions. *The International Journal of Robotics Research*, 30(4): 431–443, 2011. doi: 10.1177/0278364910370218. URL <http://ijr.sagepub.com/content/30/4/431.abstract>.
- [35] G. Palli, C. Melchiorri, G. Vassura, U. Scarcia, L. Moriello, G. Berselli, A. Cavallo, G. De Maria, C. Natale, S. Pirozzi, C. May, F. Ficuciello, and B. Siciliano. The dextrart hand: Mechatronic design and experimental evaluation of synergy-based control for human-like grasping. *The International Journal of Robotics Research*, 33(5):799–824, 2014. doi: 10.1177/0278364913519897. URL <http://ijr.sagepub.com/content/33/5/799.abstract>.
- [36] T. Mishra, P. Guha, A. Dutta, and K. S. Venkatesh. Stochastic re-grasp planning for vision aided capture of deforming and moving object. *Mechatronics*, 19(4):510–519, 2009. ISSN 0957-4158. doi: <http://dx.doi.org/10.1016/j.mechatronics.2008.12.002>. URL <http://www.sciencedirect.com/science/article/pii/S0957415808001967>.
- [37] G. Michelitsch, J. Williams, M. Osen, B. Jimenez, and S. Rapp. Haptic chameleon: a new concept of shape-changing user interface controls with force feedback. In *Proceedings of Human Factors in Computing Systems 04'*, page 1305. ACM Press, 2004. ISBN 978-1-58113-703-3. doi: 10.1145/985921.986050. URL <http://portal.acm.org/citation.cfm?doid=985921.986050>.
- [38] C. L. MacKenzie and T. Iberall. *The grasping hand*, volume 104. Elsevier, 1994. URL <https://books.google.fr/books?id=V9G5Yd46VlEC&printsec=frontcover&hl=fr#v=onepage&q&f=false>.

## BIBLIOGRAPHY

---

- [39] J. Liu, F. Feng, Y. C. Nakamura, and N. S. Pollard. A taxonomy of everyday grasps in action. In *2014 IEEE-RAS International Conference on Humanoid Robots*, pages 573–580, November 2014. doi: 10.1109/HUMANOIDS.2014.7041420.
- [40] Y. Lin and Y. Sun. Robot grasp planning based on demonstrated grasp strategies. *The International Journal of Robotics Research*, 34(1):26–42, 2015. doi: 10.1177/0278364914555544. URL <http://ijr.sagepub.com/content/34/1/26.abstract>.
- [41] C. M. Light, P. H. Chappell, P. J. Kyberd, and B. S. Ellis. A Critical Review of Functionality Assessment in Natural and Prosthetic Hands. *The British Journal of Occupational Therapy*, 62(1):7–12, 1999. doi: 10.1177/030802269906200103. URL <http://bjo.sagepub.com/content/62/1/7.abstract>.
- [42] C. M. Light, P. H. Chappell, and P. J. Kyberd. Establishing a standardized clinical assessment tool of pathologic and prosthetic hand function: normative data, reliability, and validity. *Archives of physical medicine and rehabilitation*, 83(6):776–783, 2002.
- [43] K. Lee and M. Jung. Investigation of hand postures in manufacturing industries according to hand and object properties. *International Journal of Industrial Ergonomics*, 46:98–104, March 2015. ISSN 01698141. doi: 10.1016/j.ergon.2015.01.001. URL <http://linkinghub.elsevier.com/retrieve/pii/S0169814115000104>.
- [44] J. M. F. Landsmeer. Power Grip and Precision Handling. *Annals of the Rheumatic Diseases*, 21(2):164–170, June 1962. ISSN 0003-4967. doi: 10.1136/ard.21.2.164. URL <http://ard.bmj.com/cgi/doi/10.1136/ard.21.2.164>.
- [45] K. H. Kroemer. Coupling the hand with the handle: An improved notation of touch, grip, and grasp. *Human factors*, 28(3):337–339, 1986.
- [46] G. Kootstra, M. Popović, Jørgensen, J. A., K. Kuklinski, K. Miatliuk, D. Kragic, and N. Krüger. Enabling grasping of unknown objects through a synergistic use of edge and surface information. *The International Journal of Robotics Research*, 31(10):1190–1213, 2012. doi: 10.1177/0278364912452621. URL <http://ijr.sagepub.com/content/31/10/1190.abstract>.
- [47] S. L. Kilbreath and R. C. Heard. Frequency of hand use in healthy older persons. *Australian Journal of Physiotherapy*, 51(2):119–122, 2005. ISSN 00049514. doi: 10.1016/S0004-9514(05)70040-4. URL <http://linkinghub.elsevier.com/retrieve/pii/S0004951405700404>.
- [48] A.I. Kapandji. *Anatomie fonctionnelle: Tome 1 - Membre Supérieur*. Maloine, Paris, FR, 6 edition, may 2005.

- [49] S. B. Kang and K. Ikeuchi. Toward automatic robot instruction from perception-mapping human grasps to manipulator grasps. *IEEE Transactions on Robotics and Automation*, 13(1):81–95, 1997. ISSN 1042-296X. doi: 10.1109/70.554349.
- [50] S. B. Kang and K. Ikeuchi. Robot task programming by human demonstration: mapping human grasps to manipulator grasps. In *Proceedings of the IEEE/RSJ/GI International Conference on Intelligent Robots and Systems IROS*, volume 1, pages 97–104, 1994.
- [51] S. B. Kang and K. Ikeuchi. Grasp recognition using the contact web. In *Proceedings of the IEEE/RSJ International Conference on Intelligent Robots and Systems*, volume 1, pages 194–201, jul 1992. doi: 10.1109/IROS.1992.587321.
- [52] G. Juravle, H. Deubel, and C. Spence. Attention and suppression affect tactile perception in reach-to-grasp movements. *Acta Psychologica*, 138(2):302–310, October 2011. ISSN 00016918. doi: 10.1016/j.actpsy.2011.08.001. URL <http://linkinghub.elsevier.com/retrieve/pii/S0001691811001417>.
- [53] L. A. Jones and S. J. Lederman. *Human Hand Function*. Oxford University Press, May 2006. ISBN 978-0-19-517315-4. URL <http://www.oxfordscholarship.com/view/10.1093/acprof:oso/9780195173154.001.0001/acprof-9780195173154>.
- [54] T. Iberall. Human prehension and dexterous robot hands. *The International Journal of Robotics Research*, 16(3):285–299, 1997.
- [55] T. Iberall. Grasp Planning from Human Prehension. In *IJCAI*, volume 87, pages 1153–1157. Citeseer, 1987.
- [56] F. Hemmert, S. Hamann, M. Löwe, A. Wohlauf, and G. Joost. Shape-changing mobiles: tapering in one-dimensional deformational displays in mobile phones. In *Proceedings of the fourth international conference on Tangible, embedded, and embodied interaction*, pages 249–252. ACM Press, 2010. ISBN 978-1-60558-841-4. doi: 10.1145/1709886.1709936. URL <http://portal.acm.org/citation.cfm?doid=1709886.1709936>.
- [57] P. Haggard. Planning of action sequences. *Acta Psychologica*, 99(2):201–215, July 1998. ISSN 00016918. doi: 10.1016/S0001-6918(98)00011-0. URL <http://linkinghub.elsevier.com/retrieve/pii/S0001691898000110>.
- [58] R. Gilster, C. Hesse, and H. Deubel. Contact points during multidigit grasping of geometric objects. *Experimental Brain Research*, 217(1):137–151, March 2012. ISSN 0014-4819, 1432-1106. doi: 10.1007/s00221-011-2980-9. URL <http://link.springer.com/10.1007/s00221-011-2980-9>.
- [59] F. Ficuciello, G. Palli, C. Melchiorri, and B. Siciliano. Planning and control during reach to grasp using the three predominant UB hand IV postural synergies. In *2012 IEEE*

## BIBLIOGRAPHY

---

- International Conference on Robotics and Automation (ICRA)*, pages 2255–2260, 2012. doi: 10.1109/ICRA.2012.6224922.
- [60] T. Feix, I. M. Bullock, and A. M. Dollar. Analysis of Human Grasping Behavior: Object Characteristics and Grasp Type. *IEEE Transactions on Haptics*, 7(3):311–323, July 2014. ISSN 1939-1412. doi: 10.1109/TOH.2014.2326871.
- [61] T. Feix, I. M. Bullock, and A. M. Dollar. Analysis of Human Grasping Behavior: Correlating Tasks, Objects and Grasps. *IEEE Transactions on Haptics*, 7(4):430–441, October 2014. ISSN 1939-1412. doi: 10.1109/TOH.2014.2326867.
- [62] T. Feix. *Anthropomorphic Hand Optimization based on a Latent Space Analysis*. PhD thesis, Vienna University of Technology, 2011. URL <http://me.xief.net/publications/thesis.pdf>.
- [63] S. Ekvall and D. Kragic. Grasp Recognition for Programming by Demonstration. In *Proceedings of the 2005 IEEE International Conference on Robotics and Automation*, pages 748–753, April 2005. doi: 10.1109/ROBOT.2005.1570207.
- [64] M. R. Cutkosky. On grasp choice, grasp models, and the design of hands for manufacturing tasks. *IEEE Transactions on Robotics and Automation*, 5(3):269–279, jun 1989. ISSN 1042-296X. doi: 10.1109/70.34763.
- [65] R. G. Cohen and D. A. Rosenbaum. Where grasps are made reveals how grasps are planned: generation and recall of motor plans. *Experimental Brain Research*, 157(4), August 2004. ISSN 0014-4819, 1432-1106. doi: 10.1007/s00221-004-1862-9. URL <http://link.springer.com/10.1007/s00221-004-1862-9>.
- [66] C. Cipriani, M. Controzzi, and M. C. Carrozza. Progress towards the development of the SmartHand transradial prosthesis. In *2009 IEEE International Conference on Rehabilitation Robotics*, pages 682–687, June 2009. doi: 10.1109/ICORR.2009.5209620.
- [67] M. T. Ciocarlie and P. K. Allen. Hand posture subspaces for dexterous robotic grasping. *The International Journal of Robotics Research*, 28(7):851–867, 2009.
- [68] M. Ciocarlie, C. Lackner, and P. Allen. Soft finger model with adaptive contact geometry for grasping and manipulation tasks. In *Second Joint EuroHaptics Conference and Symposium on Haptic Interfaces for Virtual Environment and Teleoperator Systems (WHC'07)*, pages 219–224, mar 2007. doi: 10.1109/WHC.2007.103.
- [69] I. M. Bullock, J. Z. Zheng, S. D. L. Rosa, C. Guertler, and A. M. Dollar. Grasp Frequency and Usage in Daily Household and Machine Shop Tasks. *IEEE Transactions on Haptics*, 6(3):296–308, July 2013. ISSN 1939-1412. doi: 10.1109/TOH.2013.6.

- [70] I. M. Bullock, R. R. Ma, and A. M. Dollar. A Hand-Centric Classification of Human and Robot Dexterous Manipulation. *IEEE Transactions on Haptics*, 6(2):129–144, April 2013. ISSN 1939-1412. doi: 10.1109/TOH.2012.53.
- [71] I. M. Bullock, T. Feix, and A. M. Dollar. The Yale human grasping dataset: Grasp, object, and task data in household and machine shop environments. *The International Journal of Robotics Research*, 34(3):251–255, March 2015. ISSN 0278-3649, 1741-3176. doi: 10.1177/0278364914555720. URL <http://ijr.sagepub.com/cgi/doi/10.1177/0278364914555720>.
- [72] I. M. Bullock, T. Feix, and A. M. Dollar. Dexterous workspace of human two- and three-fingered precision manipulation. In *2014 IEEE Haptics Symposium (HAPTICS)*, pages 41–47, Feb 2014. doi: 10.1109/HAPTICS.2014.6775431.
- [73] I. M. Bullock, T. Feix, and A. M. Dollar. Finding small, versatile sets of human grasps to span common objects. In *Robotics and Automation (ICRA), 2013 IEEE International Conference on*, pages 1068–1075, May 2013. doi: 10.1109/ICRA.2013.6630705.
- [74] G. Baud-Bovy and J. F. Soechting. Two virtual fingers in the control of the tripod grasp. *Journal of neurophysiology*, 86(2):604, 2001.
- [75] D. M. Aukes, B. Heyneman, J. Ulmen, H. Stuart, M. R. Cutkosky, S. Kim, P. Garcia, and A. Edsinger. Design and testing of a selectively compliant underactuated hand. *The International Journal of Robotics Research*, 33(5):721–735, 2014. doi: 10.1177/0278364913518997. URL <http://ijr.sagepub.com/content/33/5/721.abstract>.
- [76] C. Ansuini, M. Santello, S. Massaccesi, and U. Castiello. Effects of end-goal on hand shaping. *Journal of Neurophysiology*, 95(4):2456–2465, December 2005. ISSN 0022-3077, 1522-1598. doi: 10.1152/jn.01107.2005. URL <http://jn.physiology.org/cgi/doi/10.1152/jn.01107.2005>.
- [77] C. Ansuini, L. Giosa, L. Turella, G. Altoè, and U. Castiello. An object for an action, the same object for other actions: effects on hand shaping. *Experimental Brain Research*, 185(1):111–119, February 2008. ISSN 0014-4819, 1432-1106. doi: 10.1007/s00221-007-1136-4. URL <http://link.springer.com/10.1007/s00221-007-1136-4>.
- [78] J. Aleotti and S. Caselli. Grasp recognition in virtual reality for robot pregrasp planning by demonstration. In *Proceedings 2006 IEEE International Conference on Robotics and Automation*, pages 2801–2806, 2006. doi: 10.1109/ROBOT.2006.1642125.

## BIBLIOGRAPHY

---

- [79] N. J. Van Eck and L. Waltman. Software survey: VOSviewer, a computer program for bibliometric mapping. *Scientometrics*, 84(2):523–538, August 2010. ISSN 0138-9130. doi: 10.1007/s11192-009-0146-3. URL <http://www.ncbi.nlm.nih.gov/pmc/articles/PMC2883932/>.
- [80] M. Grebenstein. *Approaching Human Performance: The Functionality-Driven Awiwi Robot Hand*, volume 98. Springer International Publishing, 2014.
- [81] T. Feix, J. Romero, C. H. Ek, H. B. Schmedmayer, and D. Kragic. A metric for comparing the anthropomorphic motion capability of artificial hands. *IEEE Transactions on Robotics*, 29(1):82–93, feb 2013.
- [82] J. Chalfoun. *Prédiction des efforts musculaires dans le système main avant-bras : Modélisation, simulation, optimisation et validation*. PhD thesis, l'Université de Versailles Saint-Quentin-en Yvelines, 2005.
- [83] R. J. Maughan, J. S. Watson, and J. Weir. Strength and cross-sectional area of human skeletal muscle. *The Journal of Physiology*, 338(1):37–49, 1983. ISSN 1469-7793. doi: 10.1113/jphysiol.1983.sp014658. URL <http://dx.doi.org/10.1113/jphysiol.1983.sp014658>.
- [84] A. V. Hill. The series elastic component of muscle. *Proceedings of the Royal Society of London B: Biological Sciences*, 137(887):273–280, 1950. ISSN 0080-4649.
- [85] S. S. Metan, K. Prasad, and G. C. Mohankumar. FEM model an effective tool to evaluate von mises stresses in shoulder joint and muscles for adduction and abduction. *Procedia Materials Science*, 5:2090 – 2098, 2014. ISSN 2211-8128. doi: <http://dx.doi.org/10.1016/j.mspro.2014.07.544>. URL <http://www.sciencedirect.com/science/article/pii/S2211812814009092>.
- [86] H. Hatze. A Myocybernetic Control Model of Skeletal Muscle. *Biological Cybernetics*, 25(2):103–119, Jun 1977.
- [87] J. M. Winters. *Hill-Based Muscle Models: A Systems Engineering Perspective*, chapter 5, pages 69–93. Springer New York, New York, NY, 1990. ISBN 978-1-4613-9030-5. doi: 10.1007/978-1-4613-9030-5\_5. URL [http://dx.doi.org/10.1007/978-1-4613-9030-5\\_5](http://dx.doi.org/10.1007/978-1-4613-9030-5_5).
- [88] B. Tondu and S. D. Zagal. McKibben artificial muscle can be in accordance with the hill skeletal muscle model. In *proceedings of the First IEEE/RAS-EMBS International Conference on Biomedical Robotics and Biomechatronics, 2006*, pages 714–720, Feb 2006. doi: 10.1109/BIOROB.2006.1639174.

- [89] R. Perumal, A. S. Wexler, J. Ding, and S. A. Binder-Macleod. Mathematical modeling of skeletal muscle under non-isometric FES. In *proceedings of the IEEE 28th Annual Northeast Bioengineering Conference*, pages 29–30, Philadelphia, USA, Apr 2002. doi: 10.1109/NEBC.2002.999449.
- [90] F. E. Zajac. Muscle and tendon: properties, models, scaling, and application to biomechanics and motor control. *Critical reviews in biomedical engineering*, 17(4):359–411, 1989. ISSN 0278-940X 0278-940X.
- [91] S. L. Delp. *Surgery Simulation: A Computer Graphics System to Analyze and Design Musculoskeletal Reconstructions of the Lower Limb*. Stanford University Department of Mechanical Engineering, 1990. URL <https://books.google.fr/books?id=ipzVPAAACAAJ>.
- [92] M. Hayashibe, D. Guiraud, and P. Poignet. EMG-based neuromuscular modeling with full physiological dynamics and its comparison with modified hill model. In *proceedings of the 2009 Annual International Conference of the IEEE Engineering in Medicine and Biology Society*, pages 6530–6533, Minneapolis, USA, Sept 2009. doi: 10.1109/IEMBS.2009.5333147.
- [93] M. Pang, S. Guo, Z. Song, and S. Zhang. sEMG signal and hill model based continuous prediction for hand grasping motion. In *proceedings of the International Conference on Complex Medical Engineering (CME), 2013 ICME*, pages 329–333, Beijing, China, May 2013. doi: 10.1109/ICCME.2013.6548264.
- [94] M. Millard, T. Uchida, A. Seth, and S. L. Delp. Flexing computational muscle: modeling and simulation of musculotendon dynamics. *Journal of Biomechanical Engineering*, 135(135):1–11, Feb 2013.
- [95] A. Mousavi, H. Ehsani, and M. Rostami. Compliant Vs. rigid tendon models: A simulation study on precision, computational efficiency and numerical stability. In *proceedings of the 21th Iranian Conference on Biomedical Engineering (ICBME), 2014*, pages 92–97, Tehran, Iran, Nov 2014. doi: 10.1109/ICBME.2014.7043900.
- [96] L. Sun, Y. Sun, Z. Huang, J. Hou, and J. Wu. A Hill-Type Submaximally-Activated Musculotendon Model and its Simulation. In *proceedings of the 2015 14th International Symposium on Distributed Computing and Applications for Business Engineering and Science (DCABES)*, pages 439–442, Guiyang, China, Aug 2015. doi: 10.1109/DCABES.2015.116.
- [97] D. F. B. Haeufle, M. Günther, A. Bayer, and S. Schmitt. Hill-type muscle model with serial damping and eccentric force–velocity relation. *Journal of Biomechanics*, 47(6):1531–1536, Feb 2014. ISSN 0021-9290. doi: <http://dx.doi.org/10.1016/j>

## BIBLIOGRAPHY

---

- jbiomech.2014.02.009. URL <http://www.sciencedirect.com/science/article/pii/S0021929014001018>.
- [98] J. O. Ramsay, X. Wang, and R. Flanagan. A functional data analysis of the pinch force of human fingers. *Journal of the Royal Statistical Society: Series C (Applied Statistics)*, 44(1):17–30, mar 1995.
- [99] T. A. Schreuders, M. E. Roebroek, J. Goumans, J. F. van Nieuwenhuijzen, T. H. Stijnen, and H.J. Stam. Measurement error in grip and pinch force measurements in patients with hand injuries. *Physical therapy*, 83(9):806–815, 2003.
- [100] C. Lu, J. A. Stankovic, S. H. Son, and G. Tao. Feedback control real-time scheduling: Framework, modeling, and algorithms\*. *Real-Time Systems*, 23(1):85–126, 2002. ISSN 1573-1383. doi: 10.1023/A:1015398403337. URL <http://dx.doi.org/10.1023/A:1015398403337>.
- [101] S. Zodey and S. K. Pradhan. Matlab Toolbox for Kinematic Analysis and Simulation of Dexterous Robotic Grippers. *Procedia Engineering*, 97:1886–1895, 2014. ISSN 18777058. doi: 10.1016/j.proeng.2014.12.342. URL <http://linkinghub.elsevier.com/retrieve/pii/S1877705814034109>.
- [102] J. T. Belter and A. M. Dollar. Performance characteristics of anthropomorphic prosthetic hands. In *Proceedings of IEEE International Conference on Rehabilitation Robotics*, pages 921–927, Zurich, CH, jun 2011. IEEE. URL [http://www.eng.yale.edu/grablab/pubs/Belter\\_ICORR2011.pdf](http://www.eng.yale.edu/grablab/pubs/Belter_ICORR2011.pdf).
- [103] S. Narasimhan, D. Siegel, J. Hollerbach, K. Biggers, and G. Gerpheide. Implementation of control methodologies on the computational architecture for the utah/mit hand. In *proceedings of the International Conference on Robotics and Automation*, volume 3, pages 1884–1889, San Francisco, USA, Apr 1986. doi: 10.1109/ROBOT.1986.1087475.
- [104] S. C. Jacobsen, E. K. Iversen, D. F. Knutti, R. T. Johnson, and K. B. Biggers. Design of the Utah/MIT dextrous hand. In *proceedings of IEEE International Conference on the Robotics and Automation*, volume 3, pages 1520–1532, San Francisco, USA, 1986.
- [105] S. C Jacobsen, J. E. Wood, D. F. Knutti, and K. B. Biggers. The UTAH/MIT dextrous hand: Work in progress. *The International Journal of Robotics Research*, 3(4):21–50, Nov 1984.
- [106] M. Grebenstein. *Approaching human performance*. PhD thesis, Eidgenössische Technische Hochschule ETH Zürich, 2012.
- [107] L. B. Bridgwater, C. A. Ihrke, V. Diftler, M. E. Abdallah, N. A. Radford, J. M. Rogers, S. Yayathi, R. S. Askew, and D. M. Linn. The robonaut 2 hand - designed to do work

- with tools. In *proceedings of the International Conference on Robotics and Automation (ICRA)*, pages 3425–3430, St. Paul USA, May 2012. doi: 10.1109/ICRA.2012.6224772.
- [108] V. Diftler, J. S. Mehling, M. E. Abdallah, N. A. Radford, L. B. Bridgwater, A. M. Sanders, R. S. Askew, D. M. Linn, J. D. Yamokoski, F. A. Permenter, B. K. Hargrave, R. Platt, R. T. Savely, and R. O. Ambrose. Robonaut 2 - the first humanoid robot in space. In *in procedeedings of the International Conference on Robotics and Automation (ICRA)*, pages 2178–2183, Shanghai, China, May 2011. doi: 10.1109/ICRA.2011.5979830.
- [109] T. Okada. Object-Handling System for Manual Industry. *proceedings of the IEEE Transactions on Systems, Man, and Cybernetics*, 9(2):79–89, Feb 1979. ISSN 0018-9472. doi: 10.1109/TSMC.1979.4310152.
- [110] I. Yamano and T. Maeno. Five-fingered Robot Hand using Ultrasonic Motors and Elastic Elements. In *Proceedings of the 2005 IEEE International Conference on Robotics and Automation*, pages 2673–2678, Barcelona, Spain, April 2005. doi: 10.1109/ROBOT.2005.1570517.
- [111] C. Melchiorri, G. Palli, G. Berselli, and G. Vassura. Development of the UB Hand IV: Overview of Design Solutions and Enabling Technologies. *IEEE Robotics and Automation Magazine*, 20(3):72–81, sep 2013. ISSN 1070-9932. doi: 10.1109/MRA.2012.2225471.
- [112] H. Mnyusiwalla, P. Vulliez, J. P. Gazeau, and S. Zegloul. A new dexterous hand based on bio-inspired finger design for inside-hand manipulation. *IEEE Transactions on Systems, Man, and Cybernetics: Systems*, 46(6):809–817, jun 2016. ISSN 2168-2216. doi: 10.1109/TSMC.2015.2468678.
- [113] J. Butterfass, M. Grebenstein, H. Liu, and G. Hirzinger. DLR-Hand ii: next generation of a dextrous robot hand. In *proceedings of the IEEE International Conference on Robotics and Automation, 2001. Proceedings 2001 ICRA.*, volume 1, pages 109–114, 2001. doi: 10.1109/ROBOT.2001.932538.
- [114] Shadow Robot Company. *Shadow Dexterous Hand Technical Specification*. 251 Liverpool Road, London, N1 1LX, Jan 2013.
- [115] M. C. Carrozza, P. Dario, F. Vecchi, S. Rocco, M. Zecca, and F. Sebastiani. The cyberhand: on the design of a cybernetic prosthetic hand intended to be interfaced to the peripheral nervous system. In *proceedings of the 2003 IEEE/RSJ International Conference on Intelligent Robots and Systems, 2003. (IROS 2003)*, volume 3, pages 2642–2647, Oct 2003. doi: 10.1109/IROS.2003.1249269.

## BIBLIOGRAPHY

---

- [116] I. N. Gaiser, C. Pylatiuk, S. Schulz, A. Kargov, R. Oberle, and T. Werner. The FLUID-HAND III: A multifunctional prosthetic hand. *Journal of Prosthetics and Orthotics*, 21(2):91–96, Apr 2009.
- [117] Z. Xu and E. Todorov. Design of a Highly Biomimetic Anthropomorphic Robotic Hand towards Artificial Limb Regeneration. In *in proceedings of the IEEE International Conference on Robotics and Automation, 2016 (ICRA'16)*., pages 3485–3492, Stockolm, Sweden, May 2016.
- [118] H. Iwata and S. Sugano. Design of anthropomorphic dexterous hand with passive joints and sensitive soft skins. In *proceedings of the IEEE/SICE International Symposium on System Integration*, pages 129–134, Tokyo, Japan, Jan 2009. doi: 10.1109/SI.2009.5384542.
- [119] C. Gosselin, F. Pelletier, and T. Laliberte. An anthropomorphic underactuated robotic hand with 15 dofs and a single actuator. In *proceedings of the IEEE International Conference on Robotics and Automation*, pages 749–754, Pasadena, USA., May 2008. doi: 10.1109/ROBOT.2008.4543295.
- [120] Lionel Birglen, Thierry Laliberté, and Clément Gosselin. *Design and Control of the Laval Underactuated Hands*, pages 171–207. Springer Berlin Heidelberg, Berlin, Heidelberg, 2008. ISBN 978-3-540-77459-4. doi: 10.1007/978-3-540-77459-4\_7. URL [http://dx.doi.org/10.1007/978-3-540-77459-4\\_7](http://dx.doi.org/10.1007/978-3-540-77459-4_7).
- [121] K. J. DeLaurentis and C. Mavroidis. Mechanical design of a shape memory alloy actuated prosthetic hand. *Technology and Health Care*, 10(2):91–106, Jun 2002.
- [122] L. U. Odhner, L. P. Jentoft, M. R. Claffee, N. Corson, Y. Tenzer, R. R. Ma, M. Buehler, R. Kohout, R. D. Howe, and A. M. Dollar. A compliant, underactuated hand for robust manipulation. *The International Journal of Robotics Research*, 2014. doi: 10.1177/0278364913514466. URL <http://ijr.sagepub.com/content/early/2014/02/14/0278364913514466.abstract>.
- [123] T. Mouri, H. Kawasaki, K. Yoshikawa, J. Takai, and S. Ito. Anthropomorphic robot hand: Gifu hand iii. In *proceedings of the International Conference ICCAS*, pages 1288–1293, Jeonbuk, Korea, 2002.
- [124] M. S. Johannes, J. D. Bigelow, J. M. Burck, S. D. Harshbarger, M. V. Kozlowski, and V. T. Doren. An overview of the developmental process for the modular prosthetic limb. *Johns Hopkins APL Technical Digest*, 30(3):207–216, Mar 2011.
- [125] S. Jacobsen, I. McCammon, K. Biggers, and R. Phillips. Tactile sensing system design issues in machine manipulation. In *proceedings of the International Confer-*

- ence on Robotics and Automation*, volume 4, pages 2087–2096, Mar 1987. doi: 10.1109/ROBOT.1987.1087755.
- [126] F. Ficuciello, G. Palli, C. Melchiorri, and B. Siciliano. Experimental evaluation of the UB Hand IV postural synergies. In *Proceedings of IEEE/RSJ International Conference on Intelligent Robots and Systems (IROS)*, pages 1775–1780, San Francisco, CA, USA, sep 2011. IEEE. ISBN 2153-0858. URL [http://media.isr.uc.pt/autonomousgrasping/submissions/16\\_CR\\_sinergie\\_long.pdf](http://media.isr.uc.pt/autonomousgrasping/submissions/16_CR_sinergie_long.pdf).
- [127] M. G. Catalano, G. Grioli, E. Farnioli, A. Serio, C. Piazza, and A. Bicchi. Adaptive synergies for the design and control of the Pisa/IIT SoftHand. *The International Journal of Robotics Research*, 33(5):768–782, apr 2014.
- [128] M. Gabiccini, A. Bicchi, D. Prattichizzo, and M. Malvezzi. On the role of hand synergies in the optimal choice of grasping forces. *Autonomous Robots*, 31(2-3):235–252, 2011. doi: 10.1007/s10514-011-9244-1.
- [129] R. Campa, K. Camarillo, and L. Arias. Kinematic modeling and control of robot manipulators via unit quaternions: Application to a spherical wrist. In *Proceedings of 45th IEEE Conference on Decision and Control*, pages 6474–6479, San Diego, CA, USA, dec 2006. IEEE. URL [http://ieeexplore.ieee.org/xpls/abs\\_all.jsp?arnumber=4177709](http://ieeexplore.ieee.org/xpls/abs_all.jsp?arnumber=4177709).
- [130] O. Heidari, H. M. Daniali, and S. M. Varedi. Geometric design of 3r manipulators for three precision poses using dual quaternions. In *Proceedings of Second RSI/ISM International Conference on Robotics and Mechatronics (ICRoM)*, pages 601–606, Nottingham, UK, jul 2014. IACSIT and IJMSE. URL [http://ieeexplore.ieee.org/xpls/abs\\_all.jsp?arnumber=6990968](http://ieeexplore.ieee.org/xpls/abs_all.jsp?arnumber=6990968).
- [131] K. Harada and T. Anzai. Multiple sweeping using quaternion operations. *Computer-Aided Design*, 34(11):815–822, 2002. ISSN 0010-4485. URL <http://www.sciencedirect.com/science/article/pii/S0010448501001701>.
- [132] L. Radavelli, R. Simoni, E. R. De Pieri, and D. Martins. A comparative Study of the Kinematics of Robots Manipulators by Denavit-Hartenberg and Dual Quaternion. *Mecánica Computacional*, 31(15):2833–2848, nov 2012. ISSN 1666-6070.
- [133] V. Hugel and N. Jouandeau. Automatic generation of humanoid’s geometric model parameters. In *Proceedings of Proceedings of 17th annual RoboCup International Symposium (RCUP-2013)*, pages 408–419, Eindhoven, NL, jul 2014. Springer LNCS. URL [http://link.springer.com/chapter/10.1007/978-3-662-44468-9\\_36](http://link.springer.com/chapter/10.1007/978-3-662-44468-9_36).

## BIBLIOGRAPHY

---

- [134] J. S. Dai. An historical review of the theoretical development of rigid body displacements from Rodrigues parameters to the finite twist. *Mechanism and Machine Theory*, 41(1): 41–52, jan 2006. ISSN 0094114X. doi: 10.1016/j.mechmachtheory.2005.04.004.
- [135] S. L. Altmann. Hamilton, Rodrigues, and the Quaternion Scandal. *Mathematics Magazine*, 62(5):291–308, dec 1989. ISSN 0025570X.
- [136] A. Perez and J. M. McCarthy. Geometric design of RRP, RPR and PRR serial chains. *Mechanism and Machine Theory*, 40(11):1294–1311, nov 2005. ISSN 0094114X. doi: 10.1016/j.mechmachtheory.2004.12.023. URL <http://linkinghub.elsevier.com/retrieve/pii/S0094114X05000212>.
- [137] L. Yan and L. Xu. Study of diagonalization on skew self-conjugate matrix in quaternion field. In *Proceedings of Second International Conference on Computational Intelligence and Natural Computing Proceedings (CINC)*, pages 72–75, Wuhan, CN, sep 2010. IEEE. ISBN 9781424477050. URL [http://ieeexplore.ieee.org/xpls/abs\\_all.jsp?arnumber=5643889](http://ieeexplore.ieee.org/xpls/abs_all.jsp?arnumber=5643889).
- [138] J. Yang and Y. Altintas. Generalized kinematics of five-axis serial machines with non-singular tool path generation. *International Journal of Machine Tools and Manufacture*, 75:119–132, dec 2013. ISSN 08906955. doi: 10.1016/j.ijmachtools.2013.09.002. URL <http://linkinghub.elsevier.com/retrieve/pii/S0890695513001429>.
- [139] F. Tarsha-Kurdi, T. Landes, and P. Grussenmeyer. Hough-transform and extended ransac algorithms for automatic detection of 3d building roof planes from lidar data. In *Proceedings of the ISPRS Workshop on Laser Scanning*, volume 36, pages 407–412, 2007.
- [140] J. Canny. A computational approach to edge detection. *IEEE Transactions on pattern analysis and machine intelligence*, (6):679–698, 1986.
- [141] Q. He, M. Yu, L. Song, H. Ding, X. Zhang, and Z. Dai. Experimental study and model analysis of the performance of IPMC membranes with various thickness. *Journal of Bionic Engineering*, 8(1):77–85, mar 2011.
- [142] R. E. Newnham and G. R. Ruschau. Electromechanical properties of smart materials. *Journal of Intelligent Material Systems and Structures*, 4(3):289–294, 1993.
- [143] S. J. Furst and S. Seelecke. Modeling and experimental characterization of the stress, strain, and resistance of shape memory alloy actuator wires with controlled power input. *Journal of Intelligent Material Systems and Structures*, 23(11):1233–1247, 2012.
- [144] K. Jung, J. Nam, and H. Choi. Investigations on actuation characteristics of IPMC artificial muscle actuator. *Sensors and Actuators A: Physical*, 107(2):183–192, oct 2003.

- [145] T. Wallmersperger, D. J. Leo, and C. S. Kothera. Transport modeling in ionomeric polymer transducers and its relationship to electromechanical coupling. *Journal of Applied Physics*, 101(2):(024912)1–9, jan 2007.
- [146] T. G. Noh, Y. Tak, J. D. Nam, and H. Choi. Electrochemical characterization of polymer actuator with large interfacial area. *Electrochimica Acta*, 47(13):2341–2346, may 2002.
- [147] D. Vokoun, Q. He, L. Heller, M. Yu, and Z. Dai. Modeling of IPMC cantilever’s displacements and blocking forces. *Journal of Bionic Engineering*, 12(1):142–51, jan 2015. ISSN 1672-6529. doi: [http://dx.doi.org/10.1016/S1672-6529\(14\)60108-6](http://dx.doi.org/10.1016/S1672-6529(14)60108-6).
- [148] M. Bassil, J. Davenas, and M. E. Tahchi. Electrochemical properties and actuation mechanisms of polyacrylamide hydrogel for artificial muscle application. *Sensors and Actuators B: Chemical*, 134(2):496–501, sep 2008.
- [149] S. Y. Kim, H. S. Shin, Y. M. Lee, and C. N. Jeong. Properties of electroresponsive poly (vinyl alcohol)/poly (acrylic acid) IPN hydrogels under an electric stimulus. *Journal of applied polymer science*, 73(9):1675–1683, jun 1999.
- [150] K. K. Westbrook and H. J. Qi. Actuator designs using environmentally responsive hydrogels. *Journal of Intelligent Material Systems and Structures*, 19(5):597–607, 2008.
- [151] M. J. Higgins, G. G. Wallace, P. J. Molino, A. Gelmi, and H. Zhang. *Innovations in nanomaterials*, chapter Conducting polymers: Their route to nanobionics applications via atomic force microscopy, pages 41–75. Nova Science Publishers, Inc., 2015.
- [152] G. Alici, B. Mui, and C. Cook. Bending modeling and its experimental verification for conducting polymer actuators dedicated to manipulation applications. *Sensors and Actuators A: Physical*, 126(2):396–404, feb 2006.
- [153] Q. M. Wang, Q. Zhang, B. Xu, R. Liu, and L. E. Cross. Nonlinear piezoelectric behavior of ceramic bending mode actuators under strong electric fields. *Journal of Applied Physics*, 86(6):3352–3360, 1999.
- [154] B. R. Kumar and S. Ranganatha. A study of stiffness and damping characteristics of conventional fluid and smart fluid applied to squeeze film damper. *International Journal of Innovative Technology and Exploring Engineering (IJITEE)*, 3(6):30–34, nov 2013.
- [155] S. Chen and X. Liu. Spectral analysis for response of the dynamic damping force and phenomenological modeling of electro-rheological fluid. *Smart Materials and Structures*, 8(4):499–503, jun 1999.
- [156] S. Dastoor and M. Cutkosky. Design of dielectric electroactive polymers for a compact and scalable variable stiffness device. In *Proceedings of IEEE International Conference*

## BIBLIOGRAPHY

---

- on Robotics and Automation (ICRA)*, pages 3745–3750, St. Paul, MN, USA, may 2012. IEEE.
- [157] Y. Bar-Cohen. *Electroactive Polymer (EAP) Actuators as Artificial Muscles Reality, Potential, and Challenges*, chapter EAP History, Current Status, and Infrastructure, pages 4–43. SPIE The International Society for Optical Engineering, Bellingham, WA, USA, 2 edition, 2004.
- [158] Dynalloy. *Technical Characteristics of FLEXINOL Actuator Wires*. DYNALLOY Inc. Makers of Dynamic Alloys, 1562 Reynolds Avenue, Irvine, California 92614 USA, F1140Rev I.2 edition, 2015.
- [159] D. Kim, K. J. Kim, J. Nam, and Palmre V. Electro-chemical operation of ionic polymer-metal composites. *Sensors and Actuators B: Chemical*, 155(1):106–113, 2011.
- [160] H. Djojodihardjo, M. Jafari, S. Wiriadidjaja, and K.A. Ahmad. Active vibration suppression of an elastic piezoelectric sensor and actuator fitted cantilevered beam configurations as a generic smart composite structure. *Composite Structures*, 132:848–863, nov 2015.
- [161] J. H. Yoo, J. I. Hong, and W. Cao. Piezoelectric ceramic bimorph coupled to thin metal plate as cooling fan for electronic devices. *Sensors and Actuators A: Physical*, 79(1): 8–12, 2000.
- [162] W. Kim. *Model-based Design Framework for Shape Memory Alloy Wire Actuation Devices*. Dissertation, University of Michigan, jun 2016. URL [https://deepblue.lib.umich.edu/bitstream/handle/2027.42/120684/wonhekim\\_1.pdf?sequence=1&isAllowed=y](https://deepblue.lib.umich.edu/bitstream/handle/2027.42/120684/wonhekim_1.pdf?sequence=1&isAllowed=y).
- [163] F. Auricchio and L. Petrini. A three-dimensional model describing stress-temperature induced solid phase transformations: solution algorithm and boundary value problems. *International Journal for Numerical Methods in Engineering*, 61(6):807–836, 2004. ISSN 1097-0207. doi: 10.1002/nme.1086. URL <http://dx.doi.org/10.1002/nme.1086>.
- [164] B. Peultier, T. Ben Zineb, and E. Patoor. Macroscopic constitutive law of shape memory alloy thermomechanical behaviour. application to structure computation by FEM. *Mechanics of Materials*, 38(5–6):510–524, 2006. ISSN 0167-6636. doi: <http://dx.doi.org/10.1016/j.mechmat.2005.05.026>. URL <http://www.sciencedirect.com/science/article/pii/S0167663605001249>. Shape Memory Alloys.
- [165] F. Auricchio, A. Reali, and U. Stefanelli. A three-dimensional model describing stress-induced solid phase transformation with permanent inelasticity. *International Journal of Plasticity*, 23(2):207–226, 2007. ISSN 0749-6419. doi: <http://dx.doi.org/10.1016/j.ijplas.2006.02.012>. URL <http://www.sciencedirect.com/science/article/pii/S0749641906000714>.

- [166] F. Auricchio, A. Reali, and U. Stefanelli. A macroscopic 1D model for shape memory alloys including asymmetric behaviors and transformation-dependent elastic properties. *Computer Methods in Applied Mechanics and Engineering*, 198(17–20):1631–1637, apr 2009. ISSN 0045-7825. doi: <http://dx.doi.org/10.1016/j.cma.2009.01.019>. URL <http://www.sciencedirect.com/science/article/pii/S0045782509000589>.
- [167] J. Arghavani, F. Auricchio, R. Naghdabadi, A. Reali, and S. Sohrabpour. A 3-d phenomenological constitutive model for shape memory alloys under multiaxial loadings. *International Journal of Plasticity*, 26(7):976–991, 2010. ISSN 0749-6419. doi: <http://dx.doi.org/10.1016/j.ijplas.2009.12.003>. URL <http://www.sciencedirect.com/science/article/pii/S0749641909001648>.
- [168] S. J. Furst, J. H. Crews, and S. Seelecke. Numerical and experimental analysis of inhomogeneities in SMA wires induced by thermal boundary conditions. *Continuum Mechanics and Thermodynamics*, 24(4):485–504, 2012. ISSN 1432-0959. doi: 10.1007/s00161-012-0238-9. URL <http://dx.doi.org/10.1007/s00161-012-0238-9>.
- [169] S. J. Furst, J. H. Crews, and S. Seelecke. Stress, strain, and resistance behavior of two opposing shape memory alloy actuator wires for resistance-based self-sensing applications. *Journal of Intelligent Material Systems and Structures*, 24(16):1951–1968, 2013. doi: 10.1177/1045389X13486715. URL <http://jim.sagepub.com/content/24/16/1951.abstract>.
- [170] Dynalloy. *Technical Characteristics of FLEXINOL Actuator Wires*. DYNALLOY Inc. Makers of Dynamic Alloys, 1562 Reynolds Avenue, Irvine, California 92614 USA, F1140Rev I.2 edition, 2015.
- [171] L. G. Machado and D. C. Lagoudas. *Shape Memory Alloys Modeling and Engineering Applications*, chapter Thermomechanical Constitutive Modeling of SMAs, pages 121–182. In Lagoudas, [172], 2008.
- [172] D. C. Lagoudas, editor. *Shape Memory Alloys Modeling and Engineering Applications*. Springer, 2008.
- [173] A. Rubiano, J. L. Ramirez, L. Gallimard, O. Polit, and N. Jouandeau. Chaîne articulée pour une prothèse robotique comprenant une jonction souple FR1656673, Jun. 2016.